Redox Active and Lewis Acidic Pincer Complexes of Bismuth

by

Marcus B. Kindervater

Submitted in partial fulfilment of the requirements
for the degree of Master of Science

at

Dalhousie University
Halifax, Nova Scotia
August 2020

Table of Contents

LIST OF TABLES

LIST OF FIGURES

LIST OF SCHEMES

ABSTRACT

Interest in exploiting unusual reactivity from main group elements akin to that of transition metals is an increasingly popular area of chemistry. In particular, utilizing the heaviest main group elements (5^{th} and 6^{th} row) has become a quickly evolving field that has seen many recent advances in stoichiometric and catalytic applications. Logical choices of ancillary ligands, while very common in d-block chemistry, is relatively underexplored with respect to the p-block elements. Our group looks to engender and study non-VSEPR geometries in heavy main group elements in order to unlock new and useful reactivity such as redox and Lewis acid catalysis.

This thesis will investigate the use planar multidentate ligands to make new redox active and Lewis acidic bismuth centres. We envisioned that rational choices of planar ligands may offer potential for exploiting unusual electronic proprieties, as they are known for enforcing non-VSEPR geometries, and thus unlocking new reactivity. The following will aim to utilize geometric tuning to study new redox active and Lewis acidic bismuth centres.

LIST OF ABBREVIATIONS AND SYMBOLS USED

AcOH	acetic acid
α	alpha
Ln	ancillary ligand
Å	angstrom
Ar	aryl
atm	atmosphere
C_6D_6	benzene-d^6
cm	centimeter
$CDCl_3$	chloroform-d
T_c	coalesces temperature
cf.	compared to
^oC	degree Celsius
DFT	density functional theory
DCM	dichloromethane
Et_2O	diethylether
eV	electron volt
ESI	electrospray ionization
ee	enantiomeric excess
eq	equivalent
Et	ethyl
FLP	frustrated Lewis pair
Hz	hertz
HOMO	highest occupied molecular orbital
Tp^{Me2}	hydridotris(3,5-dimethylpyrazolyl)borate
IR	infrared
^iPr	*iso*-propyl
J	joule
K	Kelvin
kcal	kilocalorie
Kg	kilogram
LA	Lewis acid
LB	Lewis base
LUMO	lowest unoccupied molecular orbital
MS	mass spectrometry
mCPBA	meta-chloroperoxybenzoic acid
Mes	mesityl
MIC	meso-ionic carbene
Me	methyl
μ	micro
mmol	millimole
M	molar
MO	molecular orbital
nm	nanometer
NBO	natural bond orbital

^{n}Bu	n-Butyl
NHC	N-heterocyclic carbene
NHP	N-heterocyclic phosphenium
NMR	nuclear magnetic resonance
p-	para
ppm	parts per million
Ph	phenyl
Pn	pnictogen
π-	pi
O-py	pyridine N-oxide
σ-	sigma
SOMO	singly occupied molecular orbital
^{t}Bu	*tert*-butyl
TBDPS	*tert*-butyldiphenylsilyl
T	temperature
THF	tetrahydrofuran
BAr^{F}	tetrakis(pentafluorophenyl)borate
TD-DFT	time dependent - density functional theory
κ	transmission coefficient
TFA	trifluoroacetic acid
OTf	trifluoromethylsulfonyl
Tf	triflyl
BCF	tris(pentafluorophenyl)borane
VSEPR	valence shell electron pair repulsion
λ	wavelength
WCA	weakly coordinating anion
WBI	Weiberg bond index
DFB	1,2-diflouorobenzene
dipp	2,6-diisopropylphenyl
DMAP	4-N,N-dimethylaminopyridine
9-BBN	9-borabicyclo[3.3.1]nonane

ACKNOWLEDGMENTS

I wish to begin by thanking my supervisor Dr. Saurabh Chitnis for his training and support. Your unwavering work ethic inspires us to be our best. This opportunity has led to many successes and also some failures, experiences I hope to continue to learn from for years to come. I'd like to extend my gratitude to Dr. Alex Speed for acting as a member of my research committee and for all the assistance you have offers in my years here. Thank you to Dr. Peng Zhang for agree to act as a reader of this thesis, your effort is greatly appreciated.

Next, I would like to take the opportunities to thank my group members, past and present. Katherine Marczenko, Joe Bedard, Chloe Louise-Johnson, Toren Hynes, Josh McMillian, Samantha Jee, Joseph Zurakowski, Nick Roberts, Nick Murphy, Junyi Liu, Cali Park. Thank you all for your support, your help, your friendship, and everything in between. Your impact on my experience will not be forgotten.

Thanks to Mr. Xiao Fang for mass-spectrometry expertise. Dr. Mike Lumsden (NMR3) is thanked for assistance in NMR experiments. Katherine Marczenko and Dr. Jason Masuda are thanked for their X-ray crystallographic expertise. Dr. Alex Speed, Dr. Laura Turculet, and Dr. Allison Thompson are thanked for various chemicals which contributed to this work.

The Sipekne'katik education department is sincerely thanked for funding my time here at Dalhousie. The Natural Sciences and Engineering Council (NSERC) of Canada, Canada Foundation for Innovation (CFI) and the Chemistry Graduate Student Society (CGSS) are thanked for funding as well.

Chapter 1: Introduction

1.1 State of the Art in Catalysis

The use of transition metal complexes to perform challenging organic transformations has been a popular and extremely successful area of chemistry for much of the last century. Miyaura and coworkers developed stereospecific C-C cross-coupling reactions mediated by palladium catalysts.[1] The Buchwald-Hartwig amination is a fundamentally important reaction in the synthesis of arylamines, with particular importance in pharmaceutical and agrochemical industries.[2–4] Other heavy transition metal complexes, such those based on rhodium, have been utilized by Schrock and Osborn to develop efficient hydrogenation of olefins.[5] While each of the examples mentioned above are powerful and important in their own right, they use rare and expensive metal catalysts which has prompted researchers to seek cheaper and more abundant alternatives.

Moving away from the third and fourth row metals, the use of second row transition metals such as copper, nickel, iron and cobalt was a natural progression of this field. Copper is inexpensive and non-toxic and recently copper catalyzed C-H functionalization reactions of heterocyclic substrates has been extensively studied with important applications in the natural product synthesis.[6] Nickel has been widely used for Suzuki–Miyaura and Negishi cross-coupling catalysis due to its ability to undergo facile oxidative addition and access to multiple stable oxidation states.[7] Arguably one of the most successful applications of base metal catalysis is the Haber-Bosch process which utilizes a

heterogenous iron catalyst to convert molecular nitrogen to ammonia. [8] While homogenous iron catalysis is not as well developed, recent reports have shown its ability to perform transformation such as the hydroboration of pinacolborane and 1,3,2-diazaborolanes and the hydrosilylation of carbonyl compounds under mild conditions.[9,10] A number of iron β-diketiminate complexes have been shown to perform reactions such as hydrodefluorination of aryl and vinyl fluorides, intramolecular hydroamination chemistry, as well as high yielding catalytic inter- and intramolecular hydrophosphination reactions in recent years.[11] Lastly, recent years have seen a growing number of reports showing cobalt's ability to catalyze challenging cross-coupling and cycloaddition reactions.[12,13]

There are two main modes of homogenous catalysis, redox and Lewis acid catalysis. It is important to note that Lewis base catalysis is also a rich field of study but is less relevant to this work and therefore will not be discussed in detail in this thesis. Transition metals are well suited for redox catalysis because they have d-orbitals that are relatively close in energy and allow for facile and reversible changes in oxidation state. In contrast, p-block elements have much wider s/p orbital energy gaps that do not easily facilitate reversible redox reactivity.[14] Therefore, examples of main group redox catalysis are limited. However, Lewis acidic main group compounds are very common and widely employed to perform catalytic transformations. The following sections will give a brief introduction of main group redox and Lewis acid catalysis.

1.2 Main Group Redox Catalysis

1.2.1 Iodine

Example of iodine redox catalysis have been known for several years now.[15] Independent reports by Kita *et al.,* and Ochiai *et al.,* in 2005 using catalytic amounts of an iodoarene(III) species to catalyze the oxidative spirocyclization of phenols and carbonyls using meta-chloroperoxybenzoic acid (mCPBA) as a terminal oxidant (**Figure 1**).[16,17] These studies highlighted the potential for hypervalent iodine as a new class of organcatalysts. Successive reports by the Kita group since 2005, with both catalytic amounts of iodine(I) or iodine(III), have shown 4-iodotoluene or 4-iodotoluene bis(trifluoroacetate) with stoichiometric mCPBA to perform the catalytic spirocyclization of phenols to lactones in yields upwards of 60% with loadings as low as 1-5 mol%.[18] The potential of these catalytic iodoarene species was more recently extended to carbon-carbon bond forming reactions involving phenols. They report an assumed mechanism involving a reactive phenoxenium ion generated by a

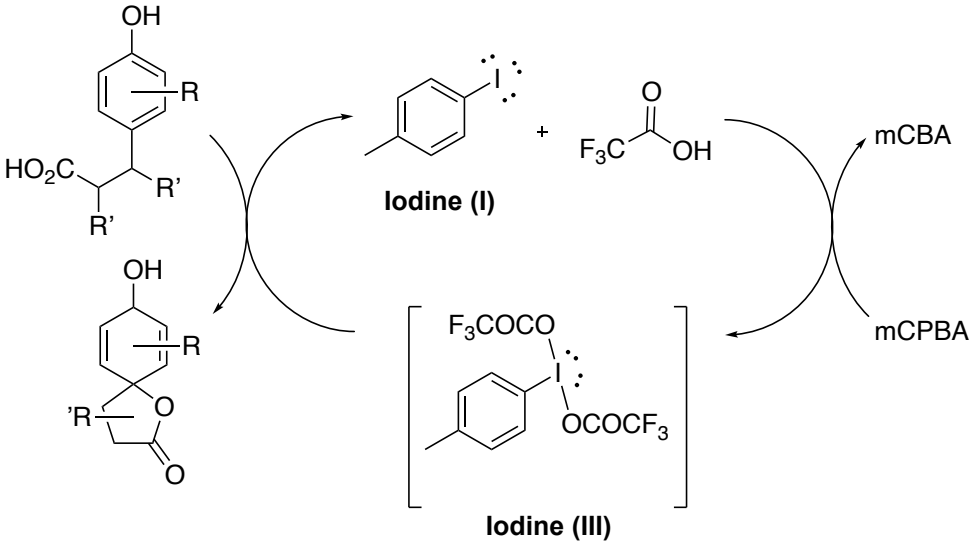

Figure 1. Catalytic iodine (I)/(III) redox cycle for the spirocyclization of phenols and lactones.

iodoarene(III)-TFA species.[19] The first iodoarene-catalyzed intramolecular carbon-nitrogen bond forming reaction was achieved using a protic 2,2,2-trifluoroethanol (CF_3CH_2OH) solvent and was the first reported hypervalent iodine(III) catalytic cycle that did not employ a strong acid while still proceeding under mild conditions.[20]

Even more impressive is that *asymmetric* hypervalent iodine compounds have been reported to catalytically perform enantioselective oxidative transformations (**Scheme 1**).[21] The first version of this process were developed by Wirth *et al.,* which employed a chiral organoiodane species in the presence of stoichiometric mCPBA as a oxidizer and p-toluenesulfonic acid monohydrate as a source of nucleophilic tosylate ions. The reaction was performed at room temperature and did not turnover at elevated temperatures, which suggested that the rate-determined step is the oxidation of the iodoarene.[22] They noted fairly poor enantioselectivities (<30% ee) in this work, however it was later reported that additional stabilization of a chelating group significantly improved the enantioselectivity up to nearly 40% ee during the during the α-oxytosylation of propiophenone.[22]

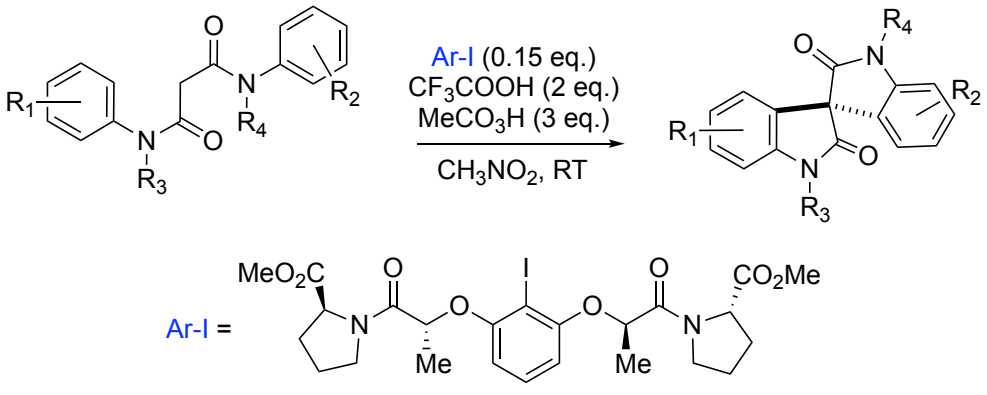

Scheme 1. Asymmetric iodine catalyzed spirocyclization through two C–C couplings.

1.2.2 Phosphorus

Phosphorus is another element that has been extensively studied in the context of main group redox catalysis. In the early 1950's Georg Wittig developed a reaction that involves conversion of an aldehyde or ketone to an alkene with a phosphonium ylide that produces the phosphine oxide as a by-product, since known as the Wittig reaction.[23] While the early work in this area was exclusively stoichiometric (**Scheme 2A**), there has been significant effort to develop an efficient catalytic protocol for this reaction. One could imagine a process in which the side product, phosphine oxide, could be reduced back to the phosphine in order to repeatedly perform the alkene conversion. While many processes involving reagents, such as $LiAlH_4$ or halodisilanes,[24,25] were known at the time they were not compatible in a one pot solutions that also contained reactive aldehydes and ketones. Therefore, O'Brian and coworkers aimed to develop a suitable reductant that could selectively regenerate the phosphine species with a retention of stereochemistry. They were successful in their endeavor as in 2009 they reported the first example of a catalytic Wittig reaction using diphenylsilane to reduce the phosphine oxide to the phosphine in a P(III)/P(V) redox cycle (**Scheme 2B**).[26] They tested their catalytic system by independently

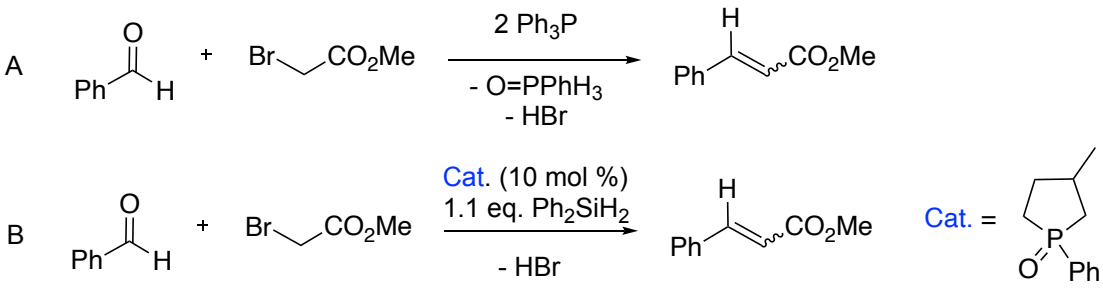

Scheme 2. A) stoichiometric and B) catalytic Wittig reaction mediated by phosphorus.

synthesizing a phosphine oxide precatalyst which in the presence of the benzaldehyde, methyl bromoacetate and diphenylsilane performed catalytic conversion to the Wittig product, methyl cinnamate, in high yield with a 10 mol% precatalyst loading. This was further confirmed by control experiments which showed no conversion to methyl cinnamate when the phosphine oxide was not present.

Inspired by the above, protocols for base-free intramolecular phosphine-catalyzed Wittig reactions were developed by Werner and co-workers several years later which proceed under neutral conditions.[27,28] Later they reported application of this method to the synthesis of benzoxepinones[29] which are synthetically useful scaffolds in organic synthesis as they often appear in natural products.[30–32]

In 2012, Radosevich *et al* reported a P(III)/P(V) catalytic cycle for the reduction of azobenzene using ammonia borane as a source of H_2. They were able to perform this transformation using a ONO tridentate pincer ligand

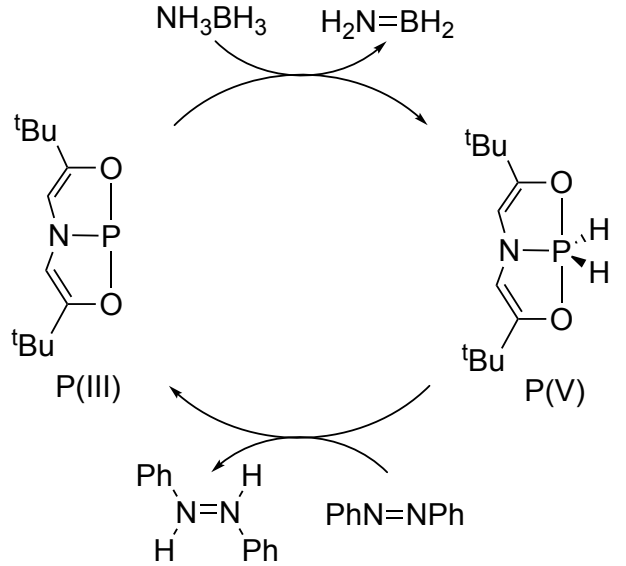

Figure 2. Catalytic transfer hydrogenation of azobenzene via a P(III)/P(V) redox cycle.

coordinated to a P(III) center which imposes a distorted geometry which facilitates the reaction. This compound was first reported several decades earlier by Arduengo who credited its planar geometry for its redox activity and ability to stabilize a P(I), P(III) and P(V) oxidation states.[33] It is reported that the reaction goes through a P(V) dihydridophosphorane intermediate which they propose is generated after protonation of the P(III) center generating a electrophilic phosphonium species, which can then abstract a hydride forming P(V) species observed. This then triggers a reduction of the P(V) complex to the P(III) complex, delivering H_2 to azobenzene (**Figure 2**).[34] Radosevich also used biphilic phosphetane compounds to catalyze the synthesis of Cadogan indazoles. This is a valuable N–N bond-forming reaction which proceeds via a P(III)/P(V)=O redox pathway which was previously only possible using transition metal catalysts[35] or with reactive azides.[36] They have also very recently reported another organocatalytic method for synthesizing N- indoles, oxindoles, benzimidazoles, and quinoxalinediones derivatives. Their study employs an organophosphorus-based catalyst (1,2,2,3,4,4-hexamethylphosphetane P-oxide) and a hydrosilane reductant; a protocol reminiscent the Wittig reaction developed by Werner. The reported conversion of ortho-functionalized nitroarenes into azaheterocycles via C-N cross coupling with boronic acids enables the synthesis of azaheterocycles from readily available building blocks and truly aids to further the application of main group redox catalysis.[36]

1.2.3 Selenium

The stereoselective dichlorination of alkenes is considered to be a long standing challenge faced in synthetic chemistry. Using highly reactive reagents such as Cl_2 makes controlling stoichiometry and side product formation extremely challenging.[36] Reagents which act of sources of Cl_2, such as SO_2Cl_2 or Et_4NCl_3, have aided to solve some of the practical issues associated with this chemistry. While operation challenges have been widely addressed, selectivity issues continue to represent a significant challenge in this field. State-of-the-art stereoselective chlorination methods are limited synthetically as they often utilize dense arrays of chlorinated stereogenic centers.[37–39] Another common issue is that most known catalysts operate via an ionic reaction pathway that yields the anti-addition product.[40,41] The Denmark group in 2015 were the first to report a catalytic, syn-stereospecific dichlorination of alkenes, employing a redox-active main group element (selenium). Using PhSeSePh as a pre-catalyst, they propose that oxidation of PhSeSePh via one of a series of external oxidants, generates $PhSeCl_3$ as the active catalyst (**Scheme 3**).[42] Their method was found to be widely applicable to variety of functionalized cyclic and acyclic 1,2-disubstituted alkenes, as well as primary allylic alcohols. Importantly, this method does not produce a chloronium ion intermediate, which is credited for the syn-selectivity in contrast to the previous literature.

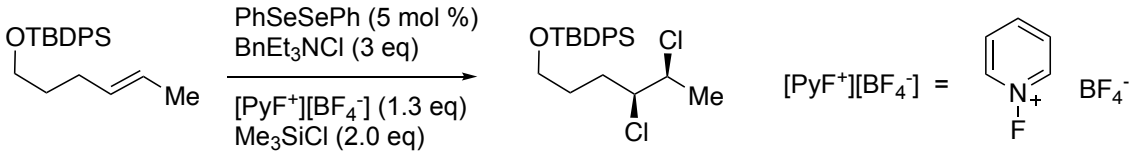

TBDPS = t*ert*-butyldiphenylsilyl

Scheme 3. Model system for the development of catalytic syn-dichlorination of alkenes via a selenium catalyst.

1.2.4 Bismuth

The last element that will be reviewed in this section is the heaviest non-radioactive element on the periodic table, bismuth. While it is typically assumed to participate mostly in Lewis acid type reactions,[43] there are a few reports in which reversible redox catalysis has been successfully performed. The Cornella group in 2020 demonstrated a Bi(III)/(V) redox couple by performing fluorination of arylboronic esters (**Scheme 4**). They hypothesized that due to the large size of Bi, it could accommodate additional neutral donor substituents which would affect its electronic and geometric proprieties. They utilized a tethered bis-anionic aryl ligand that featured a sulfonyl linker in the backbone. The tethered nature of the ligand is should aid to control geometry, and the electron withdrawing sulfonyl linker would provide electronic stabilization to the Bi(V) intermediate and make the bismuth center more electrophilic.[44] Increased electrophilicity is thought to promote the steps such as transmetallation and reductive elimination which are fundamental reactions in redox catalysis. This work systematically assessed each step, transmetallation, oxidative addition with a mild fluorinating agent, and reductive elimination of a C-F moiety and coupled them together in a Bi(III/V) catalytic cycle in order to synthesize aryl fluoride compounds. This work represent significant insight into a +3/+5 redox couple which remained elusive previous to this report.

Cornella has also recently explored another redox couple for bismuth in their work developing a transfer hydrogenation reaction of ammonia borane using

a Bi(I/III) redox couple.[45] Please refer to Chapter 2 where this topic is discussed in detail.

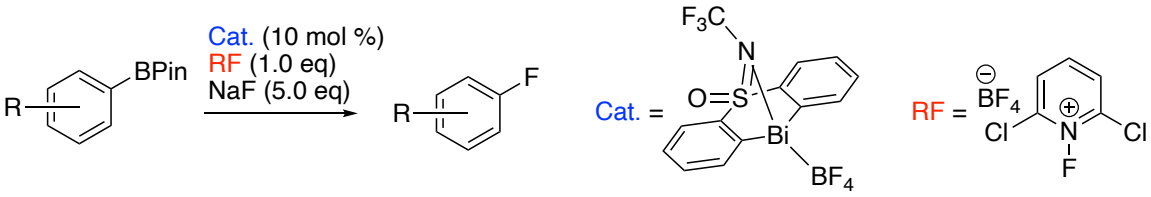

Scheme 4. Catalytic fluorination of arylboronic esters via Bi(III/V) redox couple.

1.3 Main Group Lewis Acid Catalysis

Hydroelementation or alkylelementation reaction such as hydroboration, are commonly facilitated by Lewis acid catalysis. Strong Lewis acids function by effectivity creating a dipole across the unsaturated substrate upon coordination. The key to the observed reactivity is the strong attractive forces enforced by the Lewis acid centre. The activation energy of the subsequent nucleophilic attack is lowered allowing the substrates to couple together and form a new bond.[46] The distance between the Lewis acid and the substrate after coordination is dependent on the strength of the Lewis acid (ie: a more electrophilic center leads to shorter distances) and the lower the activation barrier of the nucleophilic attack.[47] The catalyst is therefore not experiencing any change in oxidation state. The next sections will separately review s-block and p-block Lewis acid catalysis.

1.2.1 s-block Lewis acids

When thinking of early main group elements (s-block) most would first think of Grignard or organolithium reagents. However, there have been a number of compelling reports highlighting their potential in not only catalytic

transformations but in material chemistry and hydrogen storage technology.[48] The Harder group has recently reported several studies that show simple alkaline metal complexes (**Figure 3A** and **3B**) performing effective hydrogenation of substrates such as alkenes and imines under relatively mild conditions.[49–51] This area of chemistry is still in its infancy relative to transition metals but these are important contributions that further the application of transition metal-free catalysis.

1.2.2 p-block Lewis acids

Similarly, the popularity of using p-block elements as catalysts continues to grow. Compounds based on boron and phosphorus represent the majority of studies in this area, likely in part due to the convenience of an abundant NMR handle making the bonding and reactivity easier to study. First reported in 1963 by Massey *et al*., tris(pentafluorophenyl)borane (BCF) has been used in a number of reactions such hydrogenation, hydroboration, Friedel–Crafts CH silylation, hydrosilylation, and de-aromatization of N-heteroarenes. Even more difficult C-C bond forming reactions such as Michael additions, allylation

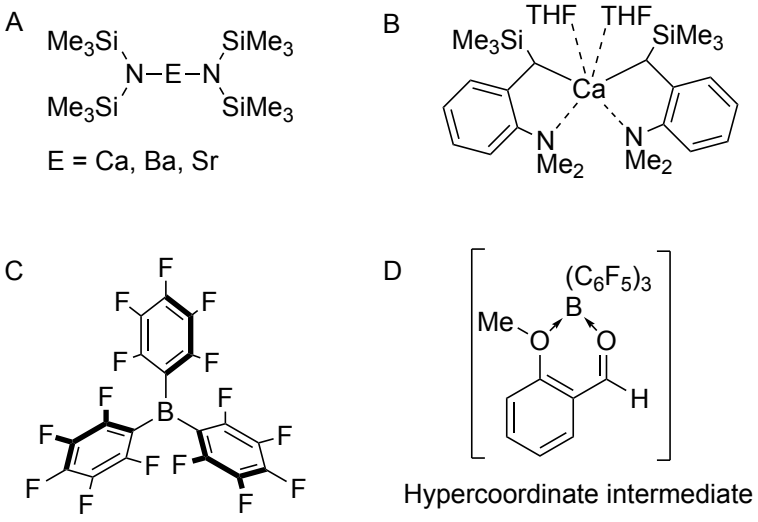

Figure 3. Select example of s-block and boron based Lewis acids.

reactions and Diels-alder reactions have been realized using the highly Lewis acidic BCF (**Figure 3C**).[52] Mechanistic insight in to the role of BCF were reported by Piers,[53–55] which showed a tetracoordinate borane species was key to the chemoselective allylstannation of *ortho*-anisaldehyde (**Figure 3D**) reported by Maruoka *et al*.[56,57]

The impressive electrophilicity of boron containing compounds has been the main defining feature of their chemistry. Two-coordinate borinium, three-coordinate borenium and four-coordinate boronium ions are a class of boron based cations that have seen extensive study in main group chemistry and are known to be very strong Lewis acids (**Figure 4A**).[52] A few example of metal-free catalysis using borenium ions have been reported, with nearly all been developed in the last decade. Arguably the most notable example of this chemistry was pioneering work by the Stephan with FLPs in which a 9-BBN stabilized borenium ion (**Figure 4B**) was able to heterolytically split H_2 in the presence of a Lewis base ($^tBu_3P$). Under the appropriate conditions, a catalytic

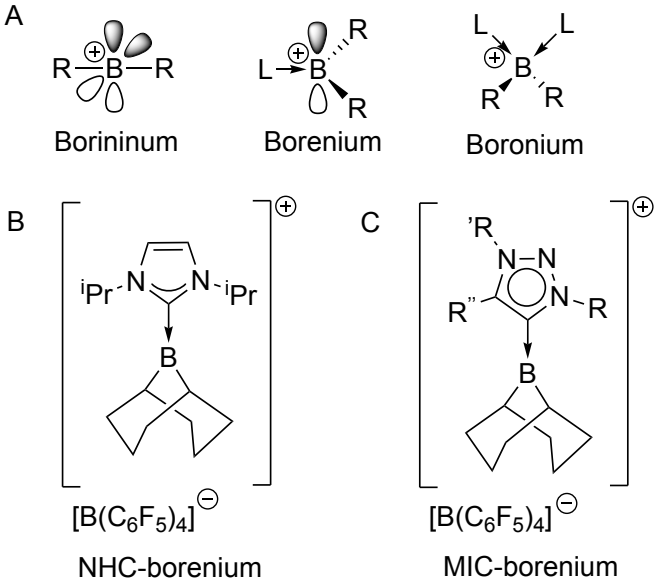

Figure 4. A) Boron based cations B) NHC-borenium C) MIC-borenium.

system for the hydrogenation of imines, enamines and 8-methylquinoline was developed via in-situ generation of a borenium catalyst.[58] More recently, the Crudden group developed a series of meso-ionic carbene (MIC)-functionalized borenium ions (**Figure 4C**) which were reported to catalyze the hydrogenation of imines and N-heterocycles under more mild conditions than that of Stephan's NHC-borenium catalysts.[59]

Generally phosphorus containing molecules are used as Lewis bases evidenced by the massive number of phosphine based ligands utilized in organometallic transition metal chemistry. That being said, phosphorus based Lewis acids have also become increasingly popular in recent years, and along with it, interest in exploiting them for catalysis. P(III) compounds are generally basic due to their energetically accessible lone pairs.[60] Discovery of the first phosphenium cations in 1964 changed the way chemists view the reactivity of these compounds.[61] Early examples of electrophilic phosphenium cations (**Figure 5A** and **5B**) were reported to perform insertions into C–H bonds, and

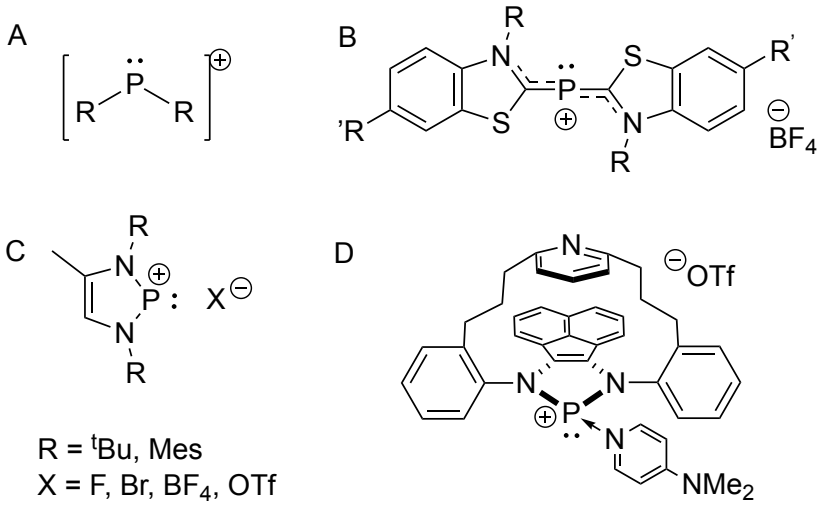

Figure 5. A) General form of a phosphenium cation. B) First phosphenium species C) First N-heterocyclic phosphenium species D) Intramolecular FLP-phosphenium stabilized by a Lewis base (DMAP).

reacted with substrates such as 1,3- and 1,4-dienes to give cyclopentene–phosphonium derivatives.[62] At the break of the 21st century, the development of N-heterocyclic phosphenium (NHPs) cations (**Figure 5C**) was reported by Nieger *et al.,* which were isovalent to N-heterocyclic carbenes. While NHCs are excellent Lewis bases, NHPs are Lewis acidic displaying the opposite reactivity as confirmed by computational and experimental methods.[63] A decade later, Ragogna *et al,* reported an intramolecular FLP comprised of an NHP and a pendant lutidine donor (**Figure 5D**), again highlighting the Lewis acidic nature of NHPs by forming an adduct with 4-N,N-dimethylaminopyridine (DMAP).[64] Computational work by Slattery and Hussein a few years later again highlight the Lewis acidic of phosphenium cations by developing a scale of fluoride ion affinities based on calculated fluorophilicities. They report that some of the phosphenium ions they tested were even more Lewis acidic than stable main group Lewis acids such as BF_3, BCl_3, $AlCl_3$ and SbF_5.[65] Activation of H_2 was reported for the P-based Lewis acid 2,4,6-tri^{t}butyl-1,3,5-triphosphabenzene. Experimental and computational results indicated a 1,4-addition of the H_2 at the phosphorus center under mild temperatures and pressure (4 atm, room temperature) after 24 hours.[66] Recently, Chitnis *et al* showed that readily accessible, air-stable P(III) and P(V) dications that were competent catalysts for hydrosilylation, C-C coupling, hydrodefluorination, and C=O bond reduction.[67–70] Importantly, they note the addition of a second positive charge greatly boosts the their Lewis acidity in these systems.

1.4 Goals of this Thesis

This thesis will investigate the use planar multidentate ligand scaffolds for making and studying redox active and Lewis acidic bismuth centres. Multidentate ligands offer stabilizing chelate effects which make them an attractive option when targeting catalysis. Planar multidentate ligands specifically are understudied in the p-block despite their wide use in transition metal chemistry. We envisioned their application to bismuth offered potential for exploiting unusual electronic proprieties as they enforce non-VSEPR geometries. This is well illustrated by comparing the molecular orbital (MO) diagrams of a planar vs. pyramidal BiH_3 molecule (**Figure 6**). Enforcing a planar geometry generates a LUMO corresponding to vacant p-orbital perpendicular to the molecular plane in contrast to the LUMO of a pyramidal species which is an anti-bonding molecular orbital.[71] A vacant p-orbital implies potential for Lewis acidy and is an interesting example of the electronic consequences of utilizing a planarity enforcing ligand. Redox active main group centres can also be accessed if the planar ligand is very electron rich and is able to donate π-electrons density into the vacant p-

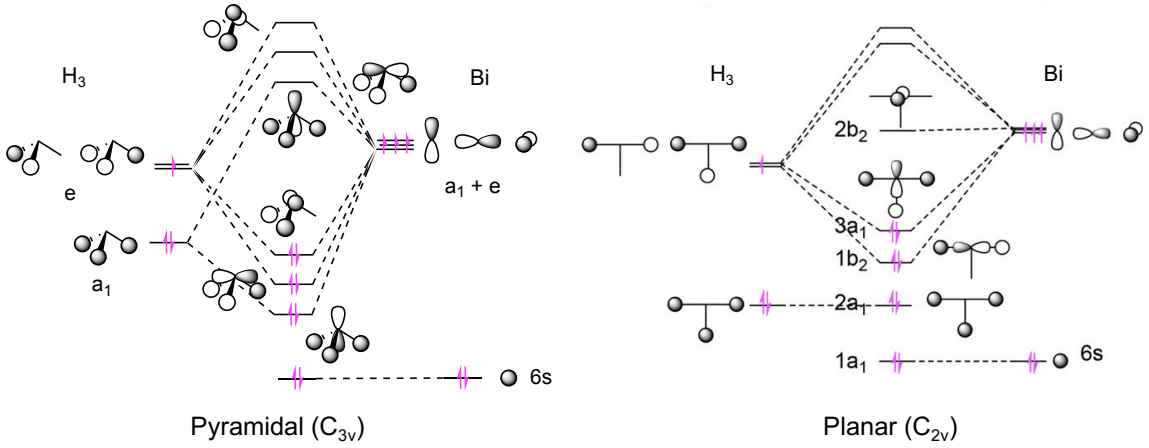

Figure 6. Molecular orbital (MO) diagram of BiH_3 in a T-shaped (right) and pyramidal (left) geometry.

orbital. Thus, the goal of this work will be to utilize geometrics, in addition to steric and electronic tuning, in order to study new redox active and Lewis acidic bismuth centres.

1.4.1 Exploring Redox Flexibility at Bismuth

Our strategy for inducing redox capabilities onto bismuth is to generate a species that lies on the cusp of two different oxidation states. The ONO-pincer ligated phosphine, first introduced by Arduengo and later applied by Radosevich, promotes oxidation state changes as it is has electronic and structural proprieties of both a P(I)/P(III). A ligand suitable for Bi(III), that is also very electron rich can donate electron density into the metal, partially reducing it (**Scheme 5**). Since the expected geometry for hypervalent Bi(I) is T-shaped (AX_3E_2, 2 lone pairs and 3 substituents), a planar tridentate ligand is well suited for this study. Combining these features we will use an electron-rich planar tridentate ligand to introduce redox flexibility at bismuth and the resulting complex may unlock redox catalysis. The synthesis of such a compound is described in chapter 2.

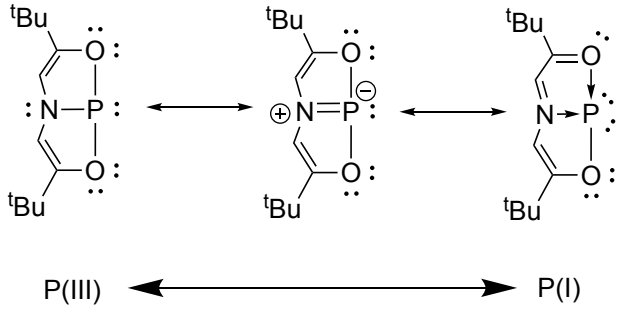

Scheme 5. Resonance contribution of a P(III) and P(I) centre enforced by a ONO-pincer ligand.

1.4.2 Exploring Lewis Acidity at Bismuth

Activation of challenging bonds can be achieved using highly Lewis acidic centres. High Lewis acidity can be exploited by introducing molecular charge.[72–

[74] In order to explore this, two bismuth dihalide complexes supported by planar tridentate ligand frameworks were studied and described in Chapter 3. One of these was converted to the dicationic bismuth centres where we observed interesting structural dynamism. We were interested in studying the reactivity and application of these dications as Lewis acid catalysts but were interrupted by the COVID-19 shutdown. Efforts to extend the our work from chapter 2 led to attempts to chemically reduce these compounds to the corresponding Bi(I) species but have so far been unsuccessful.

CHAPTER 2: STRUCTURE, BONDING AND REACTIVITY OF A PLANAR BISMUTH TRIAMIDE

2.1: Contributions

Dr. Saurabh Chitnis is thanked for the synthesis of $Bi(NMe_2)_3$, phosphorus and arsenic containing compounds, as well as for DFT calculations. Katherine Marczenko is thanked for synthetic work pertaining to the synthesis of $Sb(NMe_2)_3$, the antimony containing compounds, and for computational work. Joseph Zurakowski is thanked for characterization data pertaining to phosphorus, arsenic and antimony containing compounds.

2.2: Introduction

2.2.1 Non-VSEPR Pnictogen Compounds

Studying the relationship between electronic structure and molecular geometry has been a popular method for understanding unusual reactivity at main group centers. In particular, activation of challenging bonds and catalysis have been major goals of this field.[14,75–79] To achieve these goals, a number of groups have employed geometrically-constraining tridentate ligands on main group centers that enforce non-VSEPR geometries, which are stabilized by the chelating effect of the ligand. Strained NNN pincer ligands at phosphorus(III) cations have been shown by the Stephan group to do air-stable C–F bond reduction catalysis (**Figure 7A**).[67,68] Arduengo has employed a number of unsaturated trianionic ONO pincer ligands that were shown to enforce planar geometries at phosphorus, arsenic, and antimony centers (**Figure 7B**).[33,80,81] These 10-E-3 (10 valence electron, 3-coordinate) compounds described by

Arduengo show remarkable redox capabilities due to the presence of an unoccupied p-orbital on the central atom (**Figure 6**). Examples of 10-P-3 compounds have found applications in catalytic reductions (**Figure 7C**)[82,83] and activation of challenging substrates like ammonia.[84] Others, such as the Goicoechea, Aldridge (**Figure 7D**), and Dobrovetsky (**Figure 7E**) groups have utilized ONO pincer ligands to achieve challenging stoichiometric bond activation chemistry.[85–87] Radosevich has shown that geometrically constrained phosphorus(III) triamides can exhibit catalytic activity that proceeds via a P(III)/P(V) redox cycle (**Figure 7F**).[34] This work was quickly followed by an extensive mechanistic and kinetic study of cooperative B-H bond activation at these constrained phosphorus(III) centres.[88]

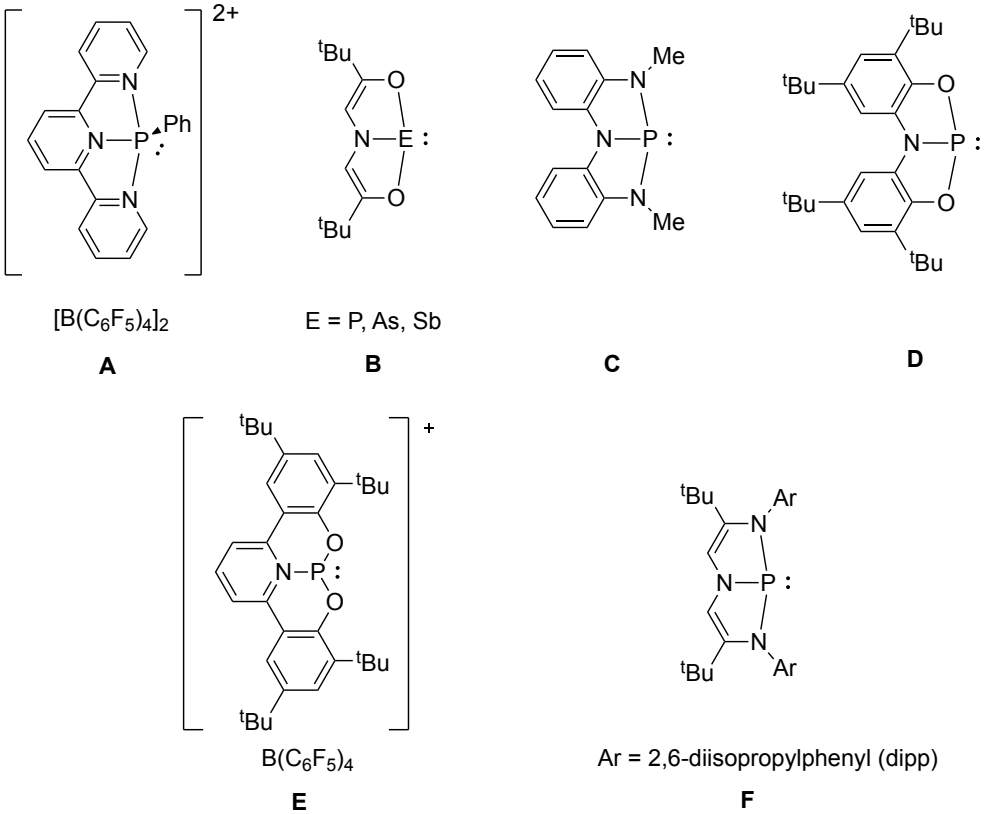

Figure 7. Select examples of pnictogen center supported by geometrically containing tridentate pincer ligands.

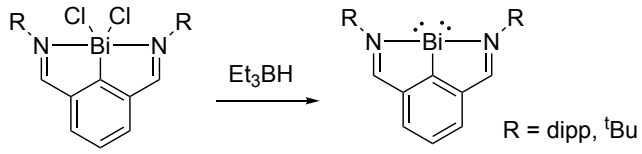

Scheme 6. Synthesis of monomeric organobismuth(I) stabilized by NCN tridentate pincer ligand.

The absence of bismuth in this field is surprising, as bismuth exhibits low toxicity,[89] a large coordination sphere,[90] multiple stable redox states,[91,92] and a high π-affinity[93]; all qualities that make it an attractive target for green catalysis. Attempts to isolate a 10-Bi-3 were unsuccessful due to the small steric profile of the ONO framework. Instead, a 20-valence electron, 9-coordinate (20-Bi-9) complex was isolated due to over coordination, with three ligands stabilizing a single bismuth center.[90] The first example of a planar tricoordinate bismuth(I) complex was reported in 2010 by the Dostál group (**Scheme 6**).[94] Reduction of NCN ligated bismuth(III) dichloride using a sacrificial reducing agent allowed for the isolation of the free bismuthinidene containing a Bi(I) centre. Recently, the Gilliard group has also isolated a free Bi(I) center by reducing a carbene-Bi(III) halide adduct using a Be(0) source (**Scheme 7**).[95] Cyclic(alkyl)(amino) carbenes are strong σ-donors, while also being π-acceptors, making them an attractive ligand for isolating a low oxidation state species. Thus, one can envision two different resonance contributions from both a Bi(I) and Bi(III) species (**Scheme 7**). In Dostál's case, the ligand enforces a planar geometry due to the rigidity of the ligand framework. While it is not a direct analogy to Arduengo's 10-E-3 compounds, one of Dostál's Bi(I) complexes has recently been shown by the Cornella group to participate in catalytic transfer hydrogenation via a Bi(I)/Bi(III)

redox cycle.[45] These examples demonstrate that orbital engineering by ligands enforcing unusual geometries is a powerful method of inducing novel reactivity with an emerging application in main group catalysis.

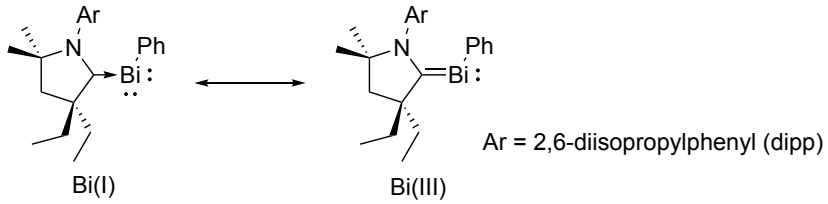

Scheme 7. Resonance contributors for a cyclic(alkyl)(amino) carbene bismuth complex.

2.2.2 Edge Inversion and Vertex Inversion

Trivalent pnictogens compounds are known to undergo inversion processes from their pyramidal geometries. The simplest example, NH_3, undergoes a vertex inversion process (**Scheme 8A**) leaving each substituent at the vertex of a triangle in the transition state. Examples of geometrically constrained trivalent pnictogen species that cannot deform in this manner are still observed to undergo inversion.[96] In these cases, edge inversion is a proposed alternative process to vertex inversion which allow more constrained compounds to adopt a t-shaped geometry at the transition state, rather than a trigonal planar geometry, and allowing the molecule to undergo inversion (**Scheme 8B**).

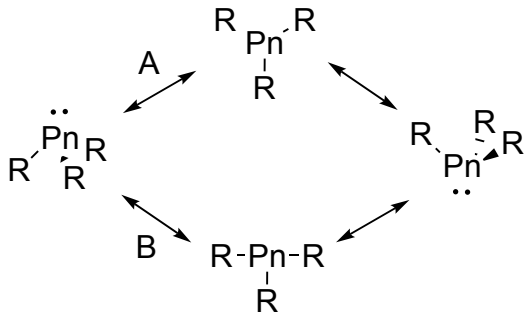

Scheme 8. Schematic of two possible inversion processes for a trivalent pnictogen compound.

The most diagnostic feature of 10-E-3 compounds, introduced by Arduengo, is their planarity. We were interested in isolating a 10-Bi-3 compound not only due to their potential applications in catalysis but also due to the T-shaped group state geometry which models the transition state proposed for edge inversion in trivalent pnictogens centers (**Scheme 8B**).[97–99] The ligand design strategy for a 10-Bi-3 compound will likely need to differ from that of its lighter analogues, due to the large size of the central atom. Therefore, it was proposed that introduction of a redox active ligand with more steric protection should prevent over-coordination. Moving away from an ONO framework to a (R)NNN(R) may allow for the isolation of an elusive 10-Bi-3 complex. These tunable tethered tri-amido ligands are not only attractive from a steric perspective, but also from an electronic perspective as well. Electing for a triamine framework should offer additional electron-richness compared to their ONO counterparts generating a metal centre that approximates the +1 oxidation state. Radosevich and coworkers have recently used a tri-amine ligand framework on P(III) centers and observed a distorted-pyramidal ground state, corresponding to a 8-P-3 geometry rather than the targeted 10-P-3 species.[82] This compound nevertheless undergoes an unusually facile inversion at phosphorus, assuming a transient 10-P-3 state along the inversion coordinate. Despite its proposed importance in unlocking new reactivity, they were unable to experimentally realize the 10-E-3 intermediate for any pnictogen triamide.[82,88] We were undeterred in the pursuit of a 10-Bi-3 compound, despite reported

instability for the phosphorus congener, as the increased bond polarity of Bi-N bonds compared to P-N bonds often promotes widely different reactivities. [100]

This chapter reports the reaction of a tri-amine ligand with a Bi(III) precursor to yield a T-shaped bismuth complex for which experimental data and DFT calculations indicate a 10-Bi-3 electronic structure.[101] These results are supplemented by follow up work done in association with several other group members which extends the use of this triamide ligand to the remaining pnictogen elements (P, As, Sb). This periodic survey allows for a comprehensive description of pnictogen triamides within the context of a single geometry-restraining substituent.

2.3: Results and Discussion

2.3.1 Syntheses

Combining a triamine ligand framework **N_3H_3** with a bismuth (III) precursor, $Bi(NMe_2)_3$, allows for the isolation of compound **1** as a dimethylamine adduct after recrystallization (**Scheme 9**). This species is relatively unstable due the volatile $HNMe_2$ ligands at room temperature. However, removal of the volatiles under high vacuum (10^{-3} mbar, 1h) allows for the isolation of free complex **2** in a good yield (**Scheme 9**, **2**). It can also be synthesized by lithiation

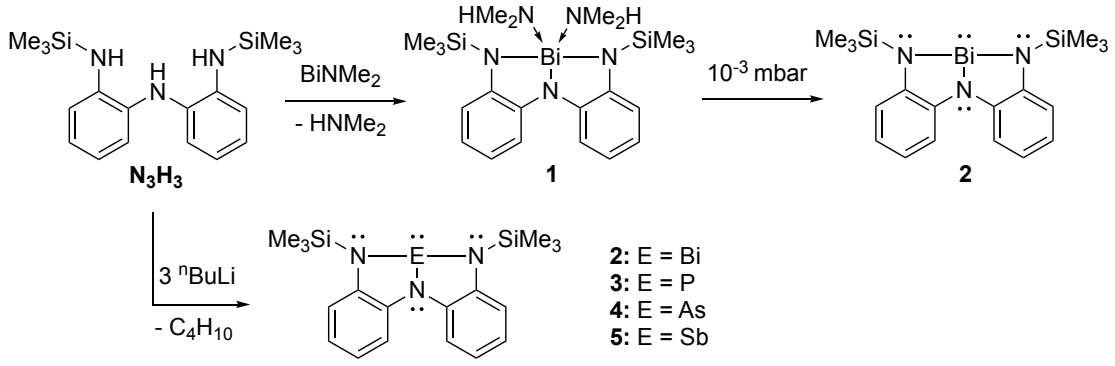

Scheme 9. Synthesis of compounds **1**-**5** from **N_3H_3**.

of **N_3H_3** and subsequently quenching with $BiCl_3$ which after work up, yields complex **2** in a lower yield (< 25%). The analogous phosphorus (**3**), and arsenic (**4**) complexes (**Scheme 9**) can be synthesized in a similar fashion via lithiation of **N_3H_3** followed by treatment of the corresponding with ECl_3 precursor with 70% and 55% yield respectively. Attempts to make complexes **3** and **4** from **N_3H_3** and $P(NMe_2)_3$ or $As(NMe_2)_3$ were unsuccessful. The antimony variant (**Scheme 9**, **5**) was isolated via amine elimination from $Sb(NMe_2)_3$, analogous to the preparation of bismuth complex **2**, and can be isolated as a dimer in the solid state in 72% yield. The aminolysis reaction for complex **5** can be done in a J Young tube at low temperature which allows for the monomeric dimethylamine adduct to be observed spectroscopically. Similar to **1**, the crystals of **5** were metastable at room temperature which limited full characterization of the compound. Compounds **2-5** are stable in the solid state and in dry, deoxygenated hydrocarbon solvent under inert atmosphere, but showed limited stability in halogenated solvents. Compound **2** has been comprehensively characterized by NMR, IR, and UV-VIS spectroscopy as well as X-ray crystallography, mass spectrometry, and elemental analysis. Only the UV-Vis characterization of compounds **3-5** will be discussed in detail, as their synthesis and other characterization was completed by Marczenko and co-authors.[102] The data from these physical methods converge upon a 10-Bi-3 electronic structure for **2** (**Scheme 10**) featuring the targeted Bi(I) metal center in a T-shaped geometry that provides the first isolable model for the transition state of edge inversion in pnictogen triamides.

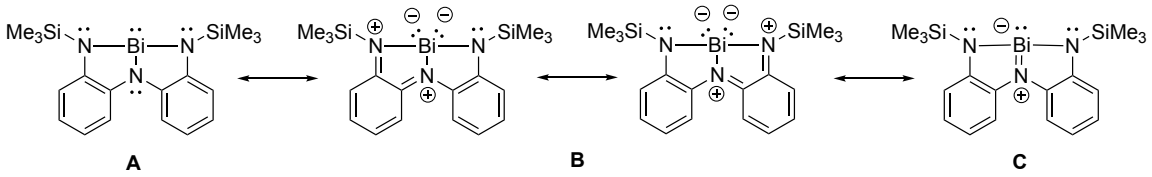

Scheme 10. Resonance forms of compound **2**.

2.3.2 Solid state

There are three major resonance forms that could be imagined for complex **2** (**Scheme 10**). The first being a triply anionic amido ligand (X_3 ligand, **Scheme 10A**) which should result in a trigonal pyramidal bismuth(III) center with a single lone pair. The second comes from the potential imine character of the ligand which would result in a monoanionic (L_2X) ligand and a bismuth(I) center with two lone pairs (**Scheme 10B**). The third can be envisioned by placing a double bond between the central nitrogen ligand and bismuth center which would correspond to a more planar bismuth(III) center with a single lone pair (**Scheme 10C**).

Visual inspection incited our interest due the deep blue color observed for complex **2** which was also reported by Dostál at the time they isolated their first formally bismuth(I) complex. Single crystal X-ray diffraction indicated a T-shaped N_3Bi core (**Figure 8**). Slight deviation from an idealized 180º dihedral due to the two aryl rings being canted by 32.2(1)º degrees is most likely to avoid C_{Ar}-H···H-C_{Ar} steric clash. At the time of publication, this degree of planarity in a pnictogen triamide was unprecedent. A related compound but untethered Bi(III) tris-arylamide $Bi[N(SiMe_3)(4\text{-}MePh)]_3$ has been structurally characterized recently and shows a non-planar, pyramidal geometry and average Bi-N distances of

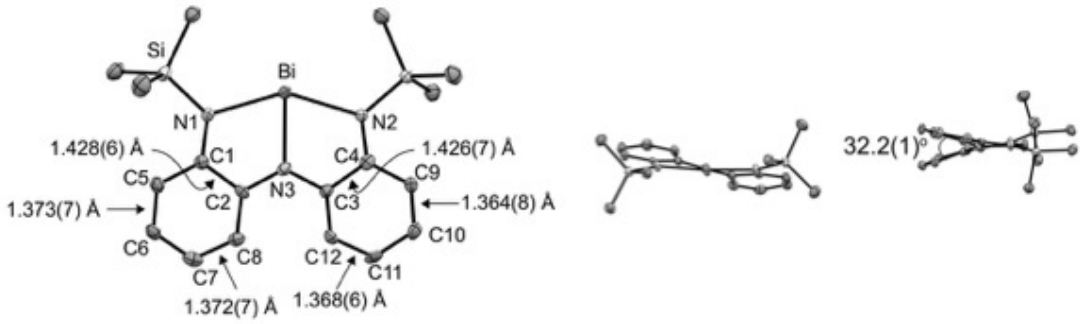

Figure 8. Views of the solid-state structure of **2**. Hydrogen atoms have been omitted. Thermal ellipsoids are drawn at the 50% probability level.

2.157 Å indicative of a typical bismuth (III) amide species.[103] From the perspective of a simple VESPR description, the T-shaped N_3Bi core observed for complex **2** [N1-Bi-N2 = 146.6(1)°, **Figure 8**] in the solid state is consistent with the presence of five stereochemically active electron pairs at the bismuth center (three bonding pairs, two nonbonding pairs), which supports an interpretation of complex **2** as a bismuth (I) center.

Structurally, the crystallographic data seems to suggest resonance form **B** (**Scheme 10**) is most appropriate (three bonds, two lone pairs). For comparison, we determined the solid-state structure of the free ligand and found that the average C-N distances are longer [1.4079(5) Å], more consistent with single bonding. It is worth noting that the C-N bond distances in the unconstrained $Bi[N(SiMe_3)(4\text{-}MePh)]_3$ are also significantly longer than in **2** ranging from 1.422(5)-1.440(5) Å.[103] In the aryl backbone, it was also observed that C5-C6, C7-C8, C9-C10, and C11-C12 bonds are markedly shorter than the C1-C2 and C3-C4 bonds (**Figure 8**) as expected from more localized double bonding character for C5-C12 and more localized single bonding character for C1-C4 due to resonance form **B** (**Scheme 10**). Thus, the structural data in the solid state

suggest assignment of complex **2** as being a bismuth (I) center stabilized by a monoanionic diimineamido- ligand (**Scheme 10B**).

2.3.3 Gas Phase

To better understand the electronics associated with our systems, an extensive gas-phase study of complex **2** was performed using dispersion-corrected DFT calculations at the PBE1-D3 level. Calculation results were kindly provided by other authors of this work, but the findings will be summarized here. The Weiberg bond index (WBI) for the four C-N bonds was calculated to be 1.2 which further supports the implied partial double bond character proposed for resonance form **B** (**Scheme 10**). Natural bond orbital (NBO) analysis revels an s-type lone pair and a p-type lone-pair at the bismuth center (**Figure 9**), which is consistent with the remaining p-orbitals being involved in one 2c-2e bond (N3-Bi, Figure 9) and one 2c-3e bond (N2-Bi-N1, **Figure 9**). Interestingly, the 6p lone pair is only partially occupied (occupancy = 1.00 e) implying that electrons are delocalized between the metal center and the ligand. The shapes and ordering of the NBO's agree well with conclusion made by Dostál, where they report a 6p occupancy of 1.5 electrons.[94] The higher occupancy is likely a result of less lone pair delocalization over their monoarene ligand versus the diarene ligand in **2**.

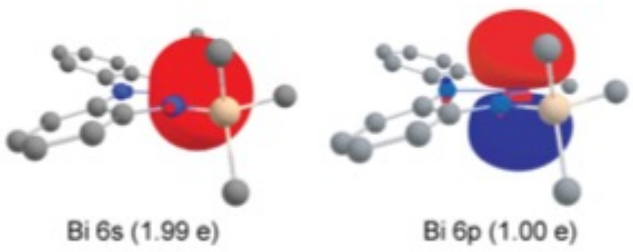

Figure 9. Natural Bond Orbitals localized on bismuth in **2** showing the 6s lone pair (left, occupancy = 1.99 e) and the 6p lone pair (right, occupancy = 1.00 e).

The Radosevich group recently reported a phosphorus analogue to **2** where instead of bulky $NSiMe_3$ substituents, they used N-methyl groups. They report a trigonal pyramidal geometry at the phosphorus center which is unlike the planar geometry at bismuth observed in **2**. To confirm conformational preferences between **2** and Radosevich's previously authenticated N-methyl derivative, a relaxed potential energy scan that mutates the N-E-N-N (E = P or Bi) dihedral angle in each molecule was performed (**Figure 10**). It was found that for Bi, the observed planar geometry is a global minimum whereas for P, the minimum corresponds to a trigonal pyramidal geometry as expected. This reversal in stability trends supports our hypothesis that larger E-N bond polarity (Bi-N vs. P-N) stabilizes transitions states involving 3c-4e bonds, and allows us to tentatively justify the stability of this unusual ground state geometry in terms of metal-ligand bond polarity. Thus, high polarity Bi-N bonds, which are monoanionic, stabilize the planar ground state geometry whereas the relatively low P-N bond polarity results in covalent bonding enforcing directionally rigid 2c-2e- bonds through 3 p-orbitals and favors the pyramidal geometry.

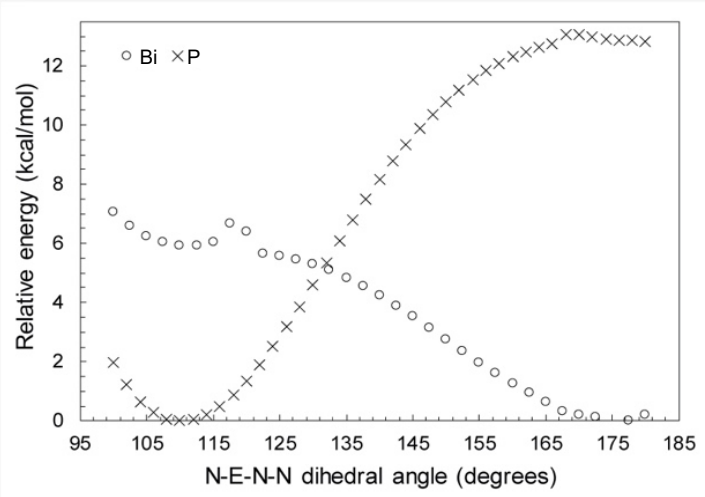

Figure 10. Relative energies of planar (N-E-N-N ≈ 180°) and distorted-pyramidal (N-E-N-N ≈ 110°) conformations in Bi (**2**) and P calculated at the PBE1PBE-D3 level.

2.3.4 Liquid state

The structure established for **2** through crystallography is apparently retained in the solution phase over at least a 100 °C temperature range as shown by a combination of variable temperature ^{1}H NMR and solid-state ^{13}C NMR spectroscopy.

As mentioned previously, compound **2** is deeply blue in both the solid state and in solution. We decided to investigate the electronic structure of **2** using UV-vis spectroscopy. Two absorption bands were found, the first appearing at 618 nm (ε = 2.3 x 104 $M^{-1}{\cdot}cm^{-1}$) with the second appearing at 525 nm (ε = 1.3 x 104 $M^{-1}{\cdot}cm^{-1}$) (**Figure 11**, left). Interestingly, Dostál also reported deep blue colors for their Bi(I) compounds, but no absorption band assignments were done by the authors.[94] In contrast, examples of pyramidal Bi(III) amides and planar boron(III) analogues of **2** are typically colorless or pale yellow.[103,104] It thus stands to reason that the electronic transitions that cause the dark color of bismithinindenes are closely related to the unusual geometry observed.

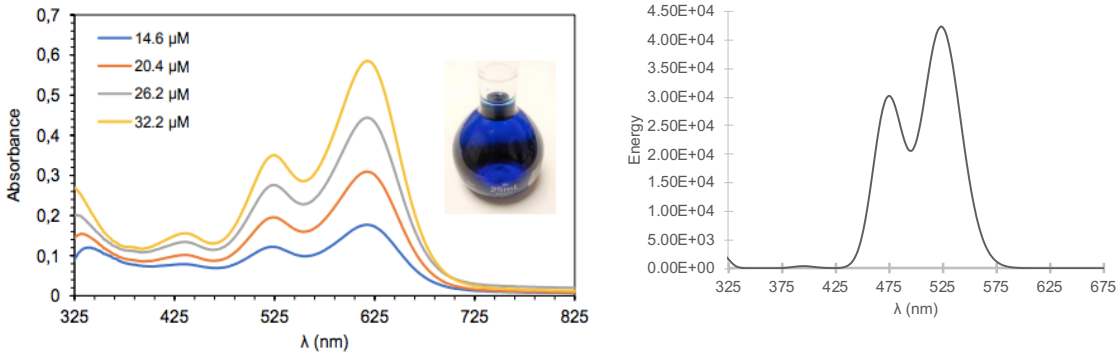

Figure 11. Left: UV-Vis spectrum of **2**. Right: DFT calculated UV-Vis spectrum of **2**.

To better understand the relationship between the electronic structure of the molecular geometry we investigated the molecular orbitals involved The HOMO of **2** is ligand-centered, whereas the HOMO-1 is a p-type lone-pair primarily at bismuth with a smaller lobe at the N3 fragment. The LUMO is a metal-centered molecular orbital (**Figure 12**). The metal-centered LUMO is consistent with the NBO picture of a partially populated p-orbital discussed previously. Despite its π-symmetry, the Bi-N3 interaction does not imply a double bond as its length [2.182(4) Å] is greater than the longest Bi-N length found in tris-amide $Bi[N(SiMe3)(4\text{-}MePh)]_3$ [2.159(3) Å].[103] We can rule out resonance form **C** for **2** (**Scheme 10)** based on the large bond distance. TD-DFT calculations show that the electronic transition at 618nm is a HOMO → LUMO transition that corresponds to a metal to ligand charge transfer. The transition at 522nm is a HOMO-1 → LUMO transition which involves primarily metal centered molecular orbitals. While there are few literature reports to compare these assignments quantitatively, the HOMO → LUMO transition observed supports

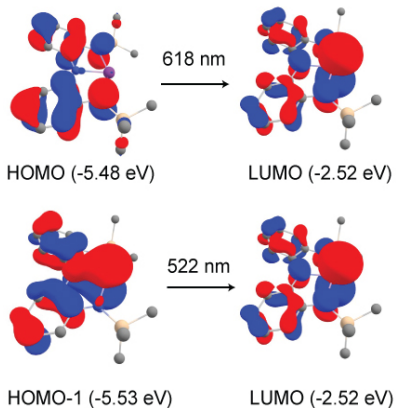

Figure 12. Calculated Kohn-Sham orbitals corresponding to observed transitions.

our assignment of **2** as a Bi(I) center as it implies the ability for the ligand to donate electrons to the metal, reducing the metal, and allowing the assignment of a second partial lone pair on the bismuth center (**Scheme 10C**).

As mention previously, parallel attempts to synthesize the phosphorus, arsenic, and antimony analogues of compound **2** were performed by Marczenko and co-workers. Being interested in the electronics of these systems we performed extensive UV-Vis studies on all four compounds (**2-5**) the results of which will be summarize here. All other characterization and analysis methods can be found in the manuscript.[102] For phosphorus (**3**) and arsenic (**4**) complexes, there were no bands found in the visible region, consistent with the TD-DFT calculation of **3** and **4** in a bent ground state geometry. TD-DFT calculations performed on compounds in a planar geometry predict strong bands to be present in the visible region all compounds described, thus suggesting a pyramidal group state for **3** and **4** as expected. For the antimony (**5**) variant, two

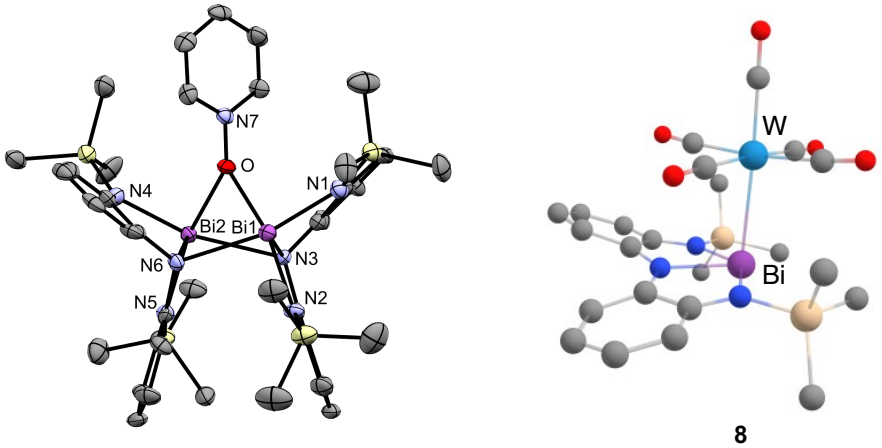

Figure 13. View of the solid-state molecular structure of **7** (left) and calculated structure of **8** (right). Hydrogen atoms have been omitted and thermal ellipsoids are drawn at the 50% probability level.

adsorption bands were observed with absorption value shifted to lower wavelengths relative to compound **2**. Values for **5** agree well with the TD-DFT model calculated for a planar monomeric N_3Sb core. To summarize, the absorption data and related TD-DTF calculations for compounds **3** and **4** suggest they exist primarily in their bent monomeric configuration in aliphatic solvents (pentane or toluene), whereas **2** and **5** exist as planar monomers. It was also found that compound **5** displayed remarkably complex temperature dependent behavior. Marczenko and co-workers were able to study this relationships using variable temperature UV-Vis experiments. The authors concluded that antimony lies on an inflection point that differentiates the behavior of the heaviest group 15 element (bismuth) and its lighter counterparts.

2.3.5 Reactivity

Collectively, this evidence suggest that in the solid, liquid and gas phases, compound **2** is a Bi(I) center, and that as one moves down group 15 there is preference for tethered pnictogen triamides to adopt a planar ground state geometry, rather than a pyramidal geometry commonly associated with these compounds.

Interpreting compound **2** as a Bi(I) with a partially occupied p-orbital perpendicular to the molecular plane implies **2** should exhibit ambiphilic behavior. That is, it should be capable of interact with both empty (or partially empty) orbital as a Lewis base while also coordinating to lone pairs (or partial lone pairs) as the Lewis acid. However, an investigation of its reactivity revealed behavior more typical of electrophilic Bi(III) compounds. Reaction of **2** with pentafluorophenol

showed complete loss of the blue color and conversion to the **N_3H_3** ligand and known compound $Bi(OC_6F_5)_3$ at all stoichiometries (**Scheme 11**, complex **6**), indicating a metathesis reaction that is well-known for bismuth(III) tris-amides.[72,105]

Addition of bulky Lewis bases such as dimethylaminopyridine (DMAP), triethylamine, and a range of triarylphosphines showed no reaction. However, a less sterically obstructed base such as pyridine N-oxide yielded compound (**7**) as a dimer (**Scheme 11**). The structure of **7** (**Figure 13**, left) shows a square-based pyramid geometry at each Bi atom, which arises from interaction of three nitrogen atoms (N1, N2, N3) and one oxygen atom with the metal (Bi1), and a fifth interaction involving a nitrogen atom (N6) from a second equivalent of **2** (**Figure 13**, left). The ligand in 7 adopts a distorted-pyramidal geometry with the long average C-N bond lengths [1.420 Å, cf. 1.374 Å in **2**], consistent with localized C-N single bonds, and the ligand is presumably more electron-rich than in **2** since the central nitrogen atoms (N3 or N6) can further coordinate a second

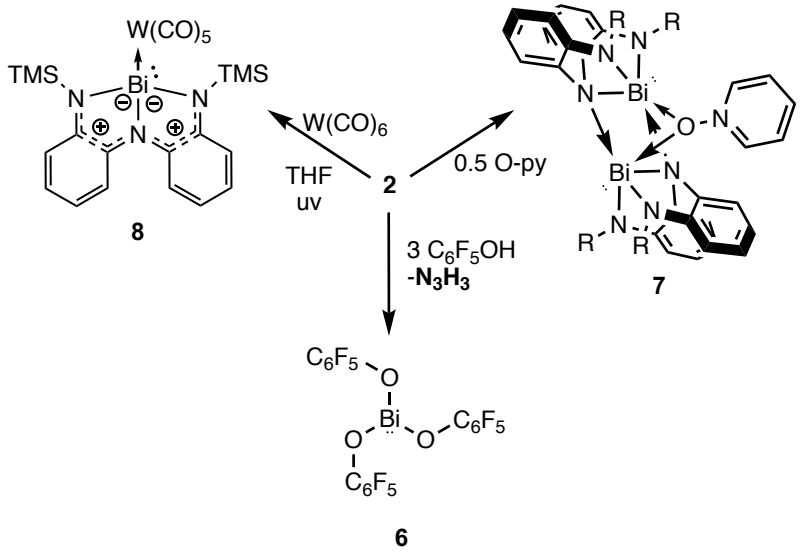

Scheme 11. Reactions of **2** with pentafluorophenol, *in-situ* generated $W(CO)_5(THF)$, and pyridine N-oxide (O-py).

metal (**Scheme 11**, **7**). In contrast, this type of intermolecular coordination was not observed in **2**. From these features, reactions with Lewis bases seems to support description as a tris-amide attached to a Bi(III) center.

We then turned our attention towards the reaction of **2** and Lewis acids. A 1:1 reaction of **2** and $W(CO)_5(THF)$ (generated in-situ via irradiation), resulted in the formation of a single product assigned as a 1:1 adduct, **8** (**Scheme 11**), based on the quantitative conversion in the NMR spectrum, IR spectroscopy (υCO = 1938, 1976, 2029, 2054 cm^{-1}), mass spectrometry ([M – CO + H_2O] ion observed), and elemental analysis. Despite multiple attempts, crystals of the 1:1 adduct (**8**) suitable for diffraction were not obtained. However, DFT calculations (PBE1PBE-D3) confirmed that the $W(CO)_5$ fragment is located perpendicular to the molecular plane (**Figure 13**, complex **8**), precisely where the 6p lone pair is envisioned. Thus, reactions with Lewis acids seem to confirm the Bi(I) electronic structure implied by resonance forms **B** (**Scheme 10**). However, we were able to isolate the 2:1 LA-LB adduct of **2** and 2 NMe_2H ligands, thus the 1.00 electron

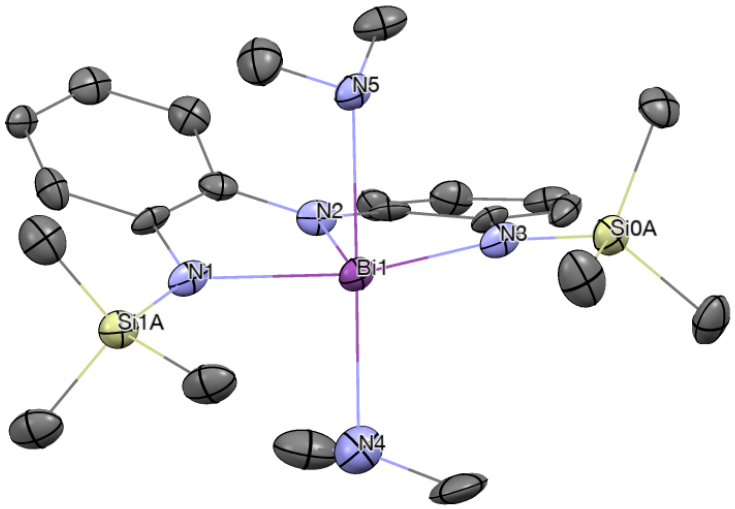

Figure 14. X-ray crystal structure of **1**. Data quality limits discussion to connectivity only.

occupancy of the perpendicular p-orbital in **2** allows for the Bi center to either accept two Lewis bases (**Figure 14**), one on the top and bottom of the molecular plane, or to act as a donor in **8** (**Figure 13**).

2.4: Conclusions and Future Work

A tethered tridentate ligand was employed to constrain the geometry of a bismuth center, realizing the first example of a planar geometry in pnictogen triamides. This work demonstrates a structural motif that is unstable for lighter congeners in group 15 as evidenced in follow up work by Marczenko and coworkers. Uniquely, **2** exhibits significant Bi(I) character but was prepared without external reductants from a Bi(III) starting material, via intramolecular electron-transfer from ligand to metal. This extends for the first time the so-called electromorphic synthesis to the 6th row elements.[33] Compound **2** provides the first structural model of the transition state proposed for edge-inversion in bismuthines and more generally in any pnictogen triamide. It is worth noting that Dostál's compounds cannot undergo inversion due to the planarity imposed by the aryl ring. Although the structural features of **2**, DFT analysis, and formation of **8** (**Scheme 11**) suggest a Bi(I) oxidation state (**Scheme 10B**), contributions from other resonance forms are sufficiently large that **2** also behaves as a classical Bi(III) source. For example, it undergoes triple metathesis reactions with RO^- sources and engages a neutral ligand (pyridine N-oxide) to give **7**. This indicates the importance of ligand choice/design to control parameters such as oxidation state and geometry at Bi; a strategy widely used in transition metal chemistry.

This ambiphilic reactivity and “redox-confused” Bi(I/III) behavior bodes well for exploring an ill-defined redox couple in the p-block.

Future and follow up work by Marczenko and coworkers, studied the effects of the central element with regard to a single triamine ligand framework. The trends observed are summarized here; 1) the tendency to adopt a planar geometry increases descending the group, 2) DFT calculations reveal that the two main factors contributing to these trends are the electronegative difference across the E–N bond (electrostatic and orbital components of bonding) and the number of electrons (Pauli repulsion) and 3) the 5th row element antimony is identified as an inflection point between the behavior of the lighter pnictogens and bismuth. Compound **2** stands out due to its planar ground state and exhibits no dimerization due to large Pauli repulsion between the subunits as well as poor orbital overlap due to the long Bi–N bonds. The Lewis acidity was experimentally found to increase in the order P ≈ Ar < Sb < Bi, which is predicted by considerations of their ground state geometries and LUMO levels (the HOMO levels are unaltered by geometric deformation). Based on these trends, studies uncovering substituent effects in this chemistry are underway in the group, with a view towards exploring the potential for applications in redox catalysis involving electrochemically flexible bismuth centres.

2.5: Experimental

2.5.1 General Considerations

Synthetic Procedures

All manipulations were performed using standard Schlenk and glovebox techniques under an atmosphere of dry nitrogen. Solvents were dried over Na/benzophenone (tetrahydrofuran, pentanes, hexanes, diethyl ether, toluene, benzene-d6) or over calcium hydride (dichloromethane, acetonitrile, 1,2-difluorobenzene, dichloromethane-d_2, acetonitrile-d_3, chloroform-d) and distilled prior to use. Reaction glassware was baked in a 130 ^{o}C oven for at least 1 h prior to use and assembled under nitrogen while hot. Melting points were obtained for samples sealed in glass capillaries and are uncorrected.

Solution Nuclear Magnetic Resonance

NMR spectra are referenced to tetramethylsilane (^{1}H, ^{13}C), 85% H_3PO_4 (^{31}P), $CFCl_3$ (^{19}F), or $B(OMe)_3$ (^{11}B) on a Bruker AV-300 spectrometer or a Bruker AV-500 spectrometer with residual solvent used for chemical shift calibration. Samples for NMR spectroscopy were prepared and sealed inside the glovebox with Parafilm before removal into ambient atmosphere. Heteronuclear NMR experiments were run using a sealed capillary containing benzene-d_6 placed within the NMR tube for solvent locking.

Solid State Nuclear Magnetic Resonance

The ^{1}H and ^{13}C cross-polarization (CP) / Magic Angle Spinning (MAS) NMR experiments were carried out on a Bruker Avance DSX NMR spectrometer with a 9.4 T magnet (400.24 MHz ^{1}H, 100.64 MHz ^{13}C, Larmor frequencies) using a probe head for rotors of 4 mm diameter. The sample was packed into the rotor inside the glovebox and removed from the Parafilm sealed vial shortly before conducting the experiments.

Vibrational Spectroscopy

Infrared spectra were obtained on an Agilent Technologies Cary 630 FTIR instrument equipped with a ZnSe ATR module. Raman spectra were obtained on a Thermo Scientific Nicolet NXR 9650 FT-Raman Spectrometer instrument equipped with a 1064 nm Nd:YVO_4 laser and InGaAs detector.

UV-Vis Spectroscopy

UV-VIS spectra were obtained on an Agilent CARY 100 spectrometer. Samples were prepared inside the glovebox in quartz cuvettes sealed with a Teflon plug prior to removal into the ambient atmosphere. Background correction was performed using a cuvette containing the analysis solvent. Variable temperature UV-Vis spectra were obtained on a portable Vernier SpectroVis spectrometer inside the glovebox. A cuvette containing the dissolved sample in pentane was cooled to ca. -100 ^{o}C using a cold port filled with copper beads. A thermocouple tip was placed in the cooled solution to provide real-time in-situ temperature measurements. The cuvette was removed from the beads and placed in the spectrometer cavity. Spectra were obtained as the sample warmed to ambient temperature.

Crystallographic Data

Single crystals diffraction experiments were performed on a Bruker D8-Quest Photon II diffractometer. Reflections were integrated using the APEX III software and solved and refined using Olex2 software. Details for individual compounds are given in **Appendix C**.

Mass Spectrometry

Electro-Spray Ionization (ESI) and Atmospheric Pressure Chemical Ionization (APCI) spectra were obtained on a Bruker micrOTOF.

Commercial Reagents

2-nitroaniline, 1-fluoro-2-nitrobenzene, pentafluorophenol were purchased from Oakwood Chemicals and used as received. Bismuth(III) chloride was purchased from Oakwood Chemicals and purified by vacuum sublimation (10^{-2} mbar, 200 ^{o}C) before use. Chlorotrimethylsilane, triethylamine were purchased from Millipore Sigma, and used after distillation under nitrogen . Pyridine N-oxide and Tungsten Hexacarbonyl were purchased from Millipore Sigma, and purified by vacuum sublimation (10^{-2} mbar, 25 ^{o}C). Phosphorus(III) chloride, ^{n}BuLi (1.6M/hexanes), lithium dimethylamide were purchased from Millipore Sigma, and used as received.

2.5.2 Synthesis of N_3H_3 and $Bi(NMe_2)_3$

The starting triamine ligand was synthesized via a series of literature procedures (**Scheme 12**).[88,106,107] **SM1** was made via an equimolar reaction between 2-nitroaniline and 1-fluoro-2-nitrobenzene in the presence of excess potassium carbonate (K_2CO_3). The product can be isolated as an orange solid after washing with cold methanol. Reduction of **SM1** with a large excess of zinc powder and ammonium chloride (NH_4Cl) generates the primary triamine ligand (**SM2**). Crude **SM2** was suitable for continuation and thus it was treated with two equivalents of trimethylchlorosilane (Me_3SiCl) and excess triethylamine (NEt_3) to produce **N_3H_3**. The crude material was purified by extraction into

dichloromethane followed by removal the triethylammonium chloride by filtration. After vigorous drying **N_3H_3** was isolated as a fine beige powder.

SM3 was prepared according to known literature procedures and was purified by sublimation.[108] **SM3** is highly sensitive to temperature, light, and moisture. It was prepared in the dark under rigorously anhydrous conditions, sublimed using the apparatus described in the cited reference, and immediately transferred it to a -30 °C freezer where it is stable for several months in the dark.

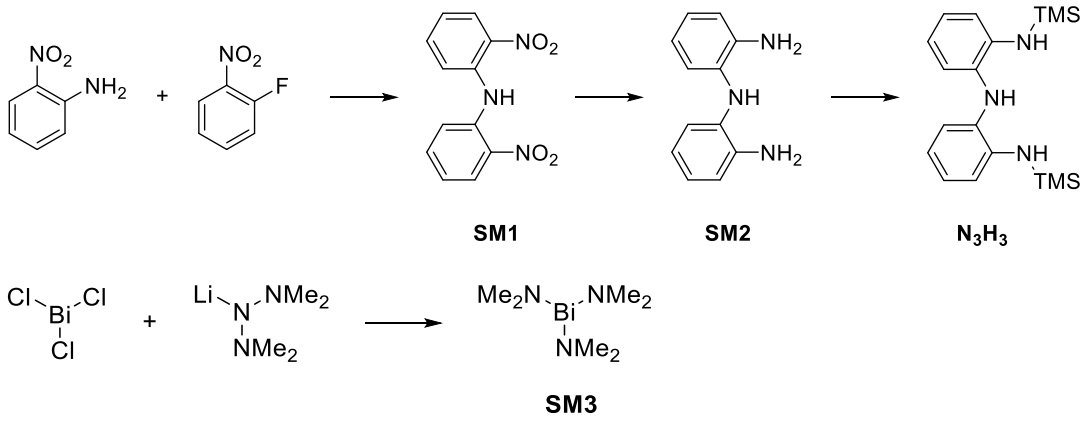

Scheme 12. Preparation of **N_3H_3** from known literature procedures.

2.5.3 Synthesis and Characterization

In-situ generated 1

Compound **1** was prepared by reacting equimolar quantities of **N_3H_3** and $Bi(NMe_2)_3$ in hexane. **1** was not isolated in macroscopic quantity due to the very labile dimethylamine ligands under a stream of nitrogen or under vacuum. Single crystals were however obtained upon cooling the reaction of solution of **N_3H_3** and $Bi(NMe_2)_3$ (**SM3**) to -30 °C. The crystals are brown in colour but their surface turns blue upon evaporation of dimethylamine from the crystals when removed from solution. The crystals were quickly transferred into pre-cooled paratone oil

and kept at -30 °C until ready for X-ray analysis. Spectroscopic data is presented for a toluene-d_8 solution of **N_3H_3** and $Bi(NMe_2)_3$ prepared by condensing the solvent onto the solid reagents in a sealed J Young tube.

^{1}H NMR (300 MHz, toluene-d_8): δ 8.02 (d, J = 7.5 Hz, 2H, C_{Ar}-H), 7.07 (d, J = 8.1 Hz, 2H, C_{Ar}-H), 6.76 (t, J = 7.8 Hz, 2H, C_{Ar}-H), 6.65 (d, J = 7.6Hz, 2H, C_{Ar}-H), 1.93 (d, J = 5.3 Hz, 1H, $N(CH_3)_2$), 0.39 (s, 18 H, $Si(CH_3)_3$)

^{13}C NMR (75 MHz, toluene-d_8): δ 149.9 (C_{Ar}), 148.6 (C_{Ar}), 137.5 (C_{Ar}), 121.3 (C_{Ar}), 120.2 (C_{Ar}), 119.2 (C_{Ar}), 115.9 (C_{Ar}), 38.2 ($N(CH_3)_2$), 2.49 ($Si(CH_3)_3$)

^{29}Si NMR (60 MHz, toluene-d_8): δ 0.2 ($Si(CH_3)_3$)

Complex 2: Preparation from $Bi(NMe_2)_3$

$Bi(NMe_2)_3$ (0.8530 g, 2.5 mmol) was dissolved in hexanes (7 mL) and cooled to -30 °C. Separately, **N_3H_3** (0.8869 g, 2.5 mmol) was dissolved in hexanes (7 mL) and cooled to -30 °C. The solution of $Bi(NMe_2)_3$ was added dropwise to the stirred solution of **N_3H_3** dropwise resulting in the formation of a dark brown solution. The reaction was warmed to room temperature and stirred overnight in the dark yielding a dark brown mixture. This mixture was filtered, concentrated to half its volume, and placed in the freezer at -25 °C for 7 days. Crystals of **2** were isolated by decanting the supernatant and before applying then dynamic vacuum (10^{-3} mbar) at room temperature to obtain **2** as a darkly colored powder (0.8010 g, 58 %).

Melting point: 121-126 °C, decomposes to brown oil

^{1}H NMR (500 MHz, benzene-d^{6}): δ 8.30 (d, J = 8.1 Hz, 2H, C_{Ar}-H), 7.39 (d, J = 7.9 Hz, 2H, C_{Ar}-H), 6.75 (t, J = 7.5 Hz, 2H, C_{Ar}-H), 6.68 (t, J = 7.24 Hz, 2H, C_{Ar}-H), 0.42 (s, 18 H, $Si(CH_3)_3$)

^{13}C NMR (126 MHz, benzene-d6): δ 152.44 (C_{Ar}), 123.33 (C_{Ar}), 123.19 (C_{Ar}), 123.10 (C_{Ar}), 117.48 (C_{Ar}), 1.99 ($Si(CH_3)_3$)

^{29}Si NMR (60 MHz, toluene-d8): δ 0.6 ($Si(CH_3)_3$)

FT-IR (ATR, ZnSe crystal): 527 (w), 563 (m), 599 (m), 630 (m), 688 (s), 725 (s), 736 (vs), 827 (vs), 881 (s), 928 (vs), 969, (vw), 1038 (w), 1051 (w), 1123 (m), 1130 (m), 1155 (s), 1196 (w), 1244 (vs), 1283 (s), 1315 (m), 1332 (s), 1407 (w), 1447 (s), 1462 (s), 1475 (m), 1535 (w), 1584 (m), 2895 (w), 2941 (m), 2945 (m), 3046 (w), 3081 (w)

UV-VIS (n-pentane): λ_{max} = 618 nm

ESI-HRMS (positive ion mode): calculated for $[M+1]^+$ = 550.1542 m/z, observed = 550.1528 m/z.

Elemental Analysis (calcd./expt.): C (39.34/39.51) H (4.77/4.69) N (7.56/8.14)

Complex 2: Preparation from N_3H_3, ^{n}BuLi and $BiCl_3$

A solution of ^{n}BuLi (1.9 mL, 1.6 M in hexane) was added dropwise to a solution of **N_3H_3** (1.0309 g, 3 mmol) in THF at -30 ^{o}C. This dark red solution was warmed to ambient temperature and stirred for 1 hour. The reaction was cooled again to -30 ^{o}C and a solution of $BiCl_3$ (0.3153 g, 1 mmol) in THF (10 mL) was added resulting in a dark blue solution. This solution was warmed to room temperature and stirred for 20 h in the dark and then volatiles were removed under vacuum. The product was extracted into pentane (20 mL), filtered through

Celite and then concentrated by half. The pentane solution was set recrystallized at -30 ^{o}C which yielded **2** as a fine powder (0.1319 g, 24 %). Characterization data the same as above.

Complex 3: Preparation from reaction of 2 with PCl_3

PCl_3 (0.0687 g, 0.5 mmol) was dissolved in toluene was added dropwise at room temperature to a solution of **2** (0.2748 g, 0.5 mmol) in toluene resulting in a reddish-brown solution. This solution was stirred for 1 hour after which the ^{31}P NMR showed quantitative conversion of PCl_3 and to a new product **3**. All volatiles were removed under vacuum and the product was extracted into pentane and filtered through Celite to remove the $BiCl_3$. Recrystallization from pentane and drying under vacuum yielded **3** as a beige powder (0.0641 g, 35 %). A low yield prompted us to also prepare **3** directly from **N_3H_3** (see below).

^{31}P NMR (121MHz, benzene-d_6): δ 155.03

Characterization data same as below.

Complex 3: Preparation from N_3H_3, ^{n}BuLi, and PCl_3

A solution of **N_3H_3** (0.6872 g, 2 mmol) in THF (15 mL) was cooled to -78 ^{o}C under dinitrogen atmosphere. A solution of ^{n}BuLi (3.75 mL, 1.6 M in hexanes) was added dropwise over 5 minutes which generated a dark red reaction solution. The reaction was allowed to stir for a total of 15 minutes before the cooling dewar was removed. The reaction was stirred for an additional 1 h at room temperature and then cooled again to -78 ^{o}C. A solution of PCl_3 (0.2746 g, 2 mmol) in THF (5 mL) was added dropwise under nitrogen to obtain a reddish-brown suspension. This suspension was stirred cold for 15 minutes and then

permitted to warm to room temperature and stirred for an additional 30 minutes resulting in a homogeneous red/brown solution. The ^{31}P NMR spectrum of an aliquot showed complete conversion and a peak at 155 ppm as the major product, similar to above. All volatiles were removed under vacuum and the solids were washed with 2 x 4 mL hexane. The washed solid was filtered and filtrate placed into the freezer at -30 ^{0}C to crystallize yielding **3** as a beige powder (0.5204 g, 70%). We were unable to grow suitable crystal for X-ray diffraction studies.

Melting point: 144 ^{o}C decomposes

^{1}H NMR (300 MHz, benzene-d_6): δ 7.33 (m, 2H, C_{Ar}-H), 6.89-6.83 (m, 4H, C_{Ar}-H), 6.77 (m, 2H, C_{Ar}-H) 0.18 (s, 18 H, $Si(CH_3)_3$)

^{13}C NMR (126 MHz, toluene-d_8): δ 143.43 (d, J = 4 Hz, C_{Ar}), 140.20 (C_{Ar}), 124.38 (C_{Ar}), 120.74 (C_{Ar}), 119.15 (d, J = 6.4 Hz, C_{Ar}), 114.74 (C_{Ar}), 0.86 (t, J = 6 Hz, $Si(CH_3)_3$)

^{31}P NMR (121MHz, benzene-d_6): δ 155.03

^{29}Si NMR (60 MHz, toluene-d_8): δ 0.7 ($Si(CH_3)_3$)

FT-IR (ATR, ZnSe crystal): 553 (w), 601 (w), 617 (w), 688 (w), 730 (s), 831 (vs), 898 (m), 952 (m), 1030 (w), 1062 (vw), 1102 (w), 1226 (s), 1248 (m, shoulder), 1304 (w), 1470 (m), 1496 (w, shoulder), 1598 (w), 2899 (vw), 2954 (w), 3064 (w)

ESI-HRMS (positive ion mode): calculated for $[M+1]^+$ = 372.1476 m/z, observed = 372.1488 m/z

Elemental Analysis (calcd./expt.): C (58.18/58.41) H (7.05/6.89) N (11.31/11.47)

Complex 7

Compound **2** (0.5496 g, 1 mmol) and pyridine N-oxide (0.0476 g, 0.5 mmol) were combined as solids before 5 mL toluene was added. The reaction was stirred at room temperature for 1 h and then dried under vacuum. The resulting dark yellow powder was dissolved in a minimal pentane, filtered and recrystallized over 1 week at -30 ^{o}C to obtain **4** as yellow/orange rectangular crystals (0.4299 g, 72 %)

Melting point: 107 ^{o}C, decomposes

^{1}H NMR (300 MHz, benzene-d_6): δ 8.04 (d, 4H, 7.9 Hz, C_{Ar}-H), 7.25 (m, 6H, C_{Ar}-H), 6.74 (t, 4H, 7.1 Hz, C_{Ar}-H), 6.59 (t, 4H, 7.1 Hz, C_{Ar}-H), 6.00 (t, 1H, 7.6 Hz, C_{Ar}-H), 5.81 (t, 2H, 7.3 Hz, C_{Ar}-H)

^{13}C NMR (75 MHz, benzene-d_6): δ 151.90 (C_{Ar}), 151.66 (C_{Ar}), 139.32 (C_{Ar}), 128.56 (C_{Ar}) 124.68 (C_{Ar}), 122.63 (C_{Ar}), 122.27 (C_{Ar}), 121.99 (C_{Ar}), 116.60 (C_{Ar}), 2.08 ($Si(CH_3)_3$)

^{29}Si NMR (60 MHz, benzene-d_6): δ 0.4 ($Si(CH_3)_3$)

FT-IR (ATR, ZnSe crystal): 469 (w), 548 (w), 627 (m), 676 (m), 734 (s), 825 (vs), 879 (m), 927 (s), 1017 (w), 1045 (w), 1119 (w), 1155 (m), 1244 (s), 1282 (m), 1330, (w), 1445 (m), 1460 (s), 1475 (m), 1572 (m), 2891 (w), 2939 (m), 3046 (w)

Elemental Analysis (calcd./expt.): C (41.23/41.29) H (4.81/4.73) N (8.21/8.11)

Complex 8

A THF solution (5 mL) of **2** (0.1648 g, 0.3 mmol) and $W(CO)_6$ (0.1056 g, 0.3 mmol) was prepared. The resulting blue reaction solution was stirred under UV irradiation for 24 h during which time the colour changed from blue to dark yellow-orange. An aliquot of this reaction, after removal of THF and redissolution

in C_6D_6, was prepared which showed quantitative conversion to **5**. This aliquot was returned to the bulk reaction mixture, and the NMR tube was rinsed twice with THF to ensure complete transfer. All volatiles were then removed from the bulk reaction mixture under vacuum to get a dark orange solid. The solid was recrystallized from a 1:2 THF/pentane mixture at -25 ^oC and dried under vacuum to obtain pure **5** (0.1598 g, 61 %). Attempts to prepare a 1:2 adduct by repeating the reaction in the presence of excess $W(CO)_6$ were not successful with the reaction generating a mixture of **5**, $W(CO)_5(THF)$ and unreacted $W(CO)_6$.

Melting point: 77 ^oC, decomposes

^1H NMR (300 MHz, benzene-d_6): δ 7.27 (dd, 2H, 8.2 Hz, 1.2 Hz, C_{Ar}-H), 6.89 (dd, 2H, 8.1 Hz, 1.3 Hz, C_{Ar}-H), 6.71 (td, 2H, 7.6 Hz, 1.3 Hz, C_{Ar}-H), 6.61 (td, 2H, 7.6 Hz, 1.4 Hz, C_{Ar}-H), 0.16 (s, 18 H, $Si(CH_3)_3$)

^{13}C NMR (126 MHz, chloroform-d): δ 154.24 (C_{Ar}), 141.47 (C_{Ar}), 124.49 (C_{Ar}), 119.61 (C_{Ar}), 118.36 (C_{Ar}), 117.22, (C_{Ar}), 2.54 $Si(CH_3)_3$). Resonances due to CO groups were not observed; presumably due to the inherently low intensity of quaternary carbons and by their proximity to a spin 1/2 ^{183}W nucleus (14% abundance)

^{29}Si NMR (60 MHz, benzene-d_6): δ 1.0 ($Si(CH_3)_3$)

FT-IR (thin film between NaCl plates): 580 (w), 632 (w), 684 (m), 731 (s), 744 (s), 760 (m), 800 (s), 832 (vs), 856 (vs), 871 (s), 882 (m), 924 (m), 1020 (m), 1055 (m), 1124 (m), 1233 (s), 1250, (s), 1259 (s), 1289 (w), 1409 (w), 1462 (m), 1473 (m), 1576 (w), 1635 (w), 1872 (w), 1938 (m, ν_{co}), 1976 (m, ν_{co}), 2029 (w, ν_{co}), 2054 (w, ν_{co}), 2851 (w), 2896 (w), 2919 (w), 3061 (w)

APCI-MS (positive ion mode): 864.3 m/z, [M – CO + H3O]+ Note: APCI-MS analysis was done under air, which accounts for the replacement of one CO ligand with H_2O (followed by protonation in positive ion mode).

Elemental Analysis (calcd./expt.): C (31.63/31.09) H (3.00/2.73) N (4.81/4.66)

Reaction of 2 with C_6F_5OH

Compound **2** (0.027 g, 0.05 mmol) and C_6F_5OH (0.0276 g, 0.15 mmol) were combined in an NMR tube and benzene-d^6 (0.75 mL) was added in one portion. The reaction was monitored by ^{19}F NMR spectroscopy and showed quantitative conversion of C_6F_5OH to $Bi(OC_6F_5)_3$. The $\mathbf{N_3H_3}$ formed as a byproduct was removed by washing with pentane (3 x 5 mL). The washed solid was then dried under vacuum to obtain $Bi(OC_6F_5)_3$ as an white powder (0.0208 g, 55 % yield). Positive identity was confirmed by comparison to the reported ^{19}F NMR spectrum.[109]

CHAPTER 3: BISMUTH (III) COMPLEXES SUPPORTED BY MONOANIONIC PINCER LIGANDS

3.1: Contributions

Dr. Saurabh Chitnis is thanked for all computational work and writing of the manuscript. Toren Hynes is thanked for the synthesis of **PNP-H** and compound **2** along with the associated starting material. Katherine Marczenko is thanked for collecting and solving X-ray crystal structure data.

3.2: Introduction

3.2.1 Monoanionic Pincer Complexes of Bismuth

Using tethered multidentate ligands to influence molecular geometry represent powerful strategy in coordination chemistry for accessing non-traditional behavior across the periodic table. These classes of ligands utilize the relationship between frontier molecular orbitals, molecular symmetry and geometric distortion to elicit interesting reactivity with application in small molecule activation and catalysis.[34,68,85,87,88,96,110] The previous chapter focused on the use of a tethered trianionic ligand however, monoanionic tridentate ligands (L_2X, where L are neutral donor atoms and X represents an anionic donor atom), also known as pincer ligands (**Scheme 13**), have been widely developed in the context of transition metal small molecule activation and catalysis. Application of

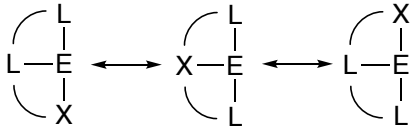

L = Neutral donor (ie: PR_2, NR_3, etc…)
X = Anionic donor (ie: OR, NR_2, etc…)

Scheme 13. Monoanionic L_2X pincer ligands.

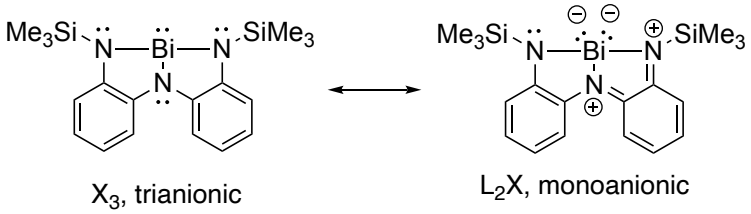

Scheme 14. Interconversion of supporting triamine ligated between its mono- and trianionic forms.

pincer ligand to p-block elements is expected to be a potentially powerful method for inducing novel reactivity as a result of the non-classical geometries often enforced by this class of ligands.

Our group is interested in prompting novel reactivity of heavy group 15 elements through the use of rational frontier molecular orbital engineering. Studying the coordination chemistry of L_2X bismuth complexes is particularly interesting because the previous chapter demonstrated a strong relationship between electronic structure and molecular geometry when supported by a tethered triamide pincer ligand (X_3, triply anionic ligand).[101,102] As described before, the analysis of our NNN-Bi complex concluded that the ligand can undergo a two-electron intramolecular oxidation of the ligand, along with a

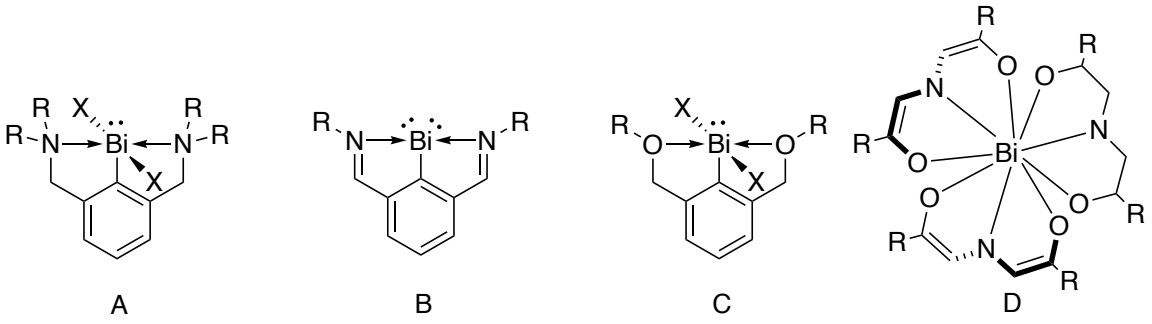

Figure 15. Monoanionic NCN, OCO and ONO pincer complexes of bismuth.

reduction of the Bi center, to become a monoanionic L_2X species (**Scheme 14**). It should be noted that the due to the ambiphilic nature of our NNN-Bi complex, the monoanionic form of the ligand manifests only under certain conditions (ie: in the presence of a strong Lewis acid $W(CO)_6$), however this work ignited our interest in furthering the application of L_2X pincer ligands to bismuth with our sights set on discovering novel behavior.

In the literature, L_2X bismuth complexes are dominated by the an NCN pincer motif that is based on a 2,5-substituted aryl ring.[94,111–114] Planar NCN-Bi complexes have been shown to be capable of small molecule activation[113,115,116] and more recently has found application is transfer hydrogenation catalysis (**Figure 15A**, **15B**).[45] Other examples of **ONO-Bi** and **OCO-Bi** pincer complexes have also been reported (**Figure 15C**, **15D**).[90,117]

3.2.2 Cationic Bismuth(III) Centers

The moderate Lewis acidity of bismuth complexes such as $Bi(Ar)_2Cl$ can be significantly increased by converting a neutral bismuth compound into its cationic derivative, such as $Bi(Ar)_2(OTf)$.[118,119] Such bismuth salts have even been shown to be useful, water stable, Lewis acid catalysts for reactions such as ring opening of epoxides, diastereoselective aldol condensations, and diastereoselective Mannich reactions.[120–122] Similarly, compounds such as $Bi(WCA)_3$ (WCA = OTf, NO_3, ClO_4, NTf_2, and O_2CCF_3) have been widely used as Lewis acid catalysts for organic synthesis such as the diastereoselective S_N1 reaction of propargylic acetates in the presence of weak carbon nucleophiles.[123,124] Most recently, works by the Lichtenberg group have reported

a number of cationic Bi(III) complexes based on bidentate aryl ligand forming a seven-membered ring also known as a bismepine. These class of complexes were previously quite elusive and isolation of the cationic bismapines was possible due to the ligands ability to planarize and generate some heteroaromatic character when donor molecules are not present. The Lewis acidity of the free cationic species was evaluated via the Guttmann-Beckett test which placed it between the Lewis acidity of BPh_3 and $AlCl_3$. It is worth noting, that in the presence of a donor solvent (ie: THF), planarity and aromaticity are disrupted.[125] Follow-up work showed that a range of these molecules can be synthesised and characterized and they were shown to quite favorably form Lewis acid-based complexes with soft Lewis bases of the form $EPMe_3$ (E = S, Se) as deduced from their "soft" Gutmann-Beckett test using a soft $EPMe_3$ (E = S, Se) Lewis base, rather than $OPEt_3$ which is typically the started for this method. They concluded using this method that cationic bismapines are potent soft Lewis acids which interact through an empty p-orbital and not a sigma antibonding orbital.[126]

Other non-carbon based chelating ligands have been explored by groups such as the Norman group who pioneered a 4-coordinate, 10-electron diarylbismuth(III) and bis(organotransitionmetal)bismuth(III) monocations stabilized by weakly coordinating tetrafluoroborate (BF_4^-) anions. X-ray crystallography concluded that Bi cations of the general type $[BiR_2(L)_2]^+$ (R = Ph, Mes, L= $OPPh_3$, $OP(NMe_2)_3$) adopt a trigonal-bipyramidal coordination geometry as would be predicted by VESPR for a 4-coordinate center with a stereochemically active lone pair on the Bi.[127–129]

More recently, precedence for using multidentate amide containing ligands has been reported in the literature. While the existence of well-defined cationic bismuth amide complexes have been reported as far back as 1988,[130] these compounds have only recently seen a resurgence in use over the past decade.[103,131] In the examples above, bulky and/or multidentate ligands are used to stabilize the cationic metal center by generating an appropriate coordination environment and allowing appropriate access to the metal all while improving the solubility of these cations.[73] An additional advantage of amide ligands, is the increase electron donation ability which may aid to stabilize low coordinate Bi cations. This effect can be seen in work by the Shimida group who reported a dianionic CNC pincer ligand to stabilize a 3-coordinate, 8-electron organobismuth monocation and its coordination complexes with a range of neutral donor substrates. They report an impressive array reversible CO_2 fixation reactions mediated by their electrophilic Bi cation.[132]

While to date a number of bulky and/or mulidentate amide ligands have been successfully employed in this area, interest in isolating rare examples of monodentate, monoanionic Bi cations has been seen in the literature. Early work in this area by the Lichtenberg group led to the discovery of the first cationic bismuth compounds based on simple amido ligands (NMe_2) and was prepared by reacting $Bi(NMe_2)_3$ with a Brønsted acid of $HBPh_4$ generating the product $Bi(NR_2)_2(L)_n(BPh_4)$ (R = Me, ^{i}Pr, Ph, L = $HNMe_2$). The isolated ion pair was observed to undergo rapid Ph transfer between Bi and B and in solution the cations reported in this proof-of-principle study were all found to be more reactive

towards a diisopropylcarbodiimide nucleophile relative to their neutral analogues.[72] Follow up works by the Lichtenberg group have included the investigation of simple cationic bismuth amides bearing aromatic substituents at nitrogen, such as $[Bi(NPh_2)_2Ln]^+[WCA]^-$, for which high reactivity can was anticipated. This led to the discovery of a double CH activation of diphenylamine ($HNPh_2$) by a masked cationic Bi amide. This is an important discovery as it represents an early example of transition-metal like behavior being promoted by rational ligand design at a highly Lewis acid Bi cations.[74] Since then, reports of cationic Bi amides performing a range of impressive Lewis acid activation of small molecules like CO have been released which exploit the increased Lewis acidity of the cationic Bi compounds.[133]

The Venugopal group reported the use of a dicationic bismuth(III) complex supported by a mono-anionic hydridotris(3,5-dimethylpyrazolyl)borate (Tp^{Me2}) ligand framework reported to catalyze the hydrosilylation of olefins. Their tridentate ligand coordinates to the bismuth centre through three σ-donor nitrogen atoms, in total donating six electrons. The cationic form is made by reacting $Tp^{Me2}BiCl_2$ with two equivalents of $[Et_3Si][B(C_6F_5)_4]$ which allowed for the isolation of $Tp^{Me2}Bi[B(C_6F_5)_4]_2$. The nitrogen substituents lack the ability to effectively quench the positive charge through π-back donation as their π-orbitals are too high in energy and have poor overlap with the large central element. The resulting bismuth species is highly electrophilic, with open coordination sites trans to the nitrogen substituents.[134] They performed hydrosilylation catalysis reacting Et_3SiH with a series of alkenes and alkynes in the presence of 1 mol%

of their bismuth dication. They observed catalytic conversion to the anti-Markovnikov hydrosilylation products at room temperature in high yield.[135] Interestingly, common side reactions such as isomerization, polymerization, hydrogenation and dehydrosilylations were not observed in this case.[136] We are interested in expanding the ligand diversity and potential TM-like reactivity shown above and will discuss new bismuth cations using tridentate pincer ligands.

3.3: Results and Discussion

3.3.1 P_2N_3-H and PNP-H ligands

This chapter highlights two phosphorus based ligands, the first an amido-diphosphorane framework (**P_2N_3-H**)[137] and the second a PNP ligand first used by the Ozerov group for palladium catalysis (**PNP-H**).[138] **P_2N_3-H** is an L_2X analogue of the NNN-pincer ligand we used in the previous chapter with two phosphinimine side arms instead of amide donors. It was synthesized from the NNN-triamine frameworks by reacting with two equivalents of a P(V) dihalide source (**Scheme 15A**). The phosphinimine groups offer additional electron donating abilities versus NNN ligand as well as increased steric protection for the

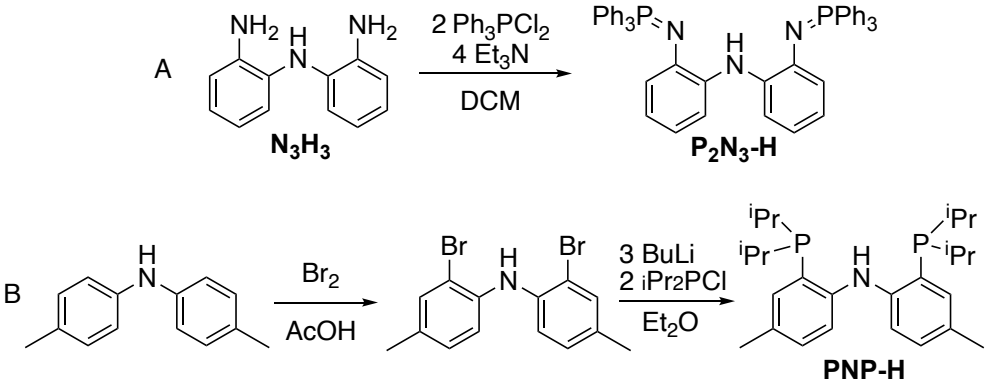

Scheme 15. Synthesis of A) **P_2N_3-H** and B) **PNP-H** ligands.

targeted Bi(I) species.[136] Similarly, **PNP-H** is a heavier to the NNN pincer ligand reported previously, with the two amide side arms being replaced by two neutral phosphine donors, again making a monoanionic L_2X framework. It can be made in a two steps from commercially available di-p-tolylamine by first brominating the ortho positions with dibromine, followed by reacting with a two equivalents of diisopropylchlorophosphine (**Scheme 15B**). This ligand is very electron rich due to the alkylphosphine substituents and should offer suitable steric bulk to aid in stabilizing hypervalent bismuth centres. Additionally both of these frameworks offer the convivence of an NMR active spin ½ nuclei, ^{31}P, which will make studying the reactivity of these systems easier. Thus, we felt these ligands were good candidates for studying low oxidation state and Lewis acidic bismuth centers.

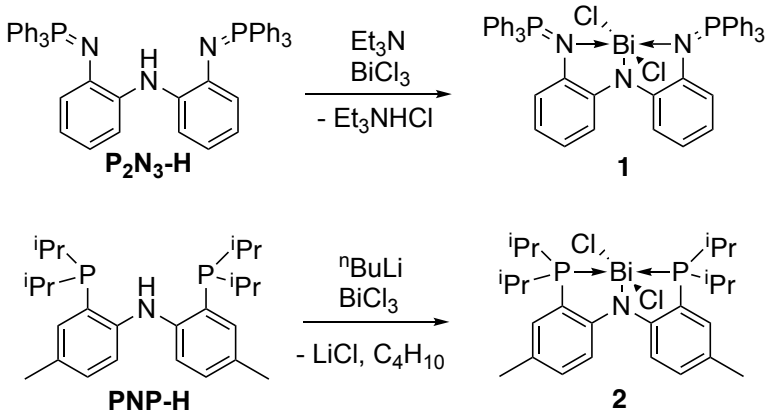

Scheme 16. Synthesis of compounds **1** and **2**.

3.3.2 Syntheses and Solid-state Structures

Deprotonation of **P_2N_3-H** or **PNP-H** with an appropriate base, ^{n}BuLi or Et_3N respectively, and metathesis with $BiCl_3$ yields compounds **1** or **2** in 65% and 64% yield respectively (**Scheme 16**). Suitable quality crystals of **1** were grown

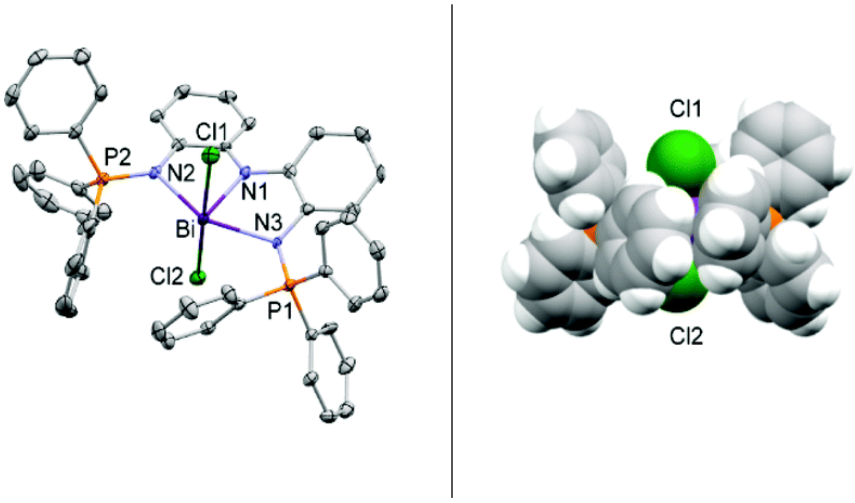

Figure 16. X-ray crystal structure of **1** (left), and space filling diagram showing bulky phosphinimine side arms (right).

from a dichloromethane solution layered with pentane at -30 °C (**Figure 16**, left). The coordination environment at bismuth looks to be a distorted square-based pyramid; five bonds (L_2X_3) along with a stereochemically-active lone pair trans to the central Bi–N moiety. The N2–Bi–N3 bond angle [146.6(2)°] is significantly smaller than the Cl–Bi–Cl angle (175.75(5)°) and is also smaller than the 180° angle predicted by VESPR for a geometry. Presumably, the deviation from 180° is due to the P_2N_3 ligand framework that enforcing a specific bite angle on the central element. The N_3Bi core of **1** is almost perfectly planar suggesting this

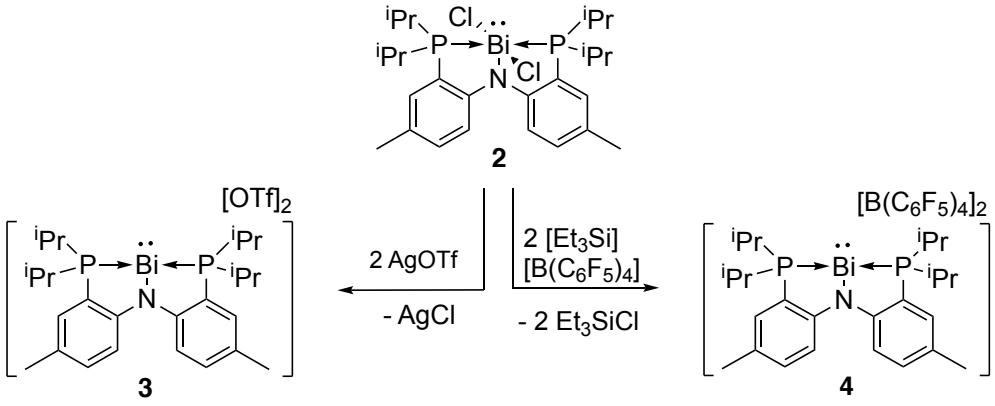

Scheme 17. Synthesis of **3** (left) and **4** (right).

ligand is quite rigid. Looking at the space filling model of the X-ray structure emphasizes the significant steric bulk of the triphenylphosphinimine side-arms (**Figure 16,** right). DFT calculations performed in this work agrees well with the solid state data presented, as multiple attempts to optimize a pyramidal geometry for **1** were not successful, and instead converged on a planar geometry in each attempt (**Figure 18)**. [139]

Attempts to grow suitable crystals of **2** X-ray diffraction studies proved challenging and prevents us from structural discussion beyond simple connectivity. However, computation performed suggested a bent geometry is preferred at the bismuth center and that their exists significant asymmetry with respect to the two P-Bi bond lengths (**Figure 17**, right). As such, we prepared the related species **3** by anion exchange of the Cl substituents using a triflate source ($AgOSO_2CF_3$) and it was isolated in 58% yield (**Scheme 17**, left). The compound is thermally sensitive in the solid state, as we observed decomposition when under vacuum at room temperature, however suitable crystal for crystallographic characterization were successfully grown from a saturated DCM solution cooled

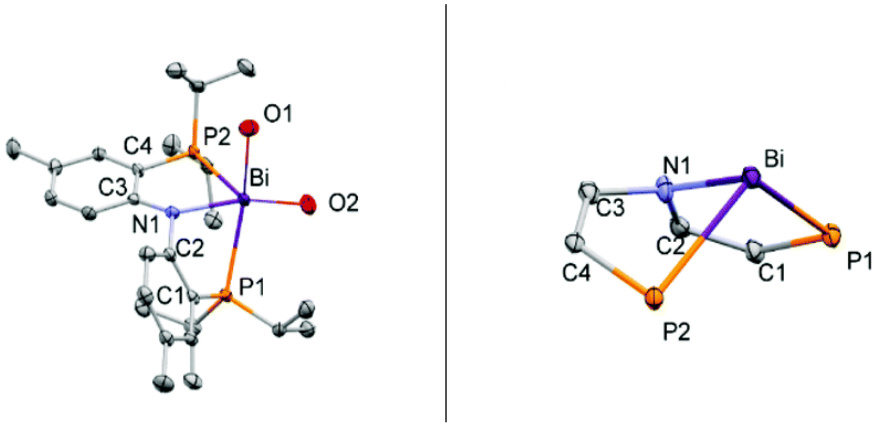

Figure 17. X-ray crystal structure of **3** (left), and a view of the PNP-Bi core showing coordination environment around Bi (right).

to -30 °C (**Figure 17**). Interestingly, a distinctly bent ligand in the solid state with a P1–Bi–P2 angle of 105.76(3)° was observed despite previously reported **PNP-M** complexes (**M** = Al, Ga, In, Sn) adopting more planar P_2N cores.[140,141] Notably, the P1–Bi bond length in **3** (2.6549(8) Å) is nearly 0.1 Å shorter than the P2–Bi bond length (2.7306(8) Å), supporting the possibility of asymmetry in the strength of the P–Bi interactions that was predicted in the calculated structure of **2**. Two O-Bi interaction are present *trans* to the N-Bi and P1-Bi bonds. The O-Bi-O angle of 119.99(8)° indicates the triflate anions are *cis* to one another. The observed deviation of the O-Bi-O from 90° is presumably due to the presence of a stereochemically active lone pair trans to the N-Bi bond. We proposed partial ionic character at the metal center based on the average Bi-O bond distance (2.72 Å) being shorter than the sum of the van der Waals radii (3.59 Å)[142] and also longer than the sum of the covalent radii (2.14 Å)[143] in a typical Bi-O bond. Lastly, the experimental data agrees well with the DFT calculated gas-phase structure of a hypothetical triflate-free **[PNP-Bi]$^{2+}$** dication (**Table 1**).

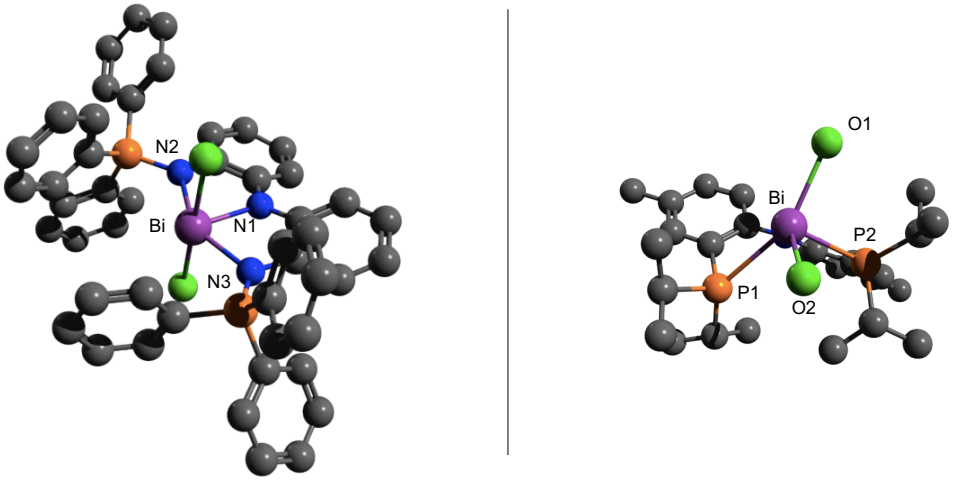

Figure 18. Calculated structure of **1** (left) and **3** (right) at the B3LYP/def2svp(d) level of theory.

Table 1. Select bond lengths and bond angles for compounds **1** and **3** in the solid state and a gas-phase calculated triflate-free **[PNP-Bi]$^{2+}$** dication.

Parameter	**1**	**3**	**[PNP-Bi]2+**
Bi—N	2.165(5) N1	2.215(3)	2.194
	2.358(5) N2	——	——
	2.371(5) N3	——	——
Bi—P	——	2.6549(8) P1	2.652
	——	2.7306(8) P2	2.715
Bi—Cl	2.703(1) Cl1	——	——
	2.721(1) Cl2	——	——
Bi—O	——	2.739(2) O1	——
	——	2.693(3) O2	——
N—Bi—N	74.0(2) N2, N2	——	——
	73.1(2) N1, N3	——	——
	146.6(2) N2, N3	——	——
P—Bi—P	——	105.76(3) P1, P2	108
N—Bi—P	——	73.12(7) N1, P1	79.3
	——	76.82(7) N1, P2	76.9
Cl—Bi—Cl	175.75(5) Cl1, Cl2	——	——
O—Bi—O	——	119.99(8) O1, O2	——

3.3.3 Solution Phase Characterization

1 is reasonably soluble in a range of organic solvents and was fully characterized by NMR spectroscopy. We observe a sharp singlet peak 23.5 ppm in the ^{31}P NMR, and ^{1}H and ^{13}C NMR both suggest chemically equivalent phosphinimine side arms consistent with a meridional arrangement of the ligand. This is consistent with the solid state and gas phase data collected which indicate a planer, C_2 symmetric, N_3Bi core. Thus, we can say that a planar ligand environment at the bismuth center observed in the solid state is maintained in solution. **1** represents the first example of a p-block complex featuring the rigid **P_2N_3** framework.[139]

2 is far less soluble compared to **1.** ^{31}P NMR data collected shows a single broad peak at 41.3 ppm. We also observed broad ^{1}H NMR signals: the first corresponds to the phosphine isopropyl methyl groups (1.37 ppm), as well as two distinct isopropyl methine resonances (2.73 and 3.22 ppm respectively) suggesting some potential asymmetry between the two phosphine substituents. We hypothesized potential dynamic behavior could be the result asymmetry specifically in the P-Bi bond strengths, which has been reported for related **PNP-B** and **PNP-P** complexes.[144,145] A variable temperature NMR experiment was performed and we observe a partial decalescence of the broad ^{31}P signal at 41.3

$$\Delta G^{\mp} = RT_c\left[ln\frac{T_c k_b}{h} - \ln k\right] = RT_c\left[23.76 - \ln\frac{T_c}{k}\right] = RT_c\left[23.76 - \ln\frac{T_c}{2.22\Delta v}\right]$$
$$= 58.76\ KJ\ mol^{-1} = 14.04\ kcal\ mol^{-1}$$

$R = 8.31\ J \cdot mol^{-1}$
$h = 6.62\ x10^{-34} J \cdot s$
$k_b = 1.38\ x10^{-34}\ m^2 \cdot Kg \cdot s^{-1} \cdot K^{-1}$

$\Delta v = 40.60\ Hz - 25.86\ Hz = 14.47\ Hz$
$T_c = 273\ K$
$k = \frac{\pi\Delta v}{\sqrt{2}} = 2.22\ \Delta v$

Assuming a transmission coefficient (κ) = 1
At coalescence temperature T = T_c

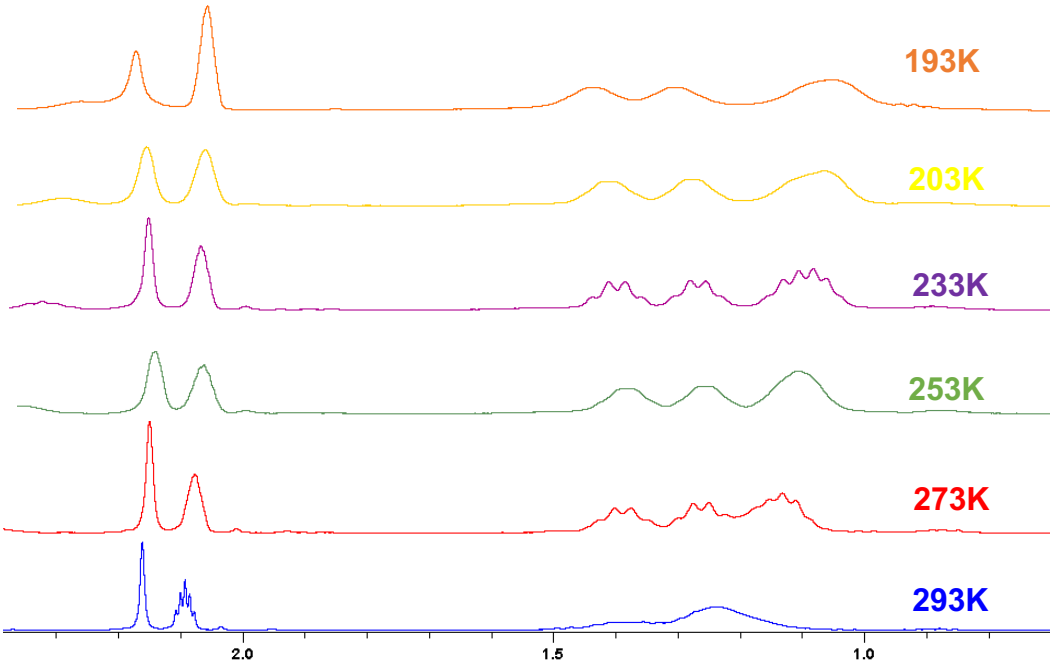

Figure 19. Simplified Eyring equation for estimating $\Delta G^{\mp}$. Variable temperature ^{1}H NMR spectra of **2** in tol-d_8 ranging from 193K to 293K.

ppm. Similarly, in our variable temperature ^{1}H NMR experiment we observe a decoalescence of the broad peak at 1.37 ppm corresponding to the isopropyl methyl protons. An activation barrier of 58.8 kJ mol^{-1} (~ 14.0 kcal mol^{-1}) was crudely estimated from the peak width (at half height) at the coalescence temperature using a simplified Eyring equation. Due to the poor peak separation even at the lowest temperature (solubility limited in toluene-d_8), multiplet analysis was not be performed (**Figure 19**). Thus, detail discussion of the dynamic nature of this system cannot be performed at the present time considering a high likelihood of other dynamic processes being present at low temperature (ie: dimerization). Nevertheless, we propose based on the observation of peak broadening and the computational data discussed above that **2** exists primarily in a bent conformation in solution.

Compound **3** was found to be metastable at room temperature in DCM and degrades after several days via chloride abstraction from the solvent as evidenced by a peak near 41 ppm in the ^{31}P NMR corresponding to **2**. The ^{1}H spectrum showed sharp isopropyl signals and a single chemical shift, unlike compound **2** (**Figure 20**). The spectrum is more consistent with a high symmetry planar ligand average geometry in solution instead of the pyramidal geometry observed for its precursor. It is also notable that the ^{31}P NMR spectrum of **3** showed a single and relatively sharp resonance at 95.1 ppm which is shifted much farther downfield compared to **2** (~41 ppm). The ^{19}F NMR shows a single sharp resonance at -78.05 ppm corresponding to the two triflate anions. These spectral features (sharp signals, downfield chemical shifts) imply a weaker Bi-

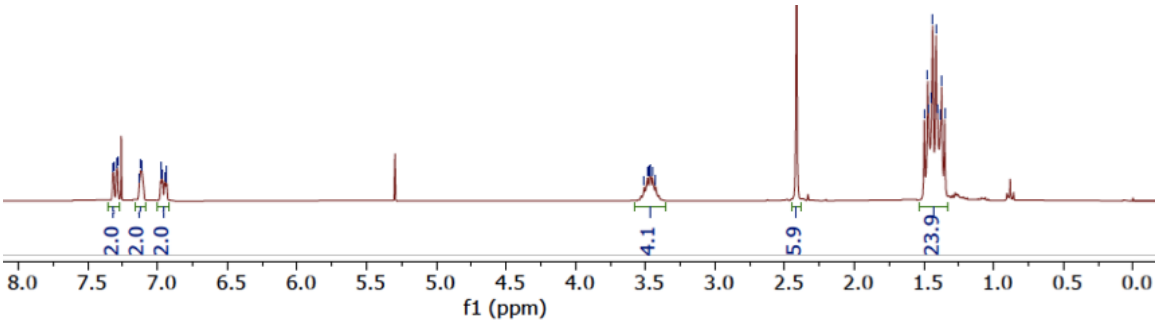

Figure 20. ^{1}H NMR spectrum of **3** in $CDCl_3$, showing sharp resonances and C_2 symmetry.

anion interaction in **3** as expected when utilizing a more weakly coordinating anion. While quantitative analysis has not been performed, the increased electrophilicity that would be predicted when exchanging X = Cl for a X= OTf would presumably strengthen the Bi-P interactions and may explain why the NMR resonances were sharper in **3** and suggest less dynamic behavior between the two Bi-P bonds compared to **2**. X-ray data implies an increased electrophilicity at Bi based on the long Bi-O observed. Thus, we propose that while the energetic minimum in the solid state is a bent geometry, **3** primarily adopts a planar geometry in solution.

Assignment of **3** as being more electrophilic may explain why it is thermally less stable and more reactive towards solvent and contaminants. To explore this further, we prepared another derivative of **2** where instead of Cl or OTf substituents, we used an even less coordinating counter anion, tetrakis(pentafluorophenyl)borate ($B(C_6F_5)_4$ or BAr^F). We converted **2** to **4** via anion exchange with $[Et_3Si][B(C_6F_5)_4]$ that is generated in situ from $[Ph_3C][B(C_6F_5)_4]$ and triethylsilane (Et_3SiH) (**Scheme 17**, right). **4** had the sharpest and most downfield ^{31}P NMR signal at 109.5 ppm presumably due to the very weakly coordinating nature of perfluoroarylborate anions and strengthening of the Bi-P

bonds due to the increased electrophilicity at Bi. This species, perhaps not surprisingly, proved to even more reactive and degrades at room temperature in 1,2-difluorobenzene and in the solid state. This prevented isolation and characterization of this proposed complex. **4** was observed to revert to **2** in the presence of chlorinated solvents, and was observed to polymerize THF very quickly upon its dissolution (**Figure 21**). Ring opening polymerization of THF has been previously overserved for highly electrophilic Bi complexes.[146]

Figure 21. Compound **4** dissolved in THF.

3.3.4 Reduction Results

Along with our interest in probing the chemistry of Bi(III) cations, were also interested in their reduction to Bi(I) compounds. Literature precedence for a Bi(I/III) redox couple has been reported recently by the Cornella group as well as previously in our group we explored a “redox-confused” species mentioned in more detail previously in this report. Thus, we attempted a series of reduction

experiments using a wide variety of reductants with the goal of generating a chemically reduced Bi(I) complex based on our L_2X pincer ligand frameworks.

Compound 1

Attempts to reduce **1** (**Scheme 18**) using a weak reducing agent such as cyclohexene showed no reaction after 24 h at elevated temperatures (60°C). Using stronger reducing agents such as metallic Mg (s) and K (s) result an insoluble black precipitate forming and a number of new unidentified peaks in the ^{31}P NMR spectrum. The precipitate is presumably metallic Bi(0) forming as a result of over reduction. Attempts to identify side products was difficult due to the limited solubility of **1**, however we suspect that a metathesis process generating a Mg(II) or K(II) pincer halide complex is highly probable.[146] Dostal used a borohydride reductant, commonly referred to as superhydride or lithium triethylborohydride, in their work and so we treated a cooled solution of **1** with a 1M THF solution of superhydride. We observed immediate precipitation of a black solid and ^{31}P NMR after only a few minutes shows regeneration of the protonated ligand. We propose this is a result of the hydride being delivered to the Bi center before undergoing a N-H reductive elimination to regenerate the free ligand (~ 20 ppm).[44] Further reduction processes would again result in over-reduction and the generation of metallic Bi which is consistent with the observed

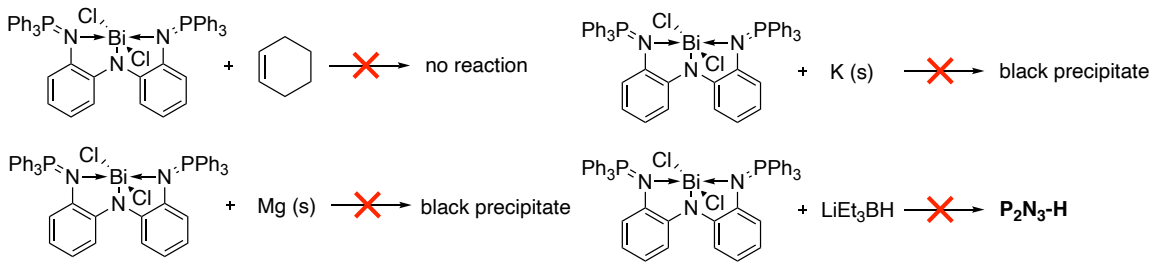

Scheme 18. Summary of P_2N_3-Bi (**1**) reduction results.

precipitate. It is worth noting that mass spectrometry was used to try identify side products of this reaction, but the poor solubility of **1** made complete analysis challenging.

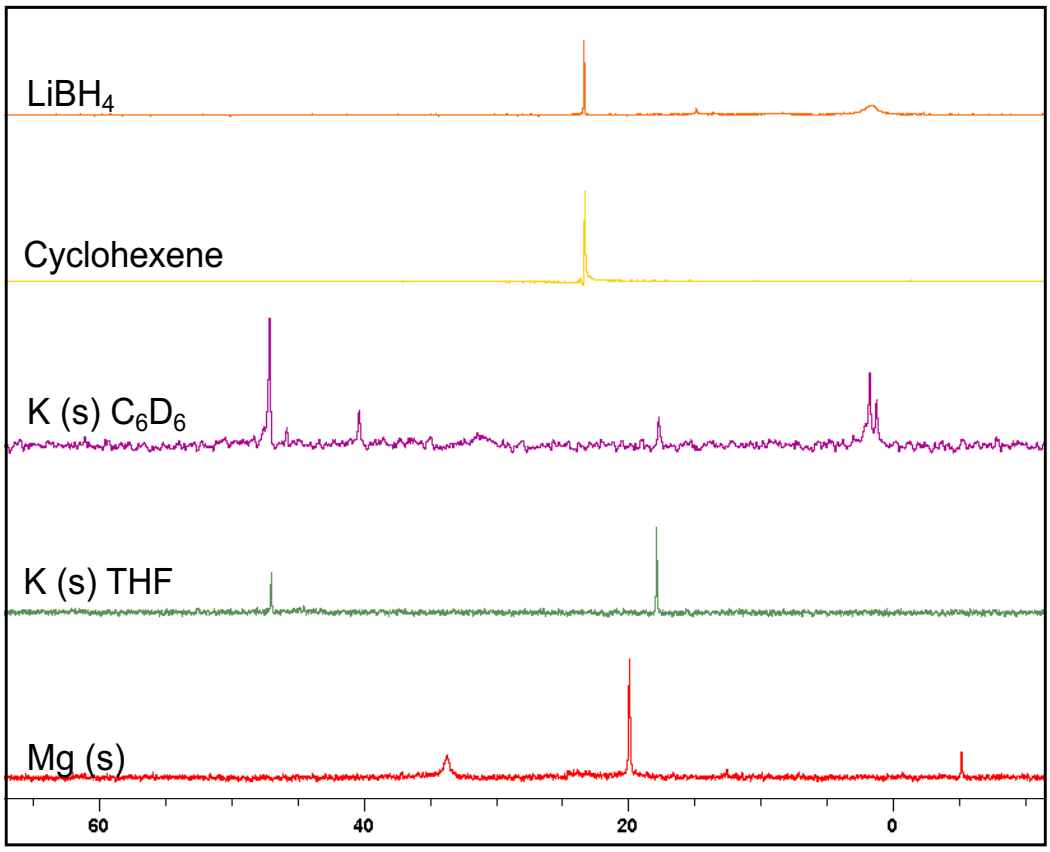

Figure 22. Stack plot of ^{31}P NMR data for attempted reductions of compound **1**. Peaks at ~20 ppm are regenerated ligand **P_2N_3-H.**

Compound 2

Parallel work using compound **2** was also performed (**Scheme 19**). The improved solubility allowed for a more rigorous analysis using a wider range of reductants. Metallic reductants such as Mg was observed to form a major product at -19.4 ppm. This was again presumed to be a Mg (II) species based on the observation of a peak at ≅ 488 m/z in an ESI mass spectrum corresponding to a protonated PNPMgCl complex (ESI-MS: M+1 ion = 488.22 m/z).

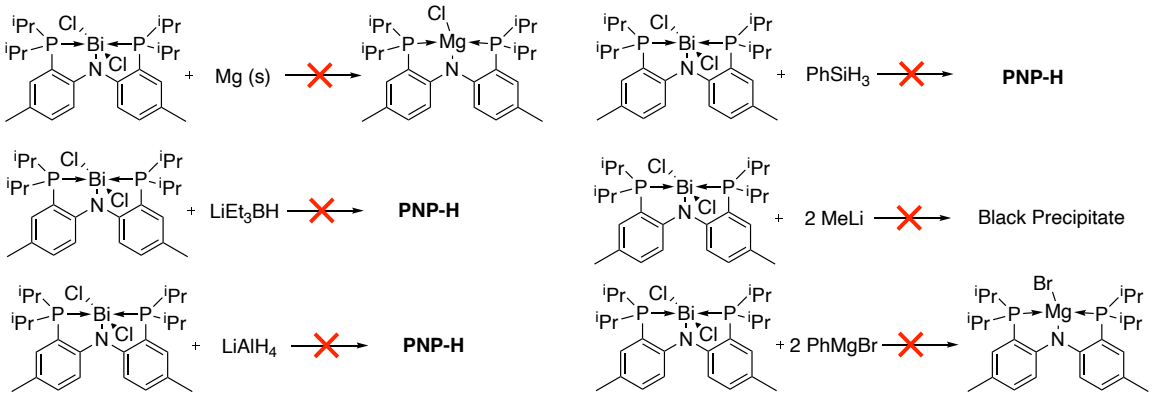

Scheme 19. Summary of attempted reduction of PNP-Bi (**2**).

Alternatively, hydride reductants were considered and so **2** was treated with two equivalents of superhydride which, similar to **1**, results in near complete conversion to the protonated ligand. Treatment of **2** with $LiAlH_4$ again saw the formation of mostly ligand and black powder. We thought perhaps that using weaker hydride sources such as $PhSiH_3$ may prevent over-reduction, however the same results were observed as the ^{31}P NMR showed near complete conversion to the protonated ligand. Although, hydride sources have been shown previously to successfully reduce Bi(III) dihalides, it seems that the Bi-N bond is too weak and reductive elimination of the ligand is preferred in our case. Our last efforts to generate a Bi(I) complex performed to try and take advantage of the apparent facile reductive eliminations observed previously. **2** was treated with two equivalents of MeLi which we postulated could generate LiCl and a dialkyl Bi(III) pincer complex. Upon heating, we hoped to reductively eliminate ethane, generating a Bi(I), however the major product by ^{31}P NMR (**Figure 23**) has a chemical shift near zero ppm suspiciously close to the of the protonated ligand. Black precipitate was observed, indicating some unwanted redox events taking place, however the side product was not identified. In a similar approach, treating

2 with the Grignard phenyl magnesium bromide (PhMgBr), which ideally would have reductively eliminate biphenyl and the target Bi(I) complex, showed a major peak near -19 ppm in the ^{31}P NMR spectrum. This value is very close to that of the attempted Mg reduction (-19.4 ppm). This seemed to suggest a PNPMgBr complex was being formed rather than the desired PNPBi(I) complex. Altogether, our unsuccessful attempted to reduce the Bi(III) dihalides is likely in part due by the relatively weak Bi-N bond cannot properly stabilize the low oxidation state Bi center.

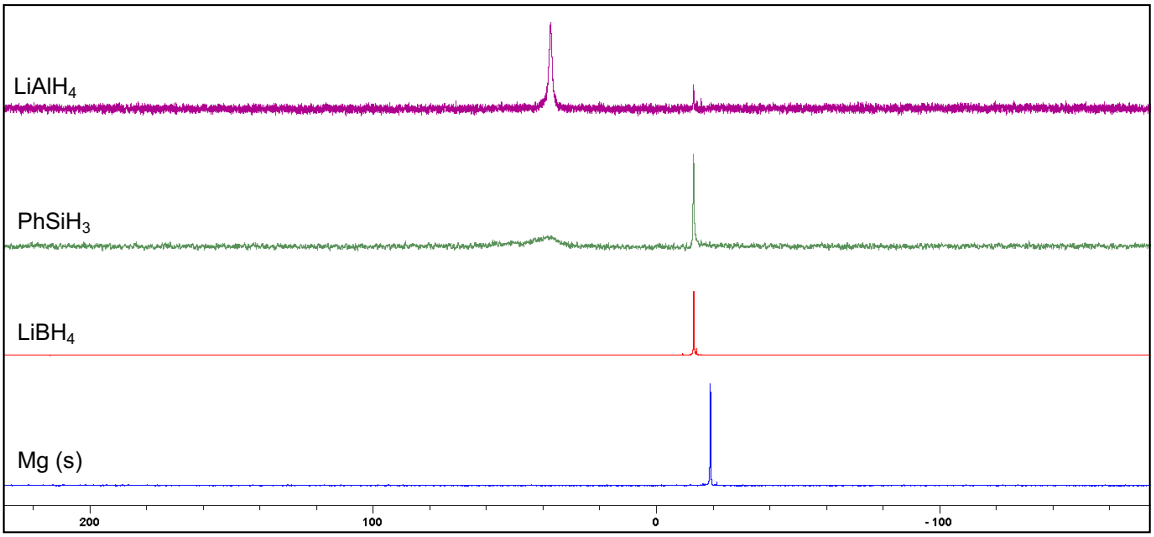

Figure 23. Select ^{31}P NMR spectra for attempted reduction of compound **2**.

3.4: Conclusions and Future Work

To conclude, this chapter reports the first example of a p-block element supported by a rigid **P_2N_3** ligand framework (**1**). We found that it enforces a planar geometry about bismuth both in solution and in the solid state. Although the we hypothesized this planar, electron rich, and bulky ligand scaffold would be

well suited for supporting a hypervalent bismuth centre, attempts to reduce this species have thus far been unsuccessful.

We also report the synthesis and characterization of the first PNP-Bi complex (**2**) along with two increasingly electrophilic analogues (**3** and **4**). Complex **2** was found to exhibit a pyramidal geometry in solution but a planar geometry in the solid state. Both complexes **3** and **4** are thermally sensitive but are planar is both the solution and solid phases, in contrast to complex **2**. The thermal and solvent sensitivity observed seem to indicate they are strongly electrophilic centres. Thus, future work will aim to explore the reactivity of the seemingly potent electrophilic bismuth centers while aiming to develop new Lewis acid catalysts.

3.5: Experimental

3.5.1 General Synthetic Procedures

All manipulations were performed using standard Schlenk and glovebox techniques under an atmosphere of dry nitrogen. Solvents were dried over Na/benzophenone (tetrahydrofuran, pentanes, hexanes, diethyl ether, toluene, benzene-d_6) or over calcium hydride (dichloromethane, acetonitrile, 1,2-difluorobenzene, dichloromethane-d_2, chloroform-d) and distilled prior to use. Reaction glassware was baked in a 130 ^{o}C oven for at least 1 hour prior to use and assembled under nitrogen while hot.

Solution NMR spectroscopy

Nuclear magnetic resonance spectra are referenced to tetramethylsilane (^{1}H, ^{13}C), 85% H_3PO_4 (^{31}P), $CFCl_3$ (^{19}F), or $B(OMe)_3$ (^{11}B) on a Bruker AV-300

spectrometer or a Bruker AV-500 spectrometer with residual solvent used for chemical shift calibration. Samples for NMR spectroscopy were prepared and sealed inside the glovebox with Parafilm before removal into ambient atmosphere. Heteronuclear NMR experiments were run using a sealed capillary containing benzene-d_6 placed within the NMR tube for solvent locking.

Vibrational spectroscopy

Infrared spectra were obtained on an Agilent Technologies Cary 630 FTIR instrument equipped with a ZnSe ATR module. Raman spectra were obtained on a Thermo Scientific Nicolet NXR 9650 FT-Raman Spectrometer instrument equipped with a 1064 nm Nd:YVO4 laser and InGaAs detector.

Crystallography

Single crystals diffraction experiments were performed on a Bruker APEX-II CCD diffractometer. Reflections were integrated using the APEX II software and solved and refined using Olex2 software. Cambridge Structural Database # 1997647, 1997649.

Commercial reagents

2-nitroaniline, 1-fluoro-2-nitrobenzene: Oakwood Chemicals, used as received

Bismuth(III) chloride, Silver(I) triflate: Oakwood Chemicals, purified by vacuum sublimation (10^{-2} mbar, 200 ^{o}C)

Triethylsilane, diisopropylchlorophosphine: Oakwood Chemicals, dried over activated molecular sieves

Triethylamine: Millipore Sigma, used after distillation under nitrogen

^{n}BuLi (1.6M/hexanes): Millipore Sigma, used as received

Triphenylmethylium Tetrakis(pentafluorophenyl)borate (Trityl BAr^F): Millipore Sigma, used as received

Starting materials

SM1: Bis(2-bromo-4-methylphenyl)amine was prepared by literature and purified by crystallization from hot ethanol.

SM2: $HN(1,2\text{-}C_6H_4N{=}PPh_3)_2$ was prepared by literature procedure and purified by crystallization from DCM/pentane.

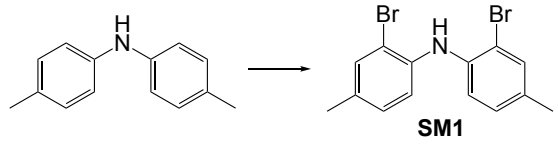

SM1

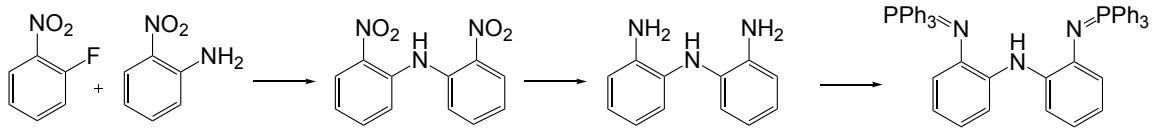

SM2

3.5.2 Synthesis of 1

$HN(1,2\text{-}C_6H_4N{=}PPh_3)_2$ (0.9105 g, 1.26 mmol) and triethylamine (0.21 mL, 1.5 mmol) were combined in THF (5 mL). This mixture was then added slowly to a stirring solution of bismuth(III) chloride (0.3975 g, 1.26 mmol) at 0 °C in THF (5 mL), resulting in the immediate appearance of a white precipitate. The reaction was allowed to stir at room temperature for 18 h and the precipitated triethylammonium chloride was removed by filtration. Volatiles were removed under *vacuum*. The product was isolated as an orange powder after washing with acetonitrile (3 x 5 mL). Crystals were grown from a 1:3 DCM/pentane solution.

Yield: 0.8089 g, 0.81 mmol (64.3%)

Elemental analysis: calcd. C 57.73, H 3.84, N 4.21; expt. C 55.93, H 3.93, N 4.41

^{1}H NMR (500 MHz, $CDCl_3$-d) δ 7.94 (dd, *J* = 12.5 Hz, 7.9 Hz, 12H, orthoC_{Ph}-H), 7.63 (t, *J* = 7.3 Hz, *overlapping*, 8H paraC_{Ph}-H and 2H Ar_{Hd}), 7.52 (td, *J* = 7.5 Hz, 2.8 Hz, 12H, metaC_{Ph}-H), 6.67 (t, *J* = 7.4 Hz, 2H, Ar_{Ha}), 6.23 (d, *J* = 7.7 Hz, 2H, Ar_{Hb}), 6.18 (t, *J* = 7.6 Hz, 2H, Ar_{Hc})

^{31}P {^{1}H} NMR (202 MHz, $CDCl_3$-d) δ 23.5 (s)

^{13}C {^{1}H} NMR (126 MHz, $CDCl_3$-d) δ 138.82 (C_Q), 134.15 (d, J_{CP} = 10.4 Hz, orthoC_{Ph}), 133.17 (paraC_{Ph}), 129.28 (d, J_{CP} = 12.4 Hz, metaC_{Ph}), 125.47 (Ar_C), 124.47 (Ar_C), 121.52 (Ar_{Cb}) 120.21 (Ar_{Cd}), 119.50 (Ar_{Ca}), 117.79 (Ar_{Cc})

Raman (cm^{-1}(int.)): 94(99), 148(52), 211(26), 233(70), 339(62), 438(29), 475(15), 543(36), 624(31), 717(33), 798(41), 846(38), 897(34), 1040(40), 1080(50), 1140(40), 1190(30), 1280(70), 1380(40), 1465(70), 1600(40), 2420(10), 2930(20)

3.5.3 Synthesis of 2

Bis(2-bromo-4-methylphenyl)amine (11.912 g, 33.55 mmol) was dissolved in Et_2O (125 mL) and cooled to -78 ^{o}C. ^{n}BuLi (1.6 M, 69.20 mL) in hexane was added dropwise to a stirring solution over 5 minutes. In another vessel $^{i}Pr_2PCl$ (10.2409 g, 67.11 mmol) was dissolved in Et_2O (50 mL) and was added to the reaction mixture dropwise over 15 minutes at -78 ^{o}C resulting in the formation of a yellow precipitate. The reaction was allowed to warm to room temperature and left to stir for 2 h which resulted in a homogenous yellow solution. $BiCl_3$ (10.5811 g, 33.55 mmol) was dissolved in Et_2O (50 mL) in a separate vessel. $BiCl_3$ was added via cannula dropwise to the cooled reaction mixture at -78 ^{o}C which resulted in a heterogenous red solution forming. The reaction was allowed to stir

overnight at room temperature. Solvent was removed *in vacuo* before extracting the residue with CH_2Cl_2 leaving an orange supernatant and a white precipitate. The solid was removed by filtration, and the CH_2Cl_2 was removed before recrystallizing the product from 1:2 CH_2Cl_2:Et_2O. (crystals can also be grown from thf/ether)

Yield: 15.3434g, 21.67 mmol (64.5%)

Elemental analysis: calcd. C 44.08, H 5.69, N 1.98; expt. C 43.93, H 5.13, N 1.91

^{1}H NMR (500 MHz, $CDCl_3$-d): δ 7.07-7.04 (m, 4H, C_{Ar}-H), 6.81 (dt, *J* = 6.8 Hz, 2.4 Hz, 2H, C_{Ar}-H) 3.22 (b, 2H, methine-C<u>H</u>), 2.73 (b, 2H, methine-C<u>H</u>), 2.04 (s, 6H, C_{Ar}-C<u>H</u>$_3$), 1.37 (b, 24H,C_{iPr}-C<u>H</u>$_3$)

^{13}C {^{1}H} NMR (126 MHz, $CDCl_3$) δ 161.60 (Ar_c), 132.60 (Ar_c), 130.69 (Ar_c), 123.53 (Ar_c), 120.32 (Ar_c), 29.68 ($Ar_{C\text{-}Me}$), 22.32 ($^iPr_{Me}$), 21.26 (C_{Me}), 19.37 ($^iPr_{CH}$)

^{31}P {^{1}H} NMR (202 MHz, $CDCl_3$-d: δ 41.31 (s)

3.5.4 Synthesis of 3

2 (5.0018 g, 7.05 mmol) was dissolved in CH_2Cl_2 (50 mL) in the dark before AgOTf (3.9895 g, 15.53 mmol) was added slowly as a solid over 10 min. The red solution quickly converts to a dark purple solution and a white precipitate is observed after 5 minutes. The reaction is allowed to stir for 1.5 hours at room temperature. The precipitate was removed by filtration, and the filtrate was dried under vacuum. Conversion by ^{31}P NMR is nearly quantitative, pure material can be isolated with extensive pentane/hexane washes or by recrystallization from 1:2 CH_2Cl_2:pentane.

Yield: 3.8475g, 4.11 mmol (58.3%)

^{1}H NMR (300 MHz, $CDCl_3$-d): δ 7.32 (dd, *J* = 8.4 Hz, 2.0 Hz, 2H, C_{Ar}-H), 7.13 (m, 2H, C_{Ar}-H), 6.97 (dt, *J* = 8.7 Hz, 2.2 Hz, 2H, C_{Ar}-H), 3.48 (m, 4H, methine-C<u>H</u>), 2.43 (s, 6H, C_{Ar}-C<u>H</u>$_3$), 1.45 (m, 24H,C_{iPr}-C<u>H</u>$_3$)

^{31}P {^{1}H} NMR (121 MHz, $CDCl_3$-d): δ 90.41 (s)

^{19}F NMR (282 MHz, $CDCl_3$-d): δ 77.06 (s)

3.5.5 Synthesis of 4

Triethylsilane (0.2558 g, 2.20 mmol) in 1,2-difluorobenzene (5 mL) was added dropwise to a stirring solution of triphenylmethylium tetrakis(3,5-bis(trifluoromethyl)phenyl)borate (1.8447 g, 2.00 mmol) in 1,2-difluorobenzene (5 mL) . The solution becomes dark and brown after 15 minutes at which point it was added dropwise to a stirring solution of **1** (0.7084g, 1.00 mmol) in 1,2-difluorobenzene (5 mL). The reaction was allowed to stir at room temperature for 2 hours which resulted in a dark green solution. Volatiles were removed under vacuum and the resulting black residue was washed vigorously with hexanes (3 x 15 mL). After washing a fine green powder was isolated.

^{31}P {^{1}H} NMR (203 MHz, 1,2-PhF_2) δ 108.97 (s)

^{19}F NMR (471 MHz, 1,2-PhF_2) δ -132.87 (s, orthoC_{Ar}-F), -163.19 (s, metaC_{Ar}-F), -167.16 (s, paraC_{Ar}-F)

^{11}B NMR (160 MHz, 1,2-PhF_2) δ -16.64 (s)

3.5.6 Reduction experimental

General remarks

Reduction experiments were performed under N_2 atmosphere in 4 dram scintillation vials. ^{31}P NMR spectra were taken in protic solvent (unless otherwise specified) and used a C_6D_6 internal standard for spectrometer locking purposes.

Compound 1, Reductant: Mg (s)

Compound **1** (0.005 g, 0.05 mmol) was dissolved in THF (0.75 mL) and treated with metallic Mg turnings (excess) and stirred at room temperature overnight. The resulting orange solution showed signs of metallic bismuth powder at the bottom of the reaction vessel and showed very weak signals in the NMR spectra in both THF and C_6D_6. The only peak that is clear is at 23 ppm and corresponds with the unreacted starting material. Due to the poor solubility, this very heterogenous reaction proceeds quite slowly. For this reason identifying, with certainty, the reaction products was not possible (see section 3.3.4 for further discussion).

Compound 1, Reductant: K (s)

Compound **1** (0.005 g, 0.05 mmol) was dissolved in THF (0.75 mL) and treated with metallic K turnings (excess) and stirred at room temperature overnight. Solubility prevent in depth analysis but some weak signals indicate a mixture of products being formed. This was reattempted over a K mirror, however black precipitate and weak NMR signals suggest the targeted Bi(I) was not formed. Signals corresponding to the starting material (24 ppm) and free ligand (3 ppm) are present however, other product were not identified.

Compound 1, Reductant: Cyclohexene

Compound **1** (0.01 g, 0.1 mmol) was dissolved in $CDCl_3$ (0.75 mL) and treated with cyclohexene (10 uL, 0.2 mmol) and stirred at room temperature for 1h. ^{31}P NMR showed only starting material (23 ppm), so the reaction was heated to 60°C for 18h, and again NMR showed no sign of a reaction.

Compound 1, Reductant: $LiEt_3BH$

Compound **1** (0.01 g, 0.1 mmol) was dissolved in THF (0.75 mL) and treated slowly with $LiEt_3BH$ (1M THF, 200 uL, 0.2 mmol) using cold beads cooled to - 30 ° C. Black powder is observed immediately, and the ^{31}P NMR spectrum showed mostly protonated ligand (3 ppm) being generated.

Compound 2, Reductant: Mg (s)

Compound **2** (0.068 g, 0.1 mmol) was dissolved in THF (0.75 mL) and treated with metallic Mg turnings (excess) and stirred at room temperature overnight. The resulting green solution showed signs of metallic bismuth powder at the bottom of the reaction vessel and the ^{31}P NMR showed a major product at -19.4 ppm. See section 3.3.4 for further discussion.

Compound 2, Reductant: $LiEt_3BH$

Compound **2** (0.0340 g, 0.05 mmol) was dissolved in THF (0.75 mL) and treated slowly with $LiEt_3BH$ (1M THF, 200 uL, 0.2 mmol) using cold beads cooled to - 30 ° C. Black powder is observed almost immediately upon addition of the reductant, and the ^{31}P NMR spectrum showed mostly protonated ligand (-13 ppm) being generated.

Compound 2, Reductant: $PhSiH_3$

Compound **2** (0.0708 g, 0.1 mmol) was dissolved in toluene (0.75 mL) and cooled to -30 ^{o}C. $PhSiH_3$ (25 uL, 0.2 mmol) was added dropwise via microsyringe. ^{31}P NMR after 30 minutes showed not reaction, thus the reaction was allowed to stir a room temperature overnight at which time black power appeared in the reaction vessel and it had degraded to mostly free ligand in the ^{31}P spectrum.

Compound 2, Reductant: $LiAlH_4$

Compound **2** (0.0708 g, 0.1 mmol) was dissolved in toluene (0.75 mL) and cooled to -30 ^{o}C. $LiAlH_4$ (0.0076 g, 0.2 mmol) was dissolved in minimal THF and added slowed to cooled reaction vessel. Nearly immediately upon addition, black power begins to precipitate out and similar to other hydride sources, protonated ligand was observed in the ^{31}P NMR spectrum.

CHAPTER 4: CONCLUSION

This thesis reports two studies to investigate the use of planar tridentate ligand scaffolds for making and studying redox active and Lewis acidic bismuth centres.

In Chapter 2 we studied a geometrically constrained tethered tridentate ligand at a bismuth center allowing for the isolation of the first planar geometry in any pnictogen triamide. That work demonstrates a structural motif that is unstable for lighter group 15 elements. Compound **2** exhibited significant Bi(I) character and was prepared without any external reductants from a Bi(III) starting material. Compound **2** provides the first structural model of the transition state proposed for edge-inversion in bismuthines and more generally in any pnictogen triamide. The structural features of **2**, DFT analysis, and reactivity studies suggest a Bi(I) oxidation state, however is was found that contributions from other resonance forms are sufficiently large that **2** can also behave as a Bi(III) complex. This ambiphilic reactivity may allow for future application in redox catalysis.

In chapter 3 we report the first example of a p-block element supported by a rigid $\mathbf{P_2N_3}$ ligand framework. We found that it enforces a planar geometry about bismuth both in solution and in the solid state. We also report the synthesis and characterization of the first **PNP-Bi** complex along with two increasingly electrophilic analogues. Complex **2** was found to exhibit a pyramidal geometry in solution but a planar geometry in the solid state. Both complexes **3** and **4** are were found to be thermally sensitive, and were found to quickly degrade via

solvent activation, in halogenated solvents. Both **3** and **4** are planar in solution and in the solid phase, in contrast to complex **2**. The thermal and solvent sensitivity observed seem to indicate they are strong electrophiles. Thus, future work will aim to explore the reactivity of the seemingly potent electrophilic bismuth centers while aiming to develop new Lewis acid catalysts.

In summary, this thesis revealed the influence of ligands on parameters such as oxidation state and geometry at bismuth. While catalysis at bismuth remains a challenging feat, this work may allow for more rational molecular design moving forward.

REFERENCES

[1] N. Miyaura, K. Yamada, A. Suzuki, Tetrahedron Lett. **1979**, 20, 3437–3440.

[2] S. Würtemberger-Pietsch, U. Radius, T. B. Marder, Dalt. Trans. **2016**, 45, 5880–5895.

[3] A. S. Guram, R. A. Rennels, S. L. Buchwald, Angew. Chemie Int. Ed. English **1995**, 34, 1348–1350.

[4] M. S. Driver, J. F. Hartwig, J. Am. Chem. Soc. **1995**, 117, 4708–4709.

[5] R. R. Schrock, J. A. Osborn, J. Am. Chem. Soc. **1976**, 98, 2134–2143.

[6] X. X. Guo, D. W. Gu, Z. Wu, W. Zhang, Chem. Rev. **2015**, 115, 1622–1651.

[7] S. Z. Tasker, E. A. Standley, T. F. Jamison, Nature **2014**, 509, 299–309.

[8] A. Fürstner, ACS Cent. Sci. **2016**, 2, 778–789.

[9] T. Ogawa, A. J. Ruddy, O. L. Sydora, M. Stradiotto, L. Turculet, Organometallics **2017**, 36, 417–423.

[10] A. J. Ruddy, C. M. Kelly, S. M. Crawford, C. A. Wheaton, O. L. Sydora, B. L. Small, M. Stradiotto, L. Turculet, Organometallics **2013**, 32, 5581–5588.

[11] R. L. Webster, Dalt. Trans. **2017**, 46, 4483–4498.

[12] S. G. Davey, Nat. Rev. Chem. **2017**, 1, 1–1.

[13] G. Cahiez, A. Moyeux, Chem. Rev. **2010**, 110, 1435–1462.

[14] P. P. Power, Nature **2010**, 463, 171–177.

[15] T. Dohi, Y. Kita, Chem. Commun. **2009**, 2073–2085.

[16] T. Dohi, A. Maruyama, M. Yoshimura, K. Morimoto, H. Tohma, Y. Kita, Angew. Chemie - Int. Ed. **2005**, 44, 6193–6196.

[17] M. Ochiai, Y. Takeuchi, T. Katayama, T. Sueda, K. Miyamoto, J. Am. Chem. Soc. **2005**, 127, 12244–12245.

[18] T. Dohi, M. Ito, K. Morimoto, Y. Minamitsuji, N. Takenaga, Y. Kita, Chem. Commun. **2007**, 4152–4154.

[19] T. Dohi, Y. Minamitsuji, A. Maruyama, S. Hirose, Y. Kita, Org. Lett. **2008**, 10, 3559–3562.

[20] T. Dohi, A. Maruyama, Y. Minamitsuji, N. Takenaga, Y. Kita, Chem. Commun. **2007**, 1224–1226.

[21] A. Claraz, G. Masson, Org. Biomol. Chem. **2018**, 16, 5386–5402.

[22] R. D. Richardson, T. K. Page, S. Altermann, S. M. Paradine, A. N. French, T. Wirth, Synlett **2007**, 2007, 538–542.

[23] G. Wittig, G. Geissler, Justus Liebigs Ann. Chem. **1953**, 580, 44–57.

[24] T. Imamoto, S. I. Kikuchi, T. Miura, Y. Wada, Org. Lett. **2001**, 3, 87–90.

[25] K. Naumann, G. Zon, K. Mislow, J. Am. Chem. Soc. **1969**, 91, 7012–7023.

[26] C. J. O'Brien, J. L. Tellez, Z. S. Nixon, L. J. Kang, A. L. Carter, S. R. Kunkel, K. C. Przeworski, G. A. Chass, Angew. Chemie - Int. Ed. **2009**, 48, 6836–6839.

[27] M. L. Schirmer, S. Adomeit, T. Werner, Org. Lett. **2015**, 17, 3078–3081.

[28] M.-L. Schirmer, S. Adomeit, A. Spannenberg, T. Werner, Chem. Eur. J. **2016**, 22, 2458–2465.

[29] A. Grandane, L. Longwitz, C. Roolf, A. Spannenberg, H. M. Escobar, C. Junghanss, E. Suna, T. Werner, J. Org. Chem. **2019**, 84, 1320–1329.

[30] S. Kim, B. N. Su, S. Riswan, L. B. S. Kardono, J. J. Afriastini, J. C. Gallucci, H. Chai, N. R. Farnsworth, G. A. Cordell, S. M. Swanson, et al., Tetrahedron Lett. **2005**, 46, 9021–9024.

[31] M. Bruder, P. L. Haseler, M. Muscarella, W. Lewis, C. J. Moody, J. Org. Chem. **2010**, 75, 353–358.

[32] N. K. Ishikawa, K. Yamaji, S. Tahara, Y. Fukushi, K. Takahashi, Phytochemistry **2000**, 54, 777–782.

[33] A. J. Arduengo, C. A. Stewart, Chem. Rev. **1994**, 94, 1215–1237.

[34] N. L. Dunn, M. Ha, A. T. Radosevich, J. Am. Chem. Soc. **2012**, 134, 11330–11333.

[35] T. Wirtanen, E. Rodrigo, S. R. Waldvogel, Chem.Eur.J. **2020**, 26, 5592–5597.

[36] S. Roscales, A. G. Csáky, Adv. Synth. Catal. **2020**, 362, 111–117.

[37] W. J. Chung, J. S. Carlson, C. D. Vanderwal, J. Org. Chem. **2014**, 79, 2226–2241.

[38] W. J. Chung, C. D. Vanderwal, Acc. Chem. Res. **2014**, 47, 718–728.

[39] C. Nilewski, E. M. Carreira, European J. Org. Chem. **2012**, 2012, 1685–1698.

[40] M. L. Poutsma, J. Am. Chem. Soc. **1965**, 87, 4285–4293.

[41] I. Roberts, G. E. Kimball, J. Am. Chem. Soc. **1937**, 59, 947–948.

[42] A. J. Cresswell, S. T. C. Eey, S. E. Denmark, Nat. Chem. **2015**, 7, 146–152.

[43] T. Ollevier, Org. Biomol. Chem. **2013**, 11, 2740–2755.

[44] I. Ugi, D. Marquarding, H. Klusacek, P. Gillespie, F. Ramirez, Acc. Chem. Res. **1971**, 4, 288–296.

[45] F. Wang, O. Planas, J. Cornella, J. Am. Chem. Soc. **2019**, 141, 4235–4240.

[46] J. Spielmann, F. Buch, S. Harder, Angew. Chemie **2008**, 120, 9576–9580.

[47] A. H. C. Horn, T. Clark, J. Am. Chem. Soc. **2003**, 125, 2809–2816.

[48] S. Harder, W. E. Piers, Dalt. Trans. **2018**, 47, 12491–12492.

[49] H. Bauer, M. Alonso, C. Fischer, B. Rösch, H. Elsen, S. Harder, Angew. Chemie Int. Ed. **2018**, 57, 15177–15182.

[50] H. Bauer, M. Alonso, C. Färber, H. Elsen, J. Pahl, A. Causero, G. Ballmann, F. De Proft, S. Harder, Nat. Catal. **2018**, 1, 40–47.

[51] H. Bauer, K. Thum, M. Alonso, C. Fischer, S. Harder, Angew. Chemie Int. Ed. **2019**, 58, 4248–4253.

[52] B. Rao, R. Kinjo, Chem. - An Asian J. **2018**, 13, 1279–1292.

[53] J. M. Blackwell, W. E. Piers, M. Parvez, Org. Lett. **2000**, 2, 695–698.

[54] J. M. Blackwell, W. E. Piers, R. McDonald, J. Am. Chem. Soc. **2002**, 124, 1295–1306.

[55] D. J. Morrison, J. M. Blackwell, W. E. Piers, in Pure Appl. Chem., Walter De Gruyter GmbH, **2004**, pp. 615–623.

[56] T. Ooi, D. Uraguchi, N. Kagoshima, K. Maruoka, J. Am. Chem. Soc. **1998**, 120, 5327–5328.

[57] A. Y. Houghton, J. Hurmalainen, A. Mansikkamäki, W. E. Piers, H. M. Tuononen, Nat. Chem. **2014**, 6, 983–988.

[58] P. Eisenberger, C. M. Crudden, Dalt. Trans. **2017**, 46, 4874–4887.

[59] P. Eisenberger, B. P. Bestvater, E. C. Keske, C. M. Crudden, Angew. Chemie - Int. Ed. **2015**, 54, 2467–2471.

[60] J. M. Bayne, D. W. Stephan, Chem. Soc. Rev. **2016**, 45, 765–774.

[61] K. Dimroth, P. Hoffmann, Angew. Chemie Int. Ed. English **1964**, 3, 384–384.

[62] A. H. Cowley, R. A. Kemp, Chem. Rev. **1985**, 85, 367–382.

[63] D. Gudat, A. Haghverdi, H. Hupfer, M. Nieger, Chem. Eur. J. **2000**, 6, 3414–3425.

[64] A. L. Brazeau, C. A. Caputo, C. D. Martin, N. D. Jones, P. J. Ragogna, Dalt. Trans. **2010**, 39, 11069–11073.

[65] J. M. Slattery, S. Hussein, Dalt. Trans. **2012**, 41, 1808–1815.

[66] L. E. Longobardi, C. A. Russell, M. Green, N. S. Townsend, K. Wang, A. J. Holmes, S. B. Duckett, J. E. McGrady, D. W. Stephan, J. Am. Chem. Soc. **2014**, 136, 13453–13457.

[67] R. J. Andrews, S. S. Chitnis, D. W. Stephan, Chem. Commun. **2019**, 55, 5599–5602.

[68] S. S. Chitnis, J. H. W. Lafortune, H. Cummings, L. L. Liu, R. Andrews, D. W. Stephan, Organometallics **2018**, 37, 4540–4544.

[69] A. E. Waked, S. S. Chitnis, D. W. Stephan, Chem. Commun. **2019**, 55, 8971–8974.

[70] S. S. Chitnis, F. Krischer, D. W. Stephan, Chem. Eur. J. **2018**, 24, 6543–6546.

[71] K. M. Marczenko, S. Jee, S. S. Chitnis, Organometallics **2020**, acs.organomet.0c00378.

[72] H. Dengel, C. Lichtenberg, Chem. Eur. J. **2016**, 22, 18465–18475.

[73] B. Ritschel, C. Lichtenberg, Synlett **2018**, 29, 2213–2217.

[74] B. Ritschel, J. Poater, H. Dengel, F. M. Bickelhaupt, C. Lichtenberg, Angew. Chemie - Int. Ed. **2018**, 57, 3825–3829.

[75] K. Chandra Mondal, S. Roy, H. W. Roesky, Chem. Soc. Rev. **2016**, 45, 1080–1111.

[76] E. Rivard, Chem. Soc. Rev. **2016**, 45, 989–1003.

[77] K. K. Milnes, L. C. Pavelka, K. M. Baines, Chem. Soc. Rev. **2016**, 45, 1019–1035.

[78] G. Frenking, M. Hermann, D. M. Andrada, N. Holzmann, Chem. Soc. Rev. **2016**, 45, 1129–1144.

[79] M.-A. Légaré, G. Bélanger-Chabot, R. D. Dewhurst, E. Welz, I. Krummenacher, B. Engels, H. Braunschweig, Science **2018**, 359, 896—900.

[80] S. A. Culley, A. J. Arduengo, J. Am. Chem. Soc. **1984**, 106, 1164–1165.

[81] C. A. Stewart, R. L. Harlow, A. J. Arduengo, J. Am. Chem. Soc. **1985**, 107, 5543–5544.

[82] W. Zhao, S. M. McCarthy, T. Y. Lai, H. P. Yennawar, A. T. Radosevich, J. Am. Chem. Soc. **2014**, 136, 17634–17644.

[83] A. J. Pistner, H. W. Moon, A. Silakov, H. P. Yennawar, A. T. Radosevich, Inorg. Chem. **2017**, 56, 8661–8668.

[84] J. Cui, Y. Li, R. Ganguly, A. Inthirarajah, H. Hirao, R. Kinjo, J. Am. Chem. Soc. **2014**, 136, 16764–16767.

[85] S. Volodarsky, R. Dobrovetsky, Chem. Commun. **2018**, 54, 6931–6934.

[86] T. P. Robinson, D. De Rosa, S. Aldridge, J. M. Goicoechea, Chem. Eur. J. **2017**, 23, 15455–15465.

[87] T. P. Robinson, D. M. De Rosa, S. Aldridge, J. M. Goicoechea, Angew. Chemie Int. Ed. **2015**, 54, 13758–13763.

[88] Y. C. Lin, E. Hatzakis, S. M. McCarthy, K. D. Reichl, T. Y. Lai, H. P. Yennawar, A. T. Radosevich, J. Am. Chem. Soc. **2017**, 139, 6008–6016.

[89] Y. Sano, H. Satoh, M. Chiba, M. Okamoto, K. Serizawa, H. Nakashima, K. Omae, J. Occup. Health **2005**, 47, 293–298.

[90] C. A. Stewart, J. C. Calabrese, A. J. Arduengo, J. Am. Chem. Soc. **1985**, 107, 3397–3398.

[91] C. Lichtenberg, Angew. Chemie Int. Ed. **2016**, 55, 484–486.

[92] R. J. Schwamm, J. R. Harmer, M. Lein, C. M. Fitchett, S. Granville, M. P. Coles, Angew. Chemie Int. Ed. **2015**, 54, 10630–10633.

[93] H. Schmidbaur, A. Schier, Organometallics **2008**, 27, 2361–2395.

[94] P. Šimon, F. de Proft, R. Jambor, A. Růžička, L. Dostál, Angew. Chemie Int. Ed. **2010**, 49, 5468–5471.

[95] G. Wang, L. A. Freeman, D. A. Dickie, R. Mokrai, Z. Benkő, R. J. Gilliard, Chem. - A Eur. J. **2019**, 25, 4335–4339.

[96] D. A. Dixon, A. J. Arduengo, J. Am. Chem. Soc. **1987**, 109, 338–341.

[97] D. A. Dixon, A. J. Arduengo, T. Fukunaga, J. Am. Chem. Soc. **1986**, 108, 2461–2462.

[98] K. Akiba, Y. Yamamoto, Heteroat. Chem. **2007**, 18, 161–175.

[99] K. Izod, E. R. Clark, J. Stewart, Inorg. Chem. **2011**, 50, 3651–3661.

[100] S. S. Chitnis, K. A. Vos, N. Burford, R. McDonald, M. J. Ferguson, Chem. Commun. **2016**, 52, 685–688.

[101] M. B. Kindervater, K. M. Marczenko, U. Werner-Zwanziger, S. S. Chitnis, Angew. Chemie - Int. Ed. **2019**, 58.

[102] K. M. Marczenko, J. A. Zurakowski, M. B. Kindervater, S. Jee, T. Hynes, N. Roberts, S. Park, U. Werner-Zwanziger, M. Lumsden, D. N. Langelaan, et al., Chem. Eur. J. **2019**, 25.

[103] C. Hering-Junghans, A. Schulz, M. Thomas, A. Villinger, Dalt. Trans. **2016**, 45, 6053–6059.

[104] K. Huang, J. L. Dutton, C. D. Martin, Chem. Eur. J. **2017**, 23, 10532–

10535.

[105] D. Mendoza-Espinosa, T. A. Hanna, Inorg. Chem. **2009**, 48, 10312–10325.

[106] A. I. Nguyen, K. J. Blackmore, S. M. Carter, R. A. Zarkesh, A. F. Heyduk, J. Am. Chem. Soc. **2009**, 131, 3307–3316.

[107] L. C. Liang, R. R. Schrock, W. M. Davis, Organometallics **2000**, 19, 2526–2531.

[108] A. H. Cowley, Inorganic Syntheses. Volume 31, **n.d.**

[109] C. M. Jones, M. D. Burkart, R. E. Bachman, D. L. Serra, S. J. Hwu, K. H. Whitmire, Inorg. Chem. **1993**, 32, 5136–5144.

[110] A. J. Arduengo, D. A. Dixon, R. L. Harlow, H. V. R. Dias, W. T. Booster, T. F. Koetzle, J. Am. Chem. Soc. **1994**, 116, 6812–6822.

[111] A. P. Soran, C. Silvestru, H. J. Breunig, G. Balázs, J. C. Green, Organometallics **2007**, 26, 1196–1203.

[112] G. Strîmb, A. Pöllnitz, C. I. Raţ, C. Silvestru, Dalt. Trans. **2015**, 44, 9927–9942.

[113] D. R. Kindra, I. J. Casely, M. E. Fieser, J. W. Ziller, F. Furche, W. J. Evans, J. Am. Chem. Soc. **2013**, 135, 7777–7787.

[114] H. J. Breunig, M. G. Nema, C. Silvestru, A. P. Soran, R. A. Varga, Dalt. Trans. **2010**, 39, 11277–11284.

[115] D. R. Kindra, W. J. Evans, Dalt. Trans. **2014**, 43, 3052–3054.

[116] L. Dostál, R. Jambor, A. Růzička, M. Erben, R. Jirásko, E. Černoškova, J. Holeček, Organometallics **2009**, 28, 2633–2636.

[117] A. Fridrichová, T. Svoboda, R. Jambor, Z. Padělková, A. Růžička, M. Erben, R. Jirásko, L. Dostál, Organometallics **2009**, 28, 5522–5528.

[118] C. Tschersich, C. Limberg, S. Roggan, C. Herwig, N. Ernsting, S. Kovalenko, S. Mebs, Angew. Chemie Int. Ed. **2012**, 51, 4989–4992.

[119] C. R. Wade, I. S. Ke, F. P. Gabbaï, Angew. Chemie - Int. Ed. **2012**, 51, 478–481.

[120] R. Qiu, Y. Qiu, S. Yin, X. Song, Z. Meng, X. Xu, X. Zhang, S. Luo, C. T. Au, W. Y. Wong, Green Chem. **2010**, 12, 1767–1771.

[121] R. Qiu, S. Yin, X. Song, Z. Meng, Y. Qiu, N. Tan, X. Xu, S. Luo, F. R. Dai, C. T. Au, et al., Dalt. Trans. **2011**, 40, 9482–9489.

[122] N. Tan, S. Yin, Y. Li, R. Qiu, Z. Meng, X. Song, S. Luo, C. T. Au, W. Y. Wong, J. Organomet. Chem. **2011**, 696, 1579–1583.

[123] T. Ollevier, Org. Biomol. Chem. **2013**, 11, 2740–2755.

[124] J. M. Bothwell, S. W. Krabbe, R. S. Mohan, Chem. Soc. Rev. **2011**, 40, 4649–4707.

[125] J. Ramler, K. Hofmann, C. Lichtenberg, Inorg. Chem. **2020**, 59, 3367–3376.

[126] J. Ramler, C. Lichtenberg, Chem.z Eur. J. **2020**, chem.202001674.

[127] C. J. Carmalt, N. C. Norman, A. G. Orpen, S. E. Stratford, J. Organomet. Chem. **1993**, 460, C22–C24.

[128] C. J. Carmalt, L. J. Farrugia, N. C. Norman, J. Chem. Soc. - Dalt. Trans. **1996**, 455–459.

[129] C. J. Carmalt, D. Walsh, A. H. Cowley, N. C. Norman, Organometallics **1997**, 16, 3597–3600.

[130] M. Veith, B. Bertsch, V. Huch, Zeitschrift f r Anorg. und Allg. Chemie **1988**, 559, 73–88.

[131] R. J. Schwamm, B. M. Day, M. P. Coles, C. M. Fitchett, Inorg. Chem. **2014**, 53, 3778–3787.

[132] B. Ming, T. Hayashi, S. Shimada, Organometallics **2007**, 26, 1816–1822.

[133] J. Ramler, J. Poater, F. Hirsch, B. Ritschel, I. Fischer, F. M. Bickelhaupt, C. Lichtenberg, Chem. Sci. **2019**, 10, 4169–4176.

[134] S. Balasubramaniam, S. Kumar, A. P. Andrews, E. D. Jemmis, A. Venugopal, Eur. J. Inorg. Chem. **2020**, 2020, 2530–2536.

[135] S. Balasubramaniam, S. Kumar, A. P. Andrews, B. Varghese, E. D. Jemmis, A. Venugopal, Eur. J. Inorg. Chem. **2019**, 2019, 3265–3269.

[136] M. S. Hill, D. J. Liptrot, C. Weetman, Chem. Soc. Rev. **2016**, 45, 972–988.

[137] P. Molina, M. J. Lidón, A. Tárraga, Tetrahedron **1994**, 50, 10029–10036.

[138] L. Fan, B. M. Foxman, O. V. Ozerov, Organometallics **2004**, 23, 326–328.

[139] M. B. Kindervater, T. Hynes, K. M. Marczenko, S. S. Chitnis, Dalt. Trans. **2020**, DOI 10.1039/D0DT01413C.

[140] J. C. DeMott, C. Guo, B. M. Foxman, D. V. Yandulov, O. V. Ozerov, Mendeleev Commun. **2007**, 17, 63–65.

[141] K. Yurkerwich, G. Parkin, in Inorganica Chim. Acta, Elsevier S.A., **2010**, pp. 157–161.

[142] M. Mantina, A. C. Chamberlin, R. Valero, C. J. Cramer, D. G. Truhlar, J. Phys. Chem. A **2009**, 113, 5806–5812.

[143] B. Cordero, V. Gómez, A. E. Platero-Prats, M. Revés, J. Echeverría, E. Cremades, F. Barragán, S. Alvarez, J. Chem. Soc. Dalt. Trans. **2008**, 2832–2838.

[144] D. E. Herbert, A. D. Miller, O. V. Ozerov, Chem. - A Eur. J. **2012**, 18, 7696–7704.

[145] J. C. Demott, P. Surawatanawong, S. M. Barnett, C. H. Chen, B. M. Foxman, O. V. Ozerov, Dalt. Trans. **2011**, 40, 11562–11570.

[146] Z. R. Turner, Inorg. Chem. **2019**, 58, 14212–14227.

APPENDIX A: NMR SPECTRA FOR CHAPTER 2

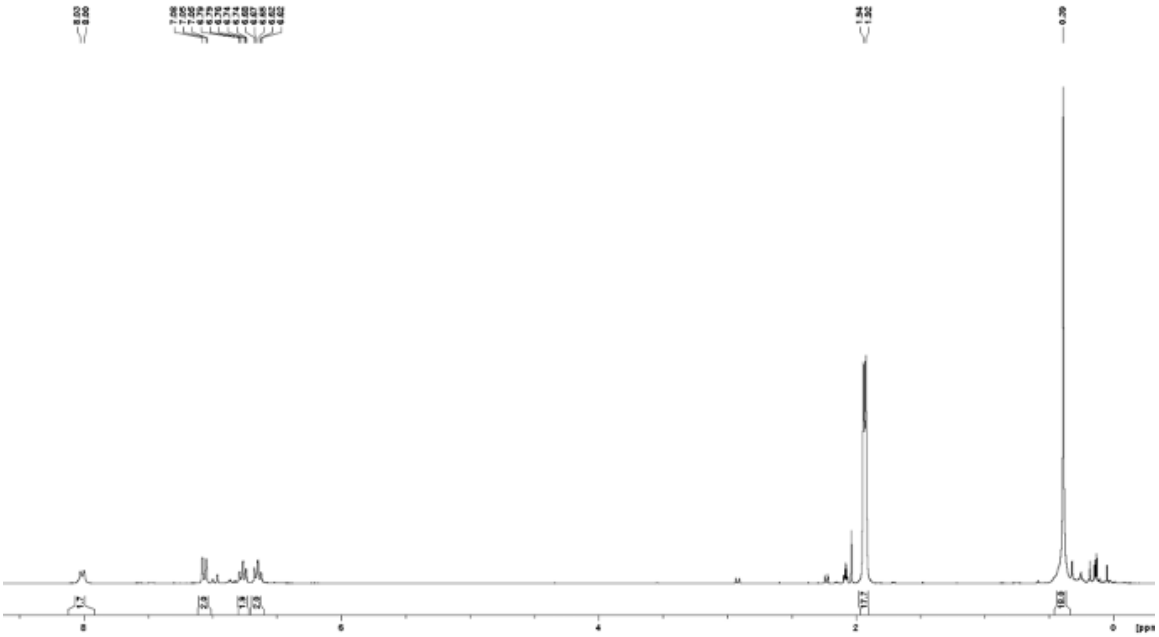

Figure A1. ^{1}H NMR spectrum of in-situ generated compound **1** tol-d_8.

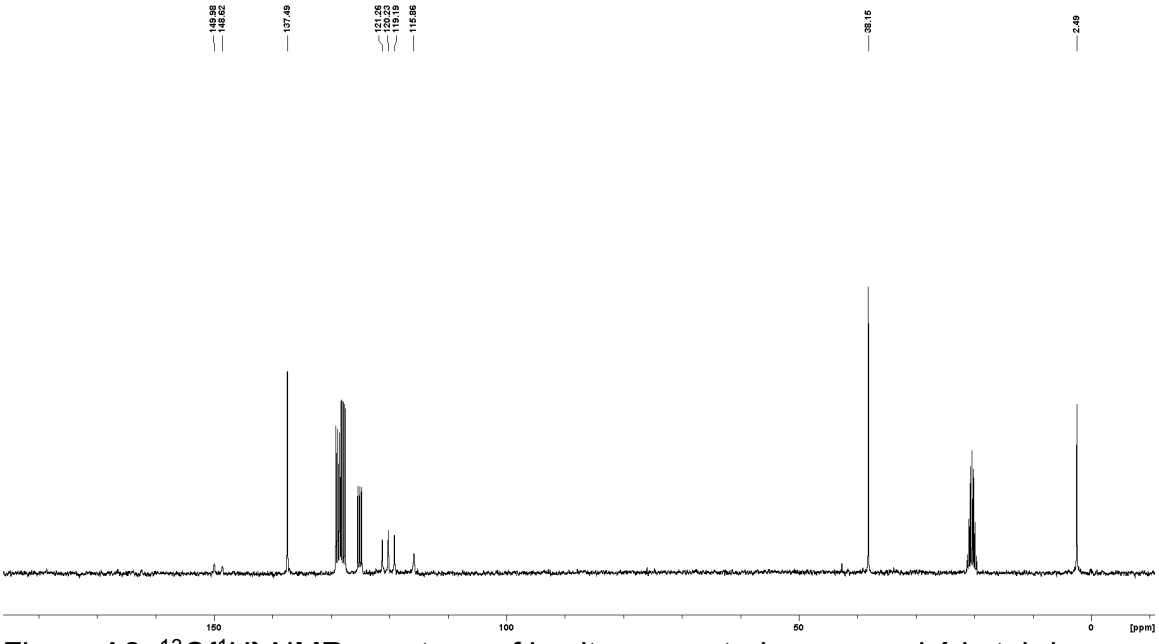

Figure A2. $^{13}C\{^{1}H\}$ NMR spectrum of in-situ generated compound **1** in tol-d_8.

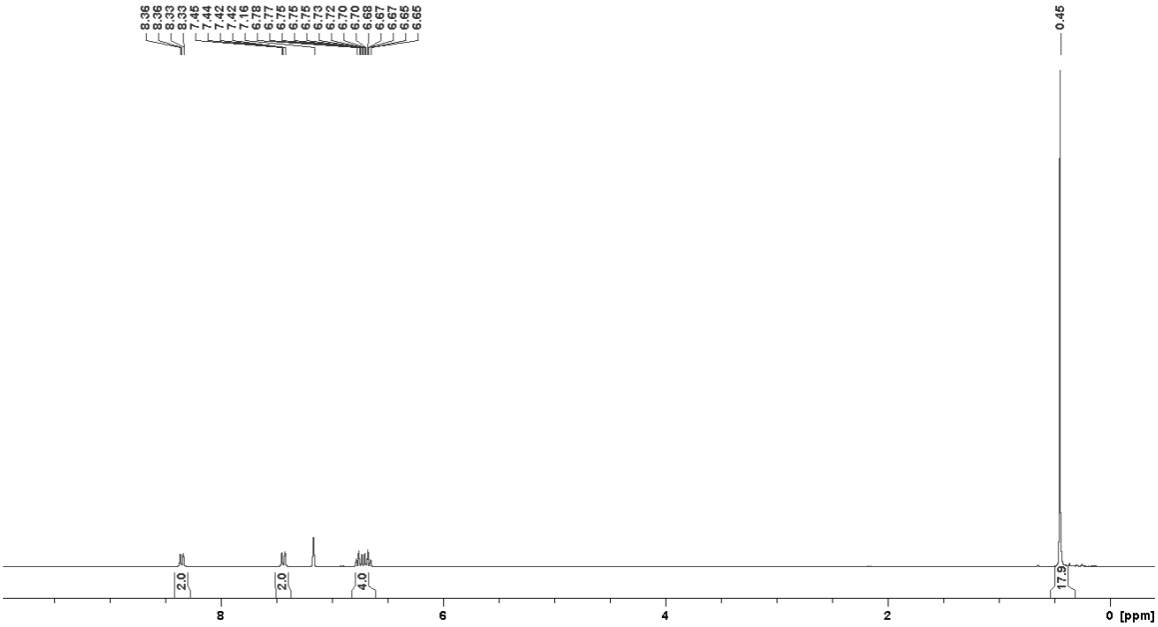

Figure A3. ^{1}H NMR spectrum of compound **2** in C_6D_6.

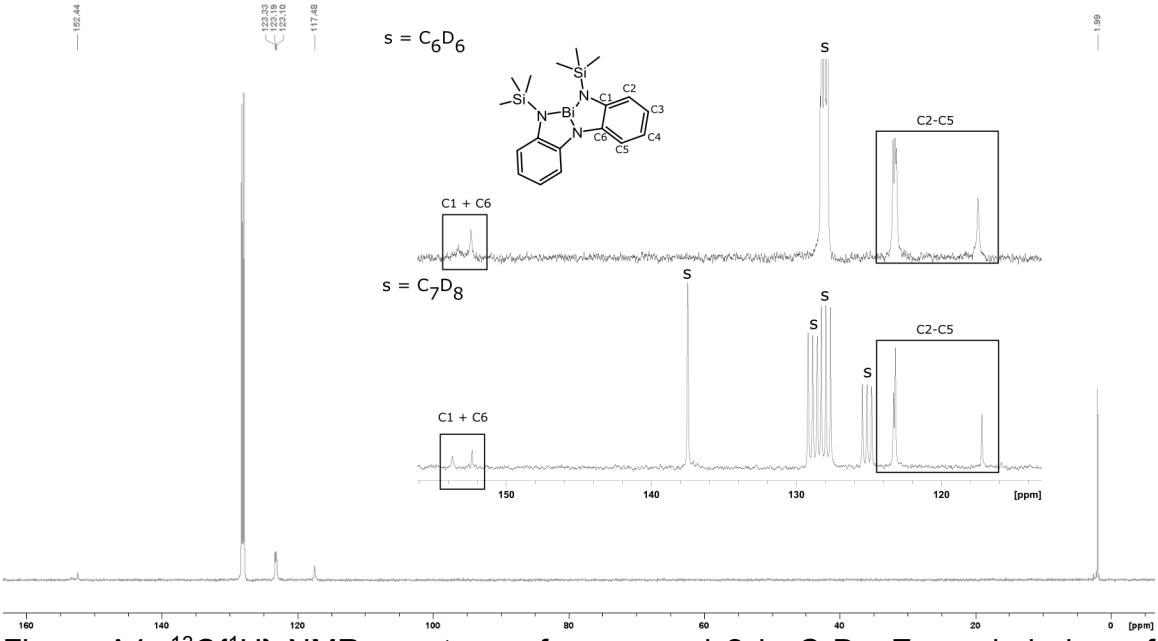

Figure A4. $^{13}C\{^{1}H\}$ NMR spectrum of compound **2** in C_6D_6. Expanded view of aromatic region in C_6D_6 and C_7D_8 showing appropriate number of peaks.

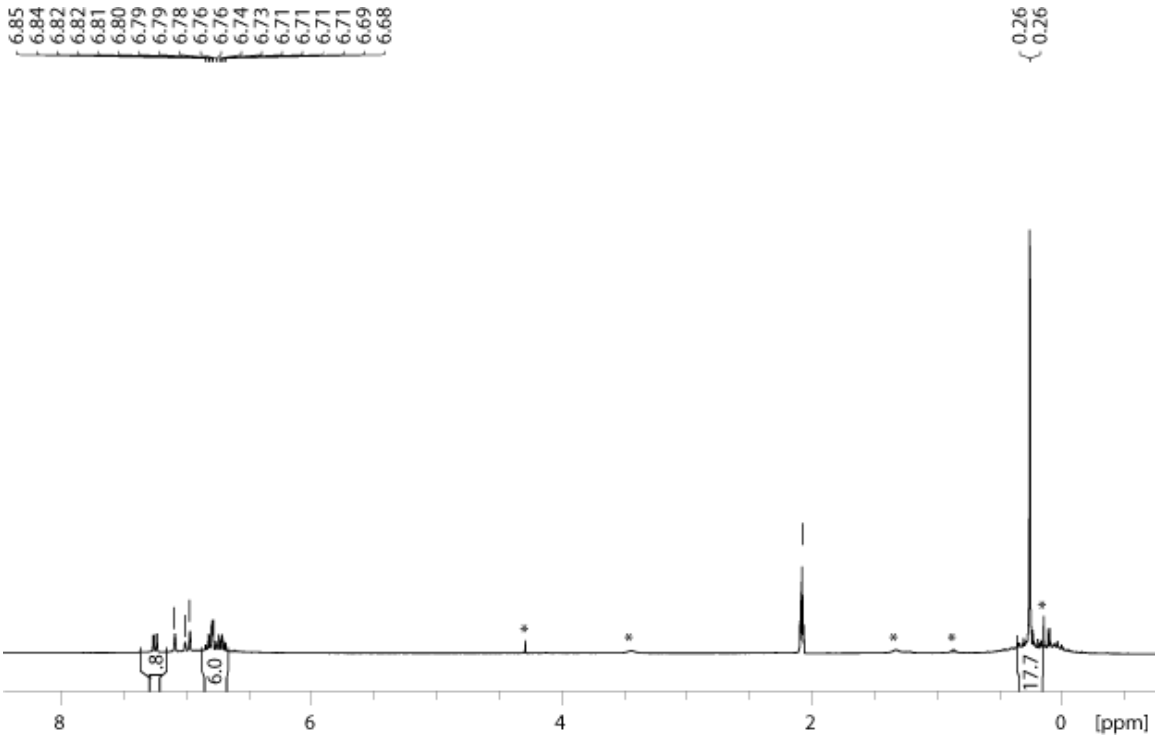

Figure A5. ^{1}H NMR spectrum of compound **3** in tol-d_8. Asterisks denote peaks due to residual DCM, THF, and pentane. Vertical lines denote toluene-d8

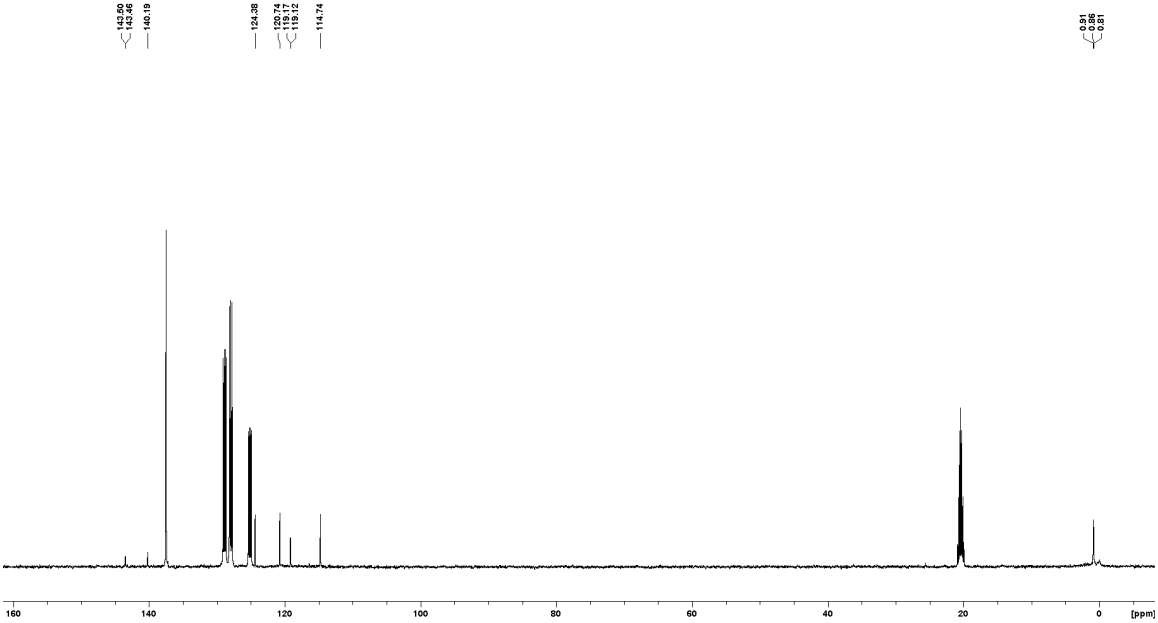

Figure A6. $^{13}C\{^{1}H\}$ NMR spectrum of compound **3** in tol-d_8.

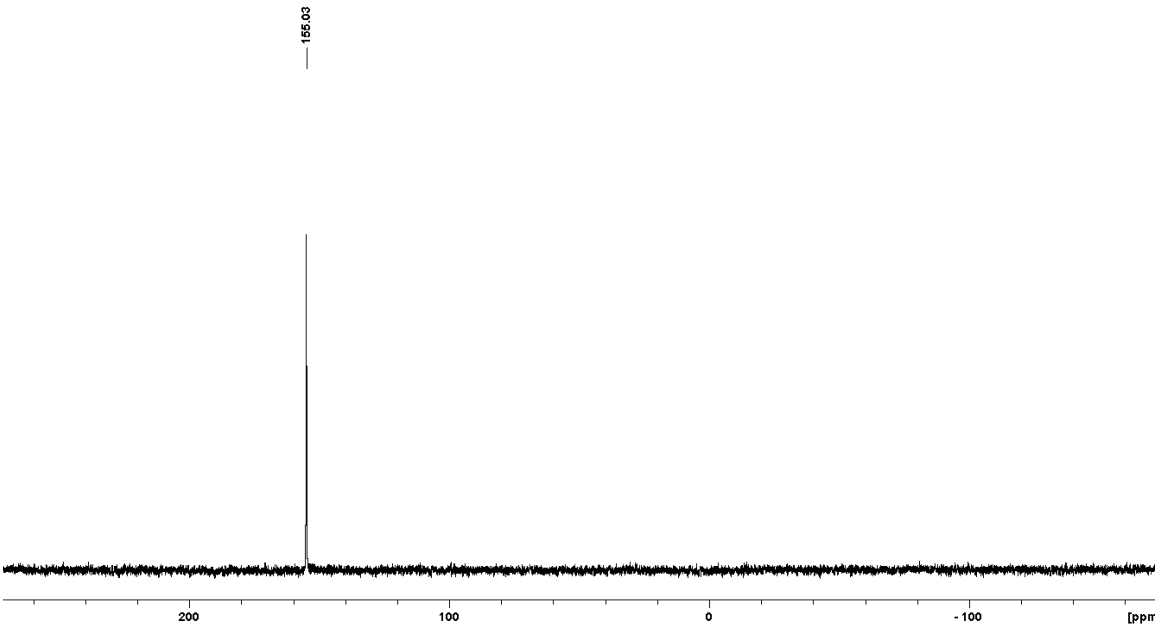

Figure A7. ^{31}P NMR spectrum of **3** in C_6D_6.

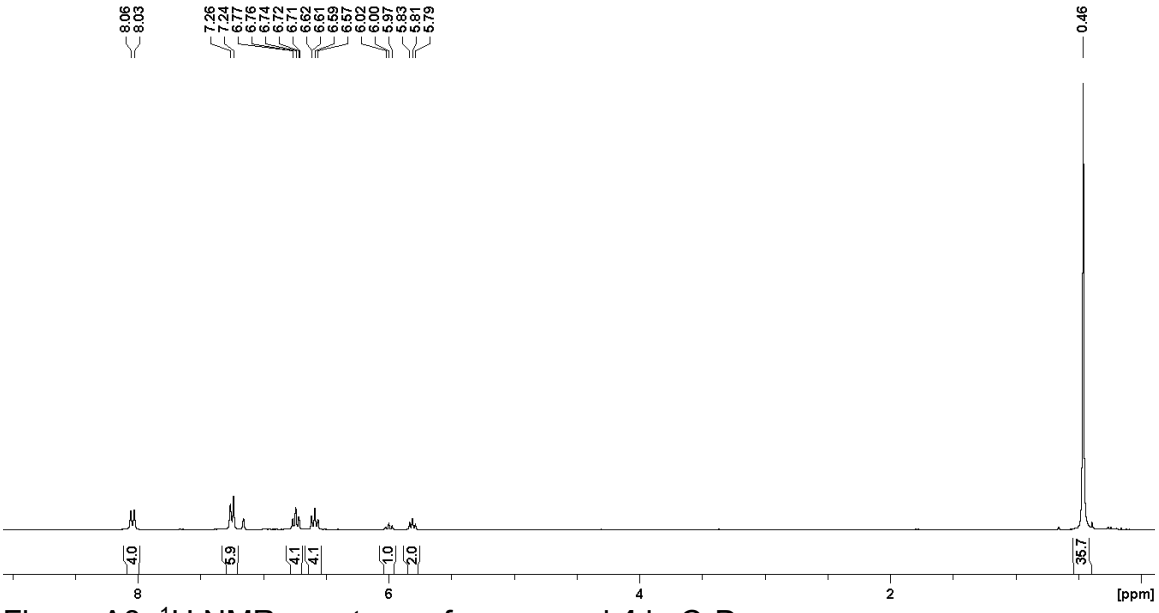

Figure A8. ^{1}H NMR spectrum of compound **4** in C_6D_6.

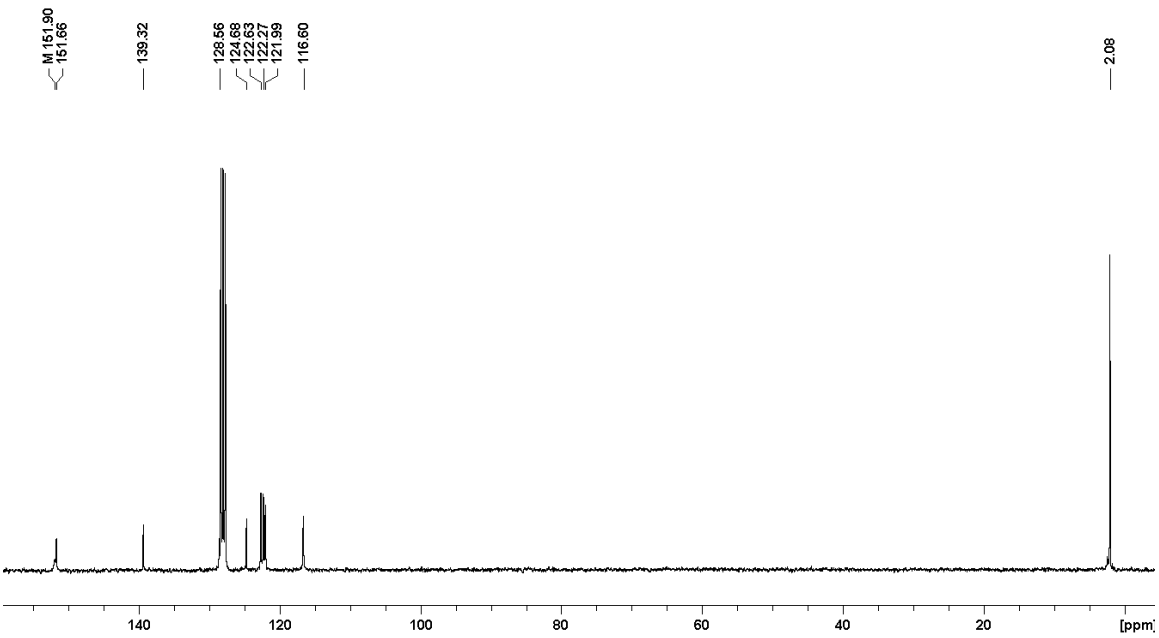

Figure A9. $^{13}C\{^{1}H\}$ NMR spectrum of compound **4** in C_6D_6.

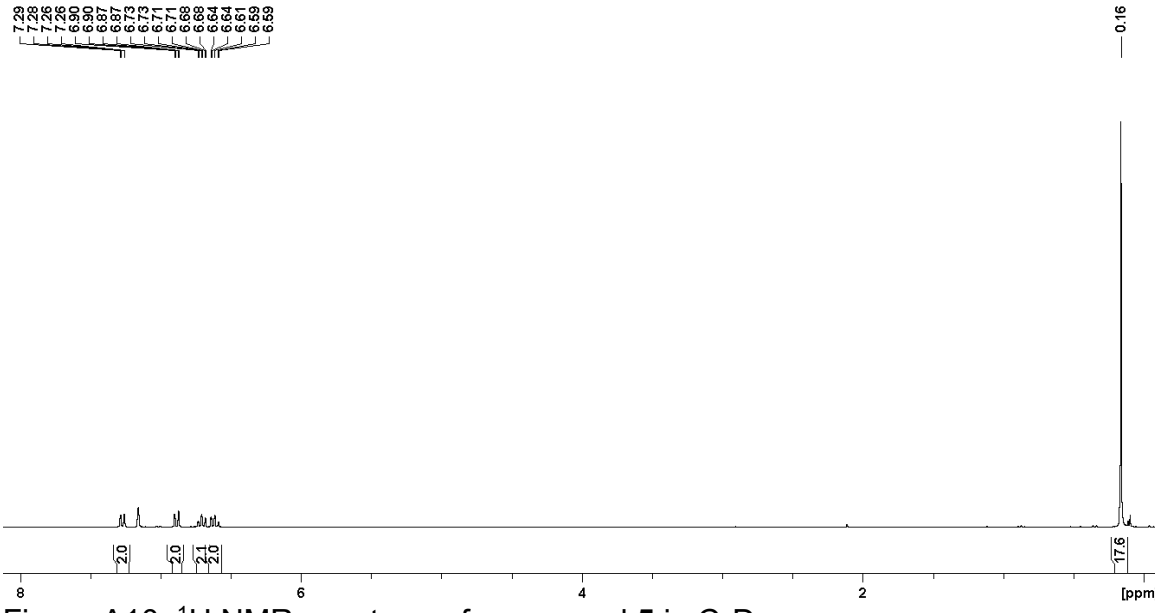

Figure A10. ^{1}H NMR spectrum of compound **5** in C_6D_6.

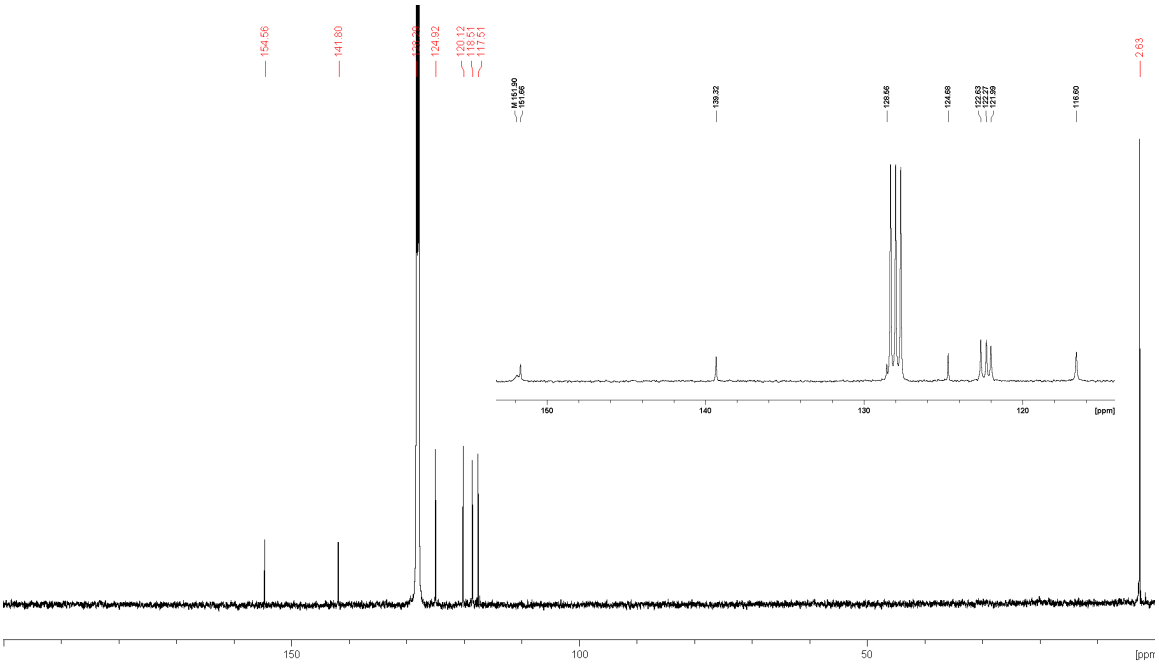

Figure A11. $^{13}C\{^{1}H\}$ NMR spectrum of compound **5** in C_6D_6. Expansion of region from 120-150 ppm shown.

APPENDIX B: NMR SPECTRA FOR CHAPTER 3

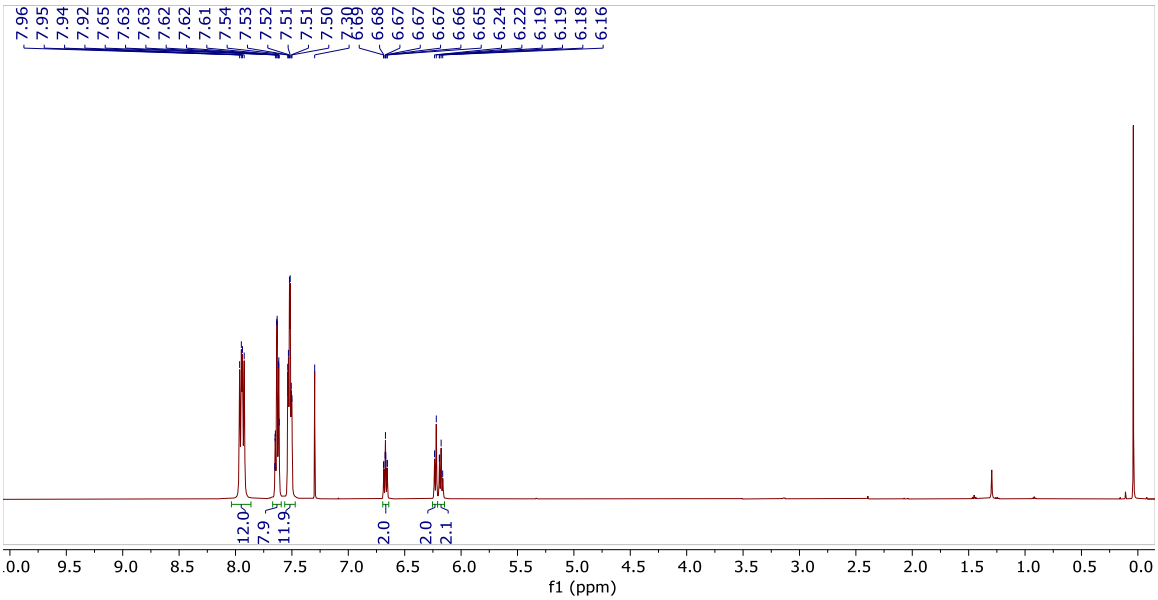

Figure B1. ^{1}H NMR spectrum of **1** in $CDCl_3$.

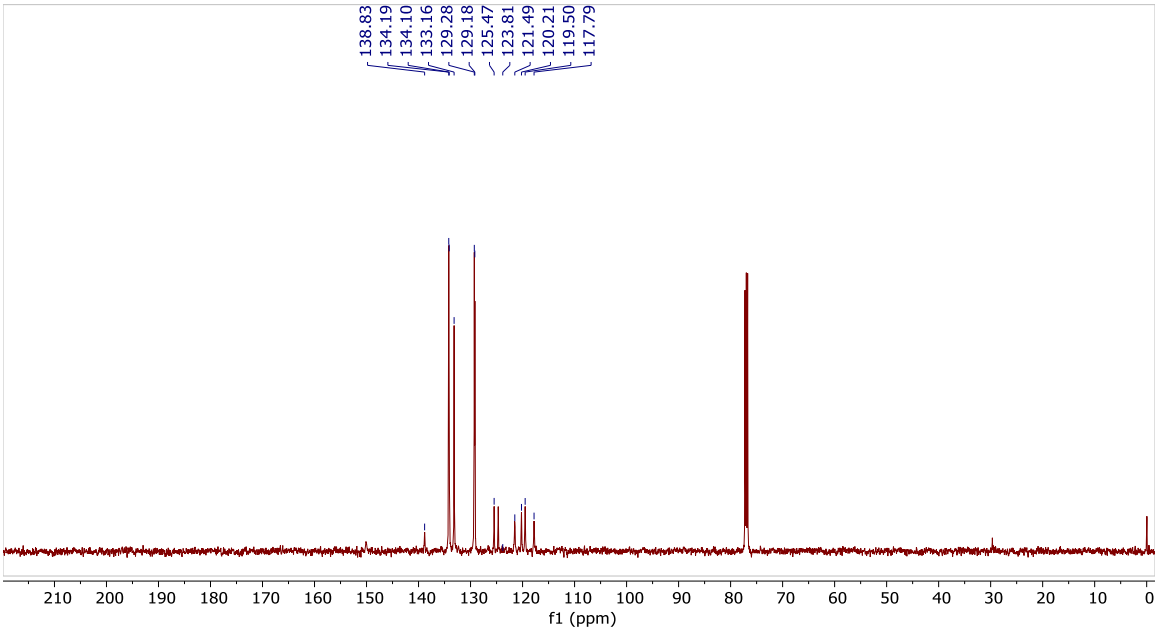

Figure B2. $^{13}C\{^{1}H\}$ NMR spectrum of **1** in $CDCl_3$.

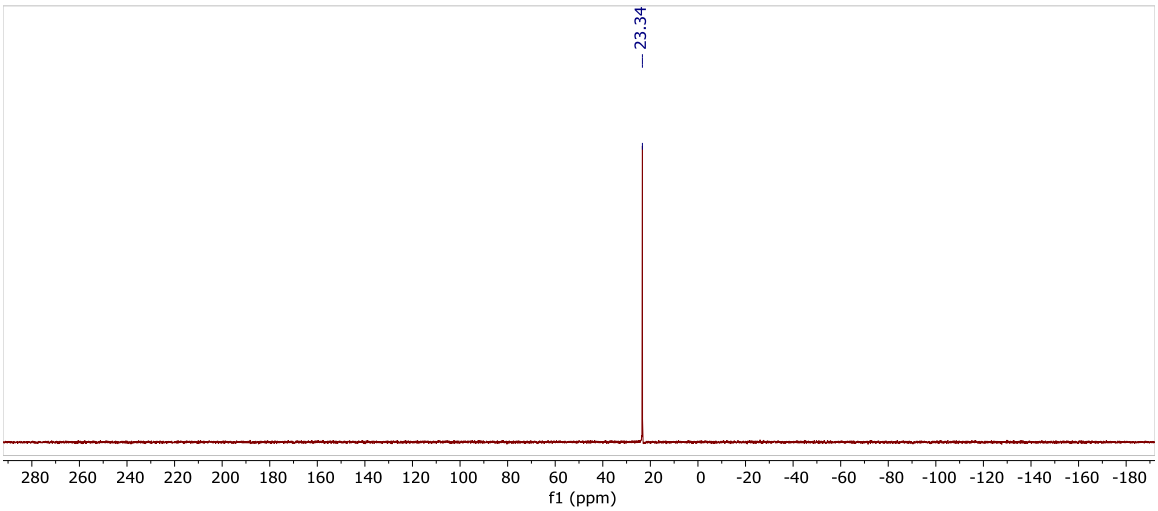

Figure B3. $^{31}P\{^{1}H\}$ NMR spectrum of **1** in $CDCl_3$.

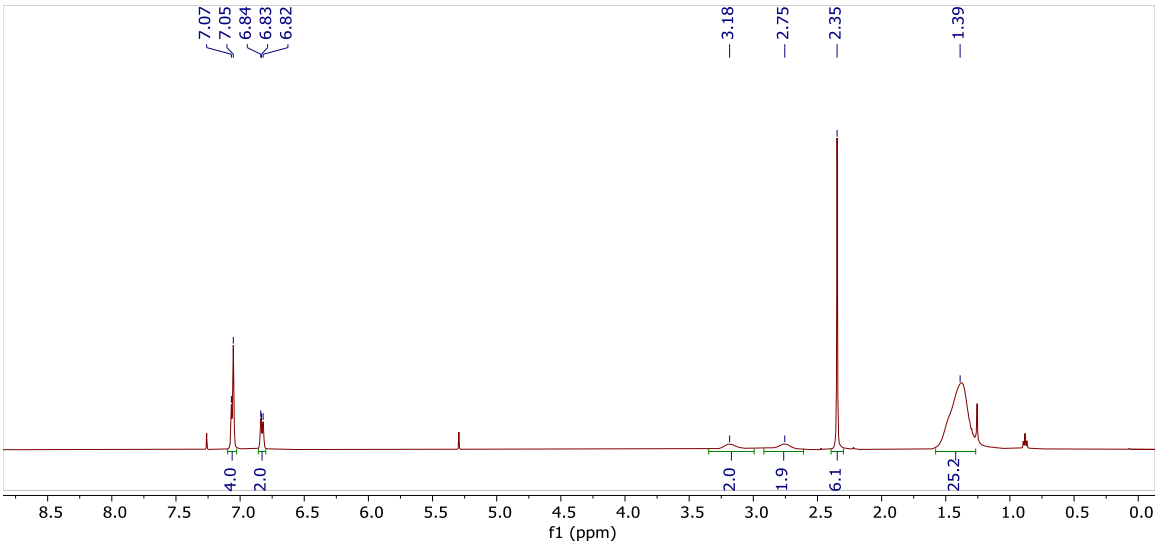

Figure B4. ^{1}H NMR spectrum of **2** in $CDCl_3$. Traces of residual pentane in deuterated solvent seen at 0.8 ppm and 1.5 ppm.

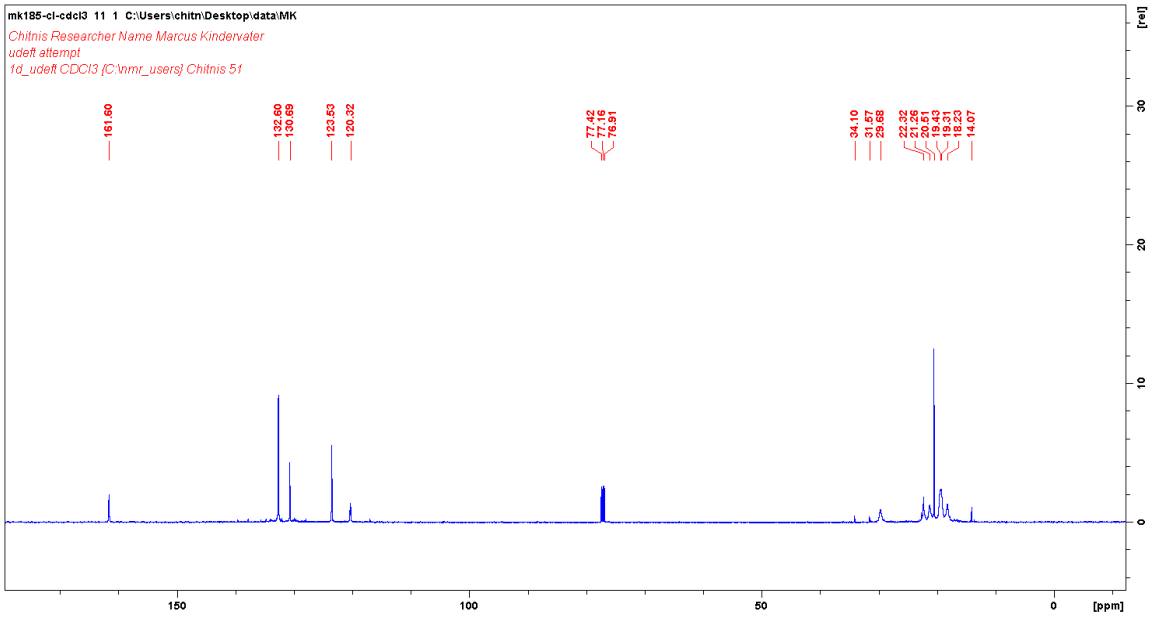

Figure B5. $^{13}C\{^{1}H\}$ NMR spectrum of **2** in $CDCl_3$.

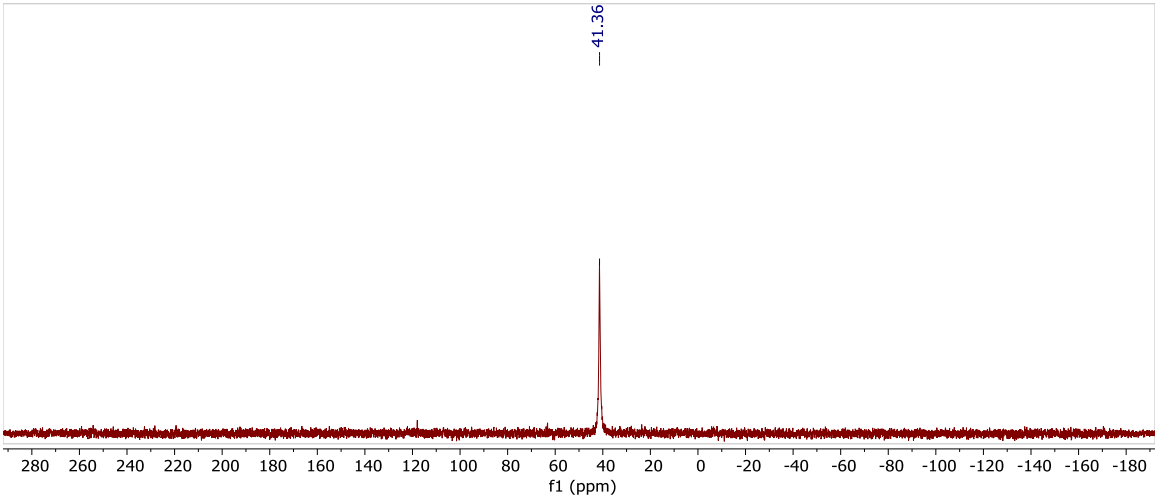

Figure B6. $^{31}P\{^{1}H\}$ NMR spectrum of **2** in $CDCl_3$.

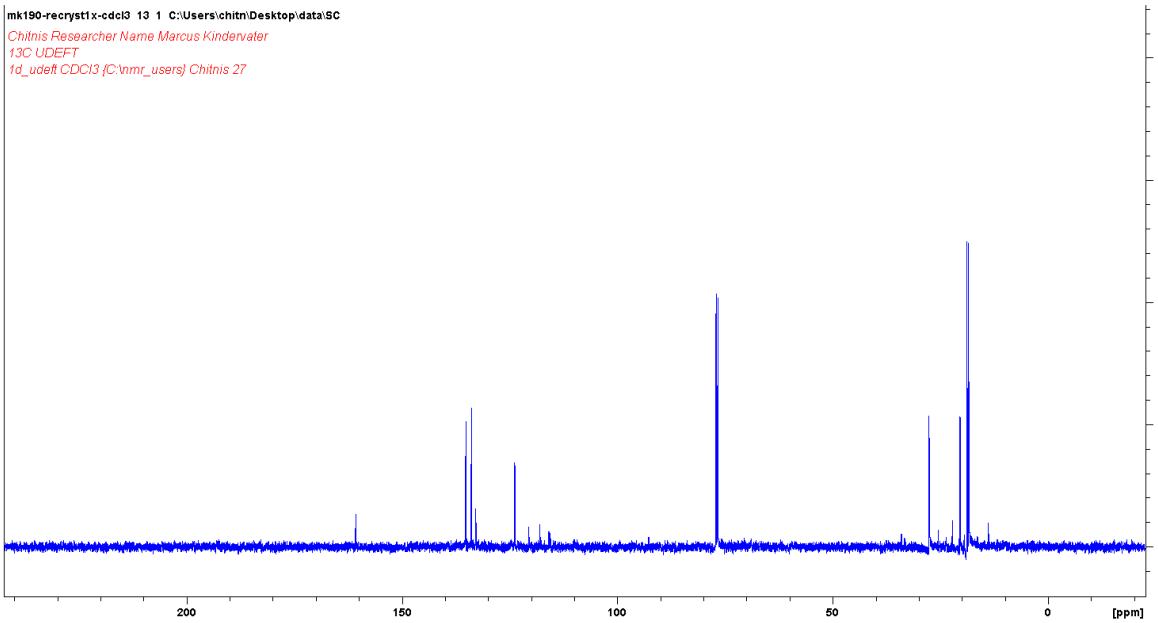

Figure B8. ^{13}C NMR spectrum of **3** in $CDCl_3$.

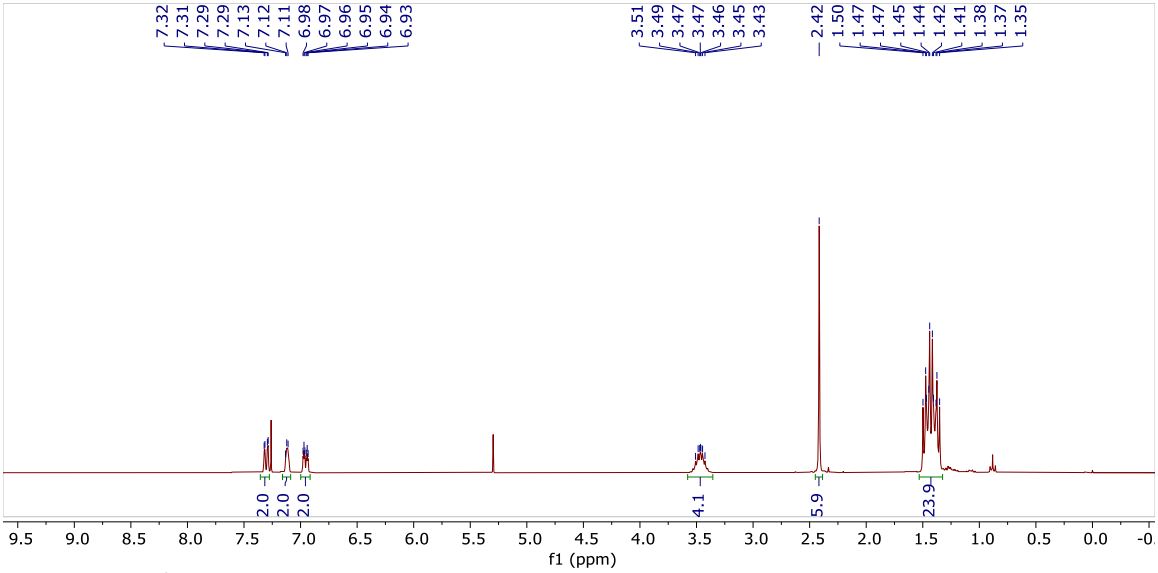

Figure B8. ^{1}H NMR spectrum of **3** in $CDCl_3$. Traces of residual pentane and DCM in deuterated solvent seen at 0.8 ppm and 1.5 and 5.4 ppm.

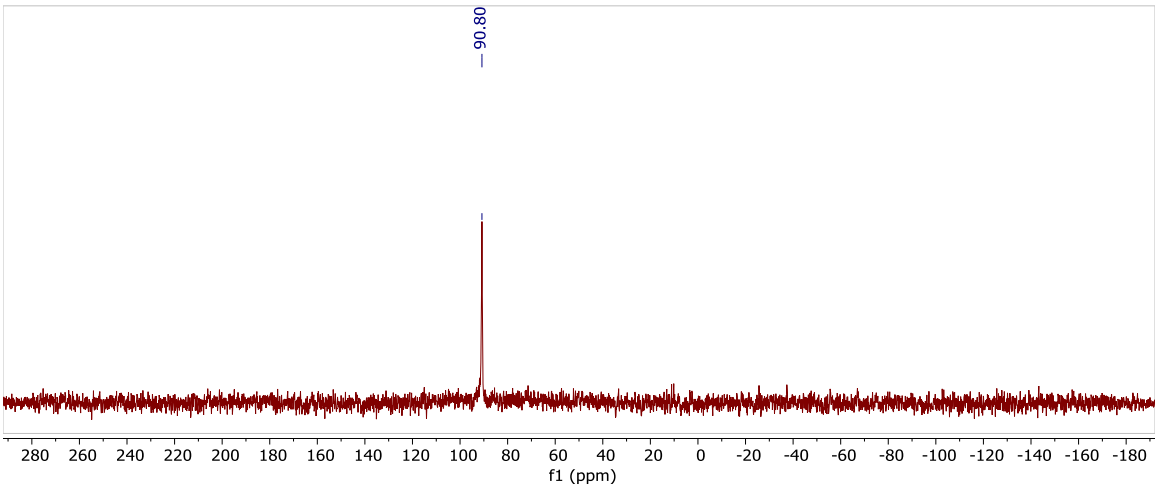

Figure B9. $^{31}P\{^{1}H\}$ NMR spectrum of **3** in $CDCl_3$.

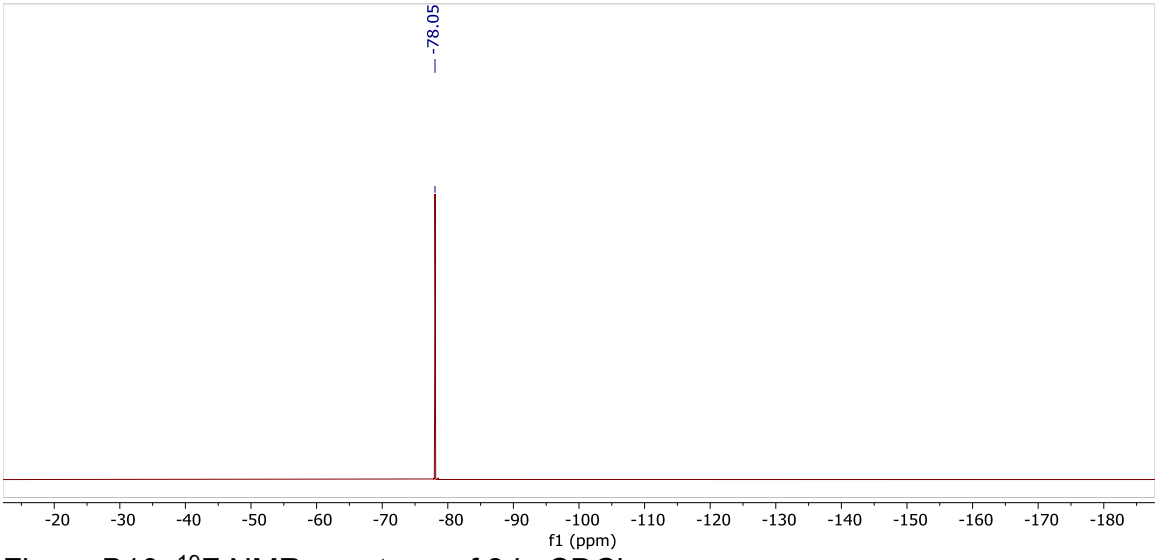

Figure B10. ^{19}F NMR spectrum of **3** in $CDCl_3$.

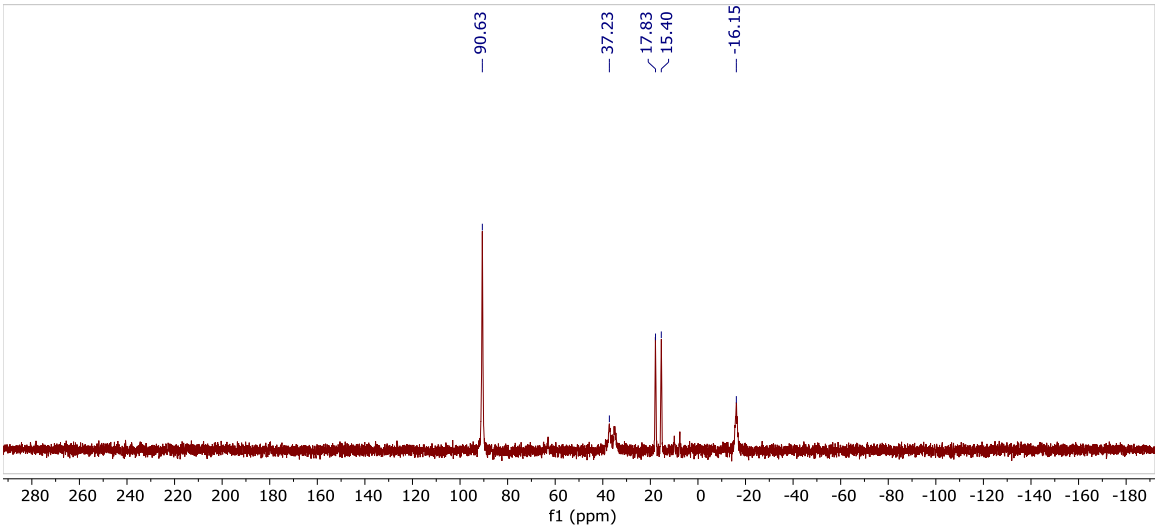

Figure B11. $^{31}P\{^{1}H\}$ NMR spectrum of **3** in protic DCM. Observing thermal degradation and formation of **2** (37.2 ppm) by solvent activation.

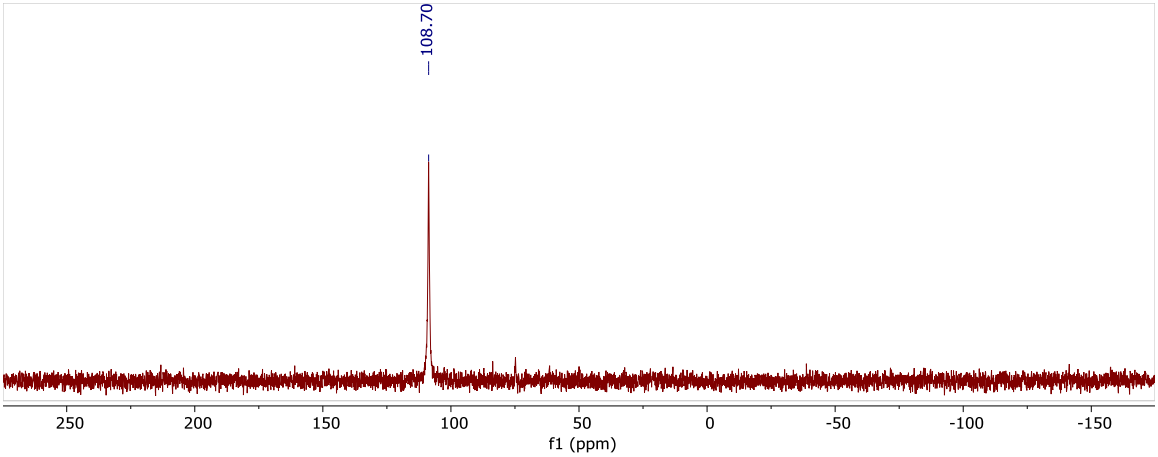

Figure B12. $^{31}P\{^{1}H\}$ NMR spectrum of **4** in 1,2-difluorobenzene.

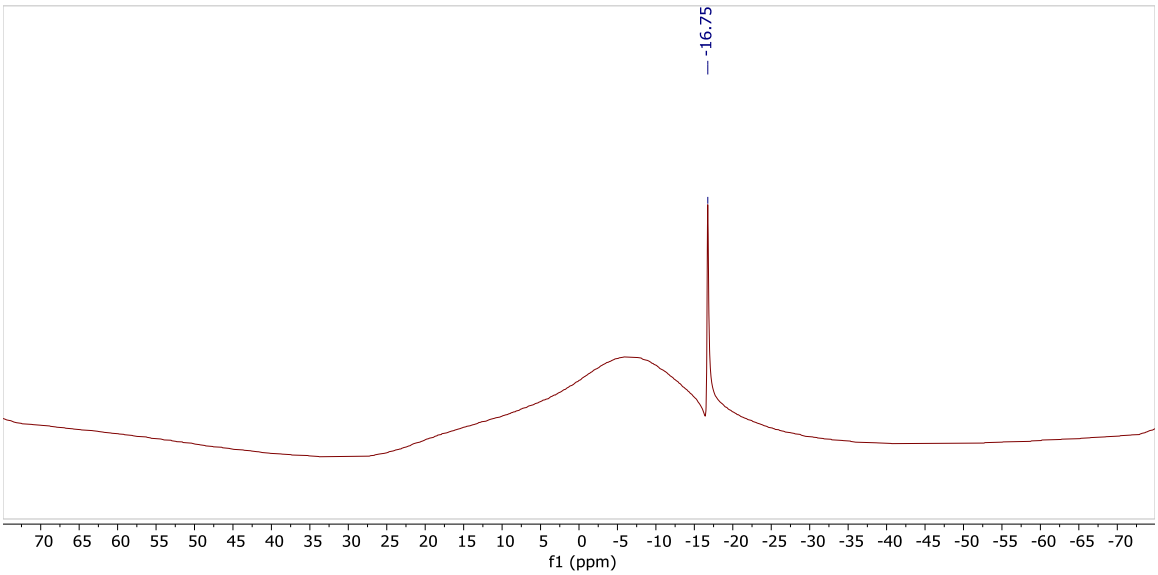

Figure B13. ^{11}B NMR spectrum of **4** in 1,2-difluorobenzene.

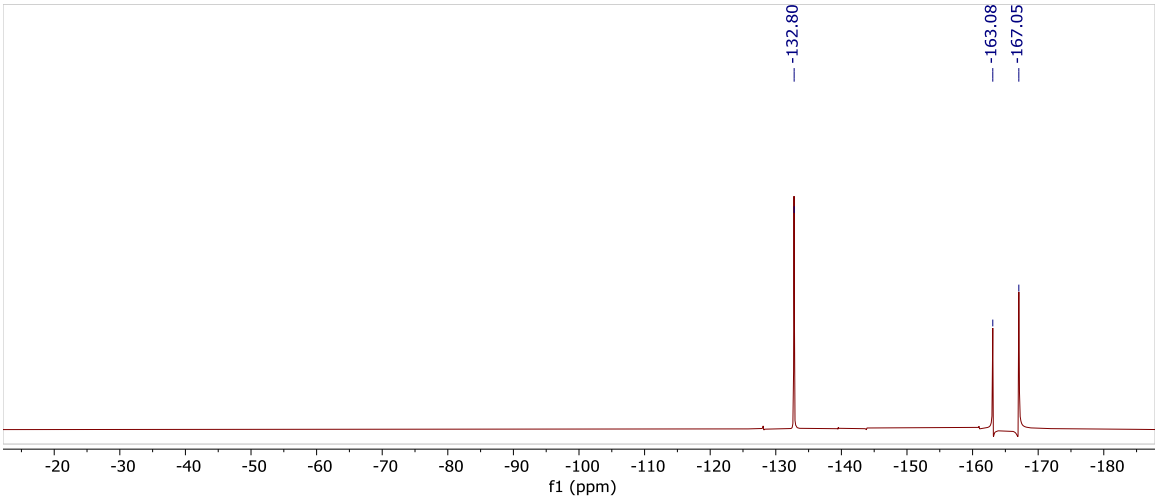

Figure B13. ^{19}F NMR spectrum of **4** in DCM. Small impurities suspected to be a result of solvent activation.

APPENDIX C: X-RAY CRYSTALLOGRAPHIC DATA

Table 2. Summary of crystal data for Chapter 2, compounds **N_3H_3**, **1**, **2** and **4**.

Compound	**N_3H_3**	**1**	**2**	**4**
Empirical formula	$C_{18}H_{29}N_3Si_2$	$C_{22}H_{40}BiN_5Si_2$	$C_{18}H_{26}BiN_3Si_2$	$C_{41}H_{57}Bi_2N_7OSi_4$
Formula weight	343.62	639.75	549.58	1194.25
Temperature/K	125(2)	124.99	131.29	125(2)
Crystal system	monoclinic	triclinic	triclinic	monoclinic
Space group	$P2_1/c$	P-1	P-1	$P2_1/c$
a/Å	10.237(4)	12.194(3)	9.8858(2)	13.0568(15)
b/Å	18.709(7)	13.995(4)	10.3897(2)	16.4347(19)
c/Å	10.697(4)	16.164(5)	11.2447(2)	21.675(3)
α/°	90	75.848(4)	96.7700(10)	90
β/°	97.407(5)	89.662(4)	111.2830(10)	90.555(2)
γ/°	90	88.712(4)	103.4480(10)	90
Volume/$Å^3$	2031.5(12)	2674.0(13)	1020.26(3)	4651.0(9)
Z	4	4	2	4
$\rho_{calc}g/cm^3$	1.123	1.589	1.789	1.706
μ/mm^{-1}	0.178	6.701	8.763	7.699
F(000)	744.0	1272.0	532.0	2328.0
Crystal size/mm^3	0.23 × 0.17 × 0.13	0.05 × 0.05 × 0.05	0.17 × 0.07 × 0.05	0.13 x 0.13 x 0.09
Radiation	MoKα (λ = 0.71073)	MoKα (λ = 0.71073)	MoKα (λ = 0.71073)	MoKα (λ = 0.71073)
2Θ range for data collection/°	4.012 to 56.74	2.598 to 58.598	3.988 to 58.482	3.11 to 58.598
Index ranges	-13 ≤ h ≤ 13, -24 ≤ k ≤ 24, -14 ≤ l ≤ 14	-16 ≤ h ≤ 16, -19 ≤ k ≤ 19, -21 ≤ l ≤ 21	-13 ≤ h ≤ 12, -14 ≤ k ≤ 13, -15 ≤ l ≤ 15	-17 ≤ h ≤ 17, -22 ≤ k ≤ 22, -29 ≤ l ≤ 29
Reflections collected	25153	33842	16099	58209
Independent reflections	5047 [R_{int} = 0.0551, R_{sigma} = 0.0479]	13351 [R_{int} = 0.0824, R_{sigma} = 0.1189]	5104 [R_{int} = 0.0513, R_{sigma} = 0.0630]	12036 [R_{int} = 0.0916, R_{sigma} = 0.0855]
Data/restraints/parameters	5047/0/214	13351/1/549	5104/0/223	12036/0/509
Goodness-of-fit on F^2	1.031	0.970	1.045	0.982
Final R indexes [I>=2σ (I)]	R_1 = 0.0479, wR_2 = 0.1097	R_1 = 0.0728, wR_2 = 0.1719	R_1 = 0.0354, wR_2 = 0.0560	R_1 = 0.0432, wR_2 = 0.0745
Final R indexes [all data]	R_1 = 0.0779, wR_2 = 0.1253	R_1 = 0.1179, wR_2 = 0.1991	R_1 = 0.0474, wR_2 = 0.0594	R_1 = 0.0842, wR_2 = 0.0875
Largest diff. peak/hole / e $Å^{-3}$	0.99/-0.25	11.54/-3.87	1.50/-2.06	1.16/-1.45

APPENDIX D: COMPUTATIONAL DETAILS

Computational details for Chapter 2

Calculations were performed using Gaussian 09.[1] Geometry optimizations and frequency calculations for **2**, **3** and **5** were carried out at the PBE1PBE-D3/def2-tzvpd or PBE1PBE-D/SVPD level (for **5**). The UV-VIS spectrum of **2** was calculated in a field of pentane (PCM model) at the same level. NBO calculations were performed on structures optimized at the SVPD level as were potential energy scans of the N-E-N-N dihedral angles.

Cartesian coordinates for compound 2

Theory: PBE1PBE-D3
Basis Set: Def2-tzvpd

7	-0.000056	1.330316	-0.000195
6	-1.208722	1.954855	-0.200287
6	-2.368223	1.124349	-0.090619
6	-1.365864	3.288768	-0.613852
6	-3.631517	1.739893	-0.228863
6	-2.614346	3.838765	-0.788833
1	-0.492939	3.879517	-0.848906
6	-3.755883	3.067477	-0.556200
1	-4.522169	1.137979	-0.101876
1	-2.705575	4.865446	-1.123010
1	-4.741692	3.504583	-0.668374
6	1.208563	1.954890	0.200071
6	2.368122	1.124489	0.090249
6	1.365597	3.288681	0.614072
6	3.631367	1.740089	0.228665
6	2.614032	3.838708	0.789276
1	0.492620	3.879278	0.849315
6	3.755632	3.067580	0.556406
1	4.522059	1.138270	0.101509
1	2.705178	4.865276	1.123821
1	4.741406	3.504724	0.668720
7	-2.179176	-0.200854	0.095808
7	2.179181	-0.200695	-0.096420
83	0.000024	-0.842810	-0.000388
14	-3.436836	-1.405186	0.254365
14	3.436989	-1.405036	-0.253865
6	4.482448	-1.090535	-1.776312
1	5.003236	-0.131721	-1.741511
1	5.234261	-1.877236	-1.889277
1	3.854406	-1.093515	-2.671156
6	4.503527	-1.506155	1.284514

1	3.882679	-1.717802	2.159378
1	5.231606	-2.316831	1.185627
1	5.053097	-0.584784	1.485145
6	2.605757	-3.074755	-0.466515
1	2.003014	-3.364255	0.399028
1	1.979190	-3.125322	-1.361016
1	3.386751	-3.833274	-0.577349
6	-2.605444	-3.074603	0.468737
1	-2.002195	-3.364675	-0.396264
1	-1.979321	-3.124323	1.363597
1	-3.386339	-3.833194	0.579746
6	-4.503421	-1.507966	-1.283861
1	-3.883592	-1.727959	-2.157417
1	-5.236482	-2.313673	-1.181039
1	-5.047209	-0.584243	-1.489456
6	-4.482331	-1.089368	1.776535
1	-5.006457	-0.132469	1.739238
1	-5.231385	-1.878298	1.892316
1	-3.853700	-1.087543	2.670975

Cartesian coordinates for 3

Theory: PBE1PBE-D3
Basis Set: Def2-tzvpd

7	-0.404837	1.328651	-1.058466
6	-1.819376	1.304774	-0.904080
6	-2.255544	0.110065	-0.305846
6	-2.694529	2.311534	-1.242810
6	-3.610187	-0.038263	-0.030693
6	-4.049672	2.153559	-0.960495
1	-2.322826	3.206857	-1.727058
6	-4.491295	0.989308	-0.354537
1	-3.989540	-0.941430	0.429720
1	-4.752859	2.934672	-1.222410
1	-5.546124	0.863006	-0.137511
6	0.317120	1.987346	-0.036405
6	1.379507	1.224045	0.457190
6	0.052064	3.242260	0.480286
6	2.170674	1.714017	1.482309
6	0.857848	3.734959	1.501149
1	-0.781328	3.821990	0.103792
6	1.909549	2.980019	1.996546
1	2.978354	1.117109	1.887519
1	0.653078	4.715405	1.914962
1	2.529261	3.369996	2.795400
7	-1.227517	-0.810853	-0.087776
7	1.511025	-0.008685	-0.216179

14	-1.427371	-2.351682	0.729446
14	3.099634	-0.707858	-0.587465
6	4.225328	0.681482	-1.124392
1	4.355857	1.432095	-0.341967
1	5.212261	0.286988	-1.383478
1	3.818642	1.184764	-2.005962
6	3.818523	-1.574814	0.905842
1	3.220965	-2.444662	1.187235
1	4.826345	-1.927528	0.667205
1	3.896956	-0.922725	1.778819
6	2.907432	-1.939019	-1.975859
1	2.242974	-2.766187	-1.720064
1	2.525979	-1.470554	-2.884984
1	3.893118	-2.361141	-2.196443
6	0.259815	-3.143689	0.823767
1	0.678073	-3.347857	-0.165526
1	0.958039	-2.506299	1.370586
1	0.183230	-4.097886	1.352694
6	-2.580232	-3.480499	-0.218506
1	-2.195474	-3.652046	-1.227776
1	-2.657402	-4.450663	0.281961
1	-3.588801	-3.073193	-0.314038
6	-2.056808	-2.039441	2.460871
1	-3.009472	-1.504631	2.473569
1	-2.195541	-2.986568	2.991193
1	-1.331915	-1.439032	3.018679
15	0.119632	-0.338437	-1.140194

Cartesian coordinates for 5

Theory: PBE1PBE-D3
Basis Set: SVPD

7	0.197328	2.018354	-0.370834
6	-0.994150	2.430000	-0.876016
6	-2.176853	2.041906	-0.129633
6	-1.154678	3.110382	-2.111547
6	-3.423021	2.597161	-0.558995
6	-2.389152	3.543443	-2.529324
1	-0.293734	3.228901	-2.765625
6	-3.525643	3.325288	-1.716012
1	-4.316184	2.381973	0.024235
1	-2.493970	4.032039	-3.498465
1	-4.500574	3.697974	-2.034382
6	1.424765	2.504084	-0.671773
6	2.560169	1.754977	-0.160241
6	1.663490	3.739996	-1.335377
6	3.865450	2.215096	-0.528403

6	2.937713	4.163451	-1.615152
1	0.822600	4.385726	-1.573758
6	4.049071	3.369233	-1.240857
1	4.727052	1.627151	-0.219447
1	3.093089	5.125572	-2.104533
1	5.059197	3.692812	-1.497059
7	-2.051253	1.171873	0.869285
7	2.336038	0.696341	0.610755
83	0.101628	0.339055	1.159267
14	-3.359243	0.512592	1.873953
14	3.572899	-0.291425	1.425693
6	4.543536	-1.270118	0.153004
1	5.143160	-0.620462	-0.499754
1	5.228135	-1.968582	0.657858
1	3.873311	-1.860522	-0.485412
6	4.710125	0.782550	2.474436
1	4.119575	1.481947	3.084348
1	5.281071	0.139183	3.161075
1	5.430997	1.369717	1.890932
6	2.679393	-1.441713	2.615083
1	2.248084	-0.890435	3.463915
1	1.892638	-2.050174	2.150832
1	3.417653	-2.146092	3.026546
6	-2.566449	-0.632568	3.137205
1	-1.999653	-1.457709	2.683590
1	-1.913861	-0.094565	3.840297
1	-3.369827	-1.098441	3.727494
6	-4.564141	-0.466036	0.818401
1	-4.076009	-1.358775	0.405157
1	-5.414137	-0.801895	1.430862
1	-4.958204	0.118409	-0.023548
6	-4.228815	1.888326	2.818725
1	-4.841415	2.539505	2.181138
1	-4.892016	1.446406	3.577982
1	-3.493843	2.519876	3.338948
6	-0.483267	-3.106815	-2.408295
6	1.261681	-2.998335	-0.252547
6	1.121863	-0.684081	-2.055285
6	-1.796755	-0.711513	-1.758042
6	-1.547194	-2.804912	0.238023
8	-0.630940	-3.869585	-3.260794
8	2.070289	-3.740069	0.092328
8	-2.283487	-3.391388	0.899629
8	1.871726	-0.058041	-2.656357
8	-2.679625	-0.164056	-2.242792
74	-0.231903	-1.786447	-0.954355

Computational details for Chapter 3

All calculations were performed using the Gaussian 16 Suite.[1] The B3LYP function was employed with Grimme's D3-BJ dispersion correction.[2] Geometries were optimized using the cc-pvdz basis set for non-Bi atoms and aug-cc-pvdz-PP + ECM60MDF at bismuth.[3] Cartesian coordinates are given below.

[PNP-Bi]$^{2+}$

Bi	-0.04062	-1.32791	-0.86824
P	1.78798	-0.66369	1.02599
P	-2.42046	-0.50828	-0.03277
N	0.17080	0.84482	-1.09128
C	-0.78570	1.71502	-0.51243
C	4.31958	1.89681	-1.00150
C	3.79666	0.96830	-0.09217
H	4.47328	0.50635	0.62906
C	-2.97438	2.15835	0.52834
H	-3.93478	1.78364	0.88294
C	2.43636	0.61275	-0.11067
C	1.56390	1.19827	-1.06199
C	-2.72013	3.52501	0.60542
C	3.44399	2.44135	-1.95786
H	3.83205	3.14390	-2.69853
C	-1.47202	3.96721	0.12609
H	-1.22885	5.03112	0.17515
C	2.09523	2.09084	-1.99953
H	1.43865	2.50706	-2.76467
C	-3.10975	-1.23063	1.54276
H	-3.10874	-2.30997	1.31056
C	-0.53578	3.09992	-0.42146
H	0.40919	3.50087	-0.78135
C	1.46540	0.08837	2.70978
H	0.89785	-0.68225	3.25606
C	3.01823	-2.05133	1.16766
H	3.91661	-1.58071	1.60215
C	-2.18077	-0.97117	2.72917
H	-1.16163	-1.34332	2.54269
H	-2.57069	-1.49477	3.61481
H	-2.12598	0.10088	2.96757
C	-2.02788	1.25307	-0.00269
C	5.77367	2.28264	-0.98131
H	5.88561	3.36231	-0.79208
H	6.24794	2.07522	-1.95353
H	6.33049	1.74085	-0.20477
C	0.63522	1.36620	2.58088

H	1.18296	2.13906	2.02177
H	0.42988	1.76004	3.58768
H	-0.32502	1.20031	2.07759
C	2.80185	0.34733	3.42245
H	3.38300	-0.56855	3.59646
H	2.58657	0.79236	4.40641
H	3.42110	1.06658	2.86530
C	-2.99397	-0.32725	-2.76265
H	-2.71116	0.73164	-2.68031
H	-3.75024	-0.41653	-3.55653
H	-2.11477	-0.90389	-3.10047
C	2.48576	-3.11811	2.13245
H	2.29589	-2.72419	3.14131
H	3.22655	-3.92614	2.22759
H	1.55341	-3.57135	1.75433
C	-4.55553	-0.79198	1.82087
H	-4.60375	0.25578	2.14867
H	-4.95357	-1.41050	2.63987
H	-5.22033	-0.92529	0.95587
C	-3.89676	-2.37757	-1.53225
H	-2.99388	-2.98410	-1.72055
H	-4.58477	-2.55360	-2.37296
H	-4.38617	-2.75595	-0.62363
C	-3.56761	-0.88377	-1.45450
H	-4.47710	-0.31319	-1.19473
C	3.37093	-2.62723	-0.20761
H	2.52181	-3.17982	-0.64517
H	4.19204	-3.35130	-0.09710
H	3.69760	-1.85521	-0.91915
C	-3.72703	4.49452	1.16336
H	-4.04272	5.21728	0.39393
H	-3.29691	5.07534	1.99459
H	-4.62512	3.98116	1.53382

References for Computations

1. M. J. Frisch, G. W. Trucks, H. B. Schlegel, G. E. Scuseria, M. A. Robb, J. R. Cheeseman, G. Scalmani, V. Barone, G. A. Petersson, H. Nakatsuji, X. Li, M. Caricato, A. V. Marenich, J. Bloino, B. G. Janesko, R. Gomperts, B. Mennucci, H. P. Hratchian, J. V. Ortiz, A. F. Izmaylov, J. L. Sonnenberg, Williams, F. Ding, F. Lipparini, F. Egidi, J. Goings, B. Peng, A. Petrone, T. Henderson, D. Ranasinghe, V. G. Zakrzewski, J. Gao, N. Rega, G. Zheng, W. Liang, M. Hada, M. Ehara, K. Toyota, R. Fukuda, J. Hasegawa, M. Ishida, T. Nakajima, Y. Honda, O. Kitao, H. Nakai, T. Vreven, K. Throssell, J. A. Montgomery Jr., J. E. Peralta, F. Ogliaro, M. J. Bearpark, J. J. Heyd, E. N. Brothers, K. N. Kudin, V. N. Staroverov, T. A. Keith, R. Kobayashi, J. Normand, K. Raghavachari, A. P. Rendell, J. C. Burant, S. S. Iyengar, J. Tomasi, M. Cossi, J. M. Millam, M. Klene, C. Adamo, R. Cammi, J. W. Ochterski, R. L. Martin, K. Morokuma, O. Farkas, J. B. Foresman and D. J. Fox, Journal, 2016.

2. S. Grimme, S. Ehrlich and L. Goerigk, J. Comput. Chem., 2011, **32**, 1456-1465.

3. T. H. D. Jr., The Journal of Chemical Physics, 1989, **90**, 1007-1023.

APPENDIX E: COPYRIGHT PERMISSIONS

Royal Society of Chemistry - License Terms and Conditions

This is a License Agreement between Marcus B. Kindervater ("You") and Royal Society of Chemistry ("Publisher") provided by Copyright Clearance Center("CCC"). The license consists of your order details, the terms and conditions provided by Royal Society of Chemistry, and the CCC terms and conditions.

All payments must be made in full to CCC.

Order Date	22-Jul-2020	Type of Use	Republish in a thesis/dissertation
Order license ID	1050019-1		
ISSN	1477-9234	Publisher	ROYAL SOCIETY OF CHEMISTRY
		Portion	Chapter/article

LICENSED CONTENT

Publication Title	Dalton transactions	Country	United Kingdom of Great Britain and Northern Ireland
Author/Editor	Royal Society of Chemistry (Great Britain)	Rightsholder	Royal Society of Chemistry
Date	01/01/2003	Publication Type	e-Journal
Language	English		

REQUEST DETAILS

Portion Type	Chapter/article	Rights Requested	Main product
Page range(s)	Advance article	Distribution	Canada
Total number of pages	5	Translation	Original language of publication
Format (select all that apply)	Electronic	Copies for the disabled?	No
Who will republish the content?	Academic institution	Minor editing privileges?	No
Duration of Use	Life of current edition	Incidental promotional use?	No
Lifetime Unit Quantity	Up to 499	Currency	CAD

NEW WORK DETAILS

Title	Synthesis and Reactivity of Three Coordinate Bismuth Pincer Complexes	Institution name	Dalhousie University
		Expected presentation date	2020-08-17
Instructor name	Marcus B. Kindervater		

ADDITIONAL DETAILS

REUSE CONTENT DETAILS

Title, description or numeric reference of the portion(s)	Synthesis and Reactivity of Three Coordinate Bismuth Pincer Complexes	Title of the article/chapter the portion is from	Squeezing Bi: PNP and P2N3 pincer complexes of bismuth
Editor of portion(s)	N/A	Author of portion(s)	Royal Society of Chemistry (Great Britain)
Volume of serial or monograph	N/A	Issue, if republishing an article from a serial	N/A
Page or page range of portion	1-5	Publication date of portion	2020-05-20

JOHN WILEY AND SONS LICENSE
TERMS AND CONDITIONS

Aug 25, 2020

This Agreement between Dalhousie University -- Marcus Kindervater ("You") and John Wiley and Sons ("John Wiley and Sons") consists of your license details and the terms and conditions provided by John Wiley and Sons and Copyright Clearance Center.

License Number	4895930104600
License date	Aug 25, 2020
Licensed Content Publisher	John Wiley and Sons
Licensed Content Publication	Angewandte Chemie International Edition
Licensed Content Title	A Redox-Confused Bismuth(I/III) Triamide with a T-Shaped Planar Ground State
Licensed Content Author	Marcus B. Kindervater, Katherine M. Marczenko, Ulrike Werner-Zwanziger, et al
Licensed Content Date	May 2, 2019
Licensed Content Volume	58
Licensed Content Issue	23
Licensed Content Pages	6
Type of use	Dissertation/Thesis

Requestor type	Author of this Wiley article
Format	Electronic
Portion	Full article
Will you be translating?	No
Title	Synthesis and Reactivity of Three Coordinate Bismuth Pincer Complexes
Institution name	Dalhousie University